2012-10-03

Passive Cardiac Properties and Titin Expression in Dilated Cardiomyopathy

McKenzie, Audree

UNIVERSITY OF CALGARY

Passive Cardiac Properties and Titin Expression in Dilated Cardiomyopathy

by

Audrée McKenzie

A THESIS

SUBMITTED TO THE FACULTY OF GRADUATE STUDIES

IN PARTIAL FULFILMENT OF THE REQUIREMENTS FOR THE

DEGREE OF MASTER OF SCIENCE

BIOMEDICAL ENGINEERING GRADUATE PROGRAM

CALGARY, ALBERTA

SEPTEMBER, 2012

Abstract

Dilated cardiomyopathy (DCM) is a frequently occurring heart disease characterized by dilation of the left or both ventricles, and systolic and diastolic dysfunctions leading to heart failure.

Considering that changes in the expression of titin have been reported to modulate the passive mechanical properties of myocardium and have been associated with human cases of DCM, this study was aimed at relating the passive mechanical properties of myofibrils to the expression of titin in the left ventricle of the Bio TO-2 hamster, a genetic animal model of human DCM, during the progression of the disease.

The results of this thesis suggest that a minor change in the expression of titin toward the stiffer N2B isoform occurs with disease progression in the left ventricle of the DCM hamster, but the change is too small to result in a measurable difference between the passive mechanical properties of the DCM and control myofibrils.

Acknowledgements

I am grateful to have had the opportunity to learn alongside the following individuals without whom this thesis would not have been possible:

Lisa Mayer, Rosalie Kolstad, Amanda Lottermoser , Holly Hanna, Hoa Nguyen and Azim Jinha, for always being willing to help,

Bogdan Iorga, for his assistance with the isolation of cardiac myofibrils,

Tak Fung, for his assistance with statistical analysis,

Venus Joumaa, Appaji Panchangam, Tim Leonard and Michael Duvall, for many hours of teaching and assistance with my research,

Walter Herzog, for his continuous support and guidance, and for his tremendous insight in the field of research, and

my family, for their love and dedication.

Table of Contents

List of Tables

List of Figures

List of Symbols, Abbreviations and Nomenclature

Symbol	Definition
ATP	adenosinetriphosphate
BDM	2,3-butanedione monoxime
BW	body weight
CARP	cardiac ankyrin repeat protein
DCM	dilated cardiomyopathy
DTT	dithiothreitol
Dys	dystrophin
EDTA	ethylenediaminetetraacetic acid
HW	weight of solution filled heart
IDC	idiopathic dilated cardiomyopathy
IF	intermediate filament
Ig	immunoglobulin
LV	left ventricle or left ventricular
MHC	myosin heavy chain
MW	molecular weight
PEVK	proline, glutamate, valine and lysine
RV	right ventricle or right ventricular
SG	sarcoglycan
SHR	spontaneously hypertensive rat
SL	sarcomere length
SP	Standard play
α	alpha
β	beta
δ	delta
γ	gamma

CHAPTER ONE: INTRODUCTION

Dilated cardiomyopathy (DCM) is a frequently occurring heart disease characterized by dilation and systolic dysfunction in the left or both ventricles, by fibrosis, and by symptoms of congestive heart failure toward the end stages of the disease (Wynne & Braunwald, 2005). It is estimated that DCM is responsible for at least half of the cases of heart failure in the US (Hershberger *et al.*, 2010). More than 75 specific diseases of the heart muscle can produce DCM. It appears to be the end result of myocardial damage originating from a variety of causes (Hershberger *et al.*, 2010), and initiating cardiac remodelling. Approximately 10 to 15% of patients with DCM, or 30 to 35% of patients with idiopathic dilated cardiomyopathy (IDC) (of unknown causes), have a familial form of the disease (Hershberger *et al.*, 2010). Mutations in over 30 different genes that encode nuclear membrane, sarcomeric, cytoskeletal, sarcolemmal and extra cellular proteins have been found to be linked to DCM (Hershberger *et al.*, 2010).

The Bio TO-2 Syrian hamster is a genetic model of human DCM. It shows systolic and diastolic dysfunctions, and pathophysiological features replicating human cases of DCM (Kawada *et al.*, 2005). It has a defect in the delta-sarcoglycan (δ-SG) gene, lacks the alpha (α), beta (β), gamma (γ) and δ-SG proteins (Sakamoto *et al.*, 1997;Kawada *et al.*, 1999), and shows a partial loss of the α- and β-dystroglycan proteins (Sakamoto *et al.*, 1997). Human cases of DCM have been attributed to a mutation in a gene encoding δ-SG.

This research was aimed at studying over time the progression of the remodelling process leading to DCM in the Bio TO-2 animal model. More specifically, this research was aimed at comparing over time the passive mechanical properties of experimental myofibrils isolated from the left ventricles (LVs) of Bio TO-2 Syrian hamsters to those of control myofibrils from the LVs of Bio F1B Syrian hamsters. Studying isolated myofibrils provides the opportunity to link passive mechanical properties to subcellular components since the connective tissues

and sarcolemma normally surrounding cells are removed. This study was also aimed at relating the passive mechanical properties of the myofibrils to the expression of titin in the LVs of Bio TO-2 and Bio F1B hamsters, since changes in the expression of titin have been reported to modulate the passive mechanical properties of myocardium (Wu *et al.*, 2002b;Cazorla *et al.*, 2000;Neagoe *et al.*, 2003;Schiaffino & Reggiani, 1996;Nagueh *et al.*, 2004;Makarenko *et al.*, 2004;Neagoe *et al.*, 2002) and have been associated with DCM (Nagueh *et al.*, 2004;Makarenko *et al.*, 2004;Neagoe *et al.*, 2002). It was hypothesized that the remodeling process leading to DCM in the Bio TO-2 Syrian hamster would involve changes over time in the mechanical properties of its LV myocardium at the myofibrillar level, which would be relatable to the expression of titin.

CHAPTER TWO: CARDIAC MUSCLE

2.1 Introduction

This chapter contains background information on the morphology of the normal heart at the macroscopic and microscopic levels, the mechanisms of passive and active force production, the structure and function of titin, and the role of titin in passive force production and its modulation.

2.2 Heart anatomy

The heart pumps blood through the vascular system, thereby supplying oxygen to all parts of the body (Weinhaus A.J. & Roberts K.P., 2009). It is an involuntary muscle. As schematically depicted in Figure 2-1 below, the septum separates the heart into two halves. The left half, which comprises a superior and an inferior chamber, namely the left atrium and ventricle, circulates oxygenated blood. Blood flows from the lungs through the pulmonary veins and into the left atrium, then through the bicuspid or mitral valve and into the LV, and finally through the aortic valve and aorta from where it is distributed throughout the body. The heart muscle receives oxygenated blood via the coronary arteries which are connected to the aorta at its origin. The right half of the heart, which also comprises a superior and an inferior chamber, namely the right atrium and ventricle, circulates deoxygenated blood. Blood flows from the body through the superior and inferior vena cava and into the right atrium, then through the tricuspid valve into the right ventricle (RV), and finally through the pulmonary valve and arteries to feed the lungs.

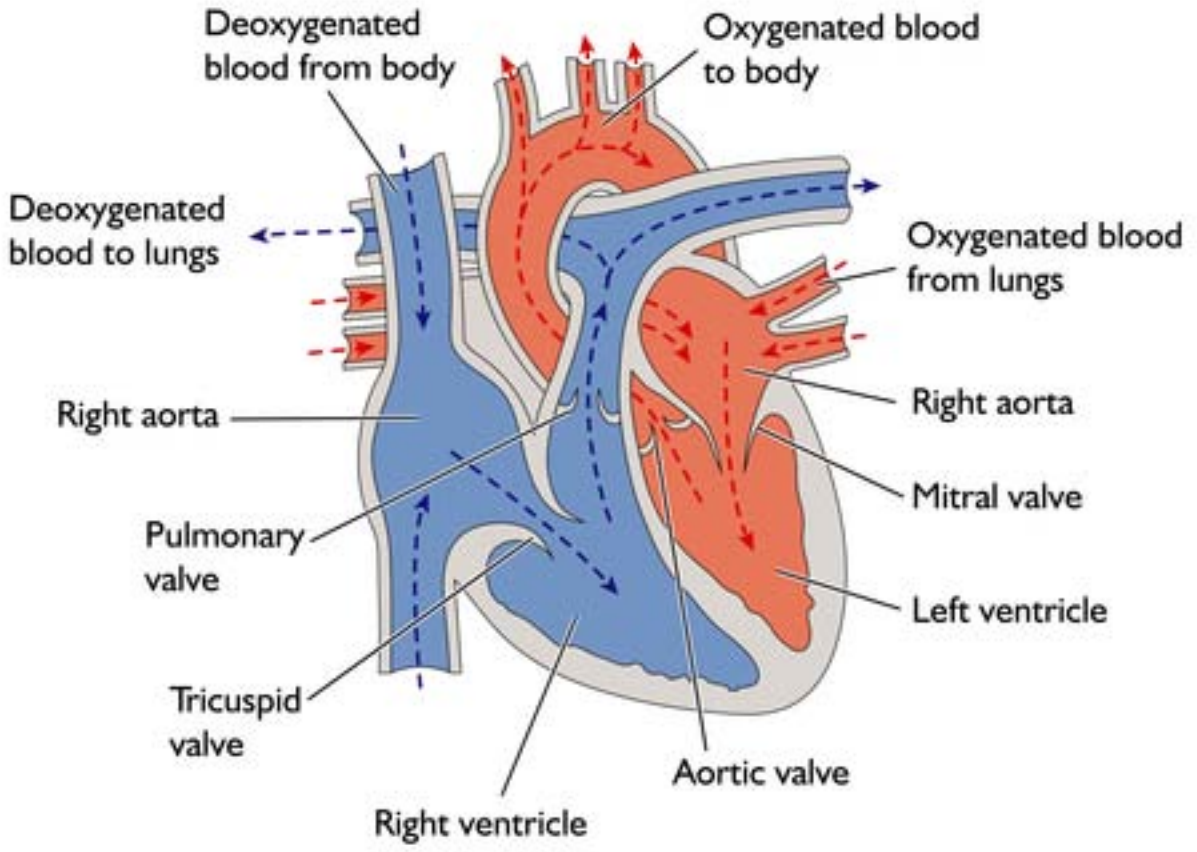

Figure 2-1 Schematic illustration of the heart (www.dreamstime.com)

The walls of the heart consist of three tissue layers. The endocardium, the innermost layer, lines the heart chambers. The epicardium is the outermost layer. The myocardium is the thick layer between the endocardium and epicardium layers. The sub-endocardium and sub-epicardium layers are often referred to as the endocardium and epicardium layers.

Papillary and trabecular muscles are often used in cardiac preparations. The former are located in the ventricles and are connected to the cusps of the atrioventricular valves. They contract to prevent inversion of these valves. The latter are muscle tissue elements in the form of rods that project from the endocardium of the right and left ventricles.

2.3 Histology of cardiac muscle

The heart consists of muscle cells connected at each end by intercalated discs, forming muscle fibres (Leeson *et al.*, 1985). The fibres are arranged into layers, which in the porcine left ventricle, were found to gradually change orientation transmurally "from +80° ± 7° (endocardium) to +30° ± 13° (midwall) and -40° ± 10° (epicardium) with 0° aligning with the circumference of the heart" (Lee *et al.*, 2012). A fine connective tissue, the endomysium, is present between the fibres. A thin cell membrane, the sarcolemma, surrounds each fibre. The muscle cells are approximately 100 µm long and 15 µm in diameter, and often split up into two or more branches at the ends (Leeson *et al.*, 1985). They are made up of myofibrils, which constitute the smallest functional units of muscle tissue. Cardiac myofibrils measure approximately 1 µm in diameter. They are partially surrounded by sarcoplasmic reticulum (Kossmann & Fawcett D.W., 1961).

2.4 Sarcomere

The cardiac muscle is involuntary but striated. Thick and thin myofilaments are organized in sarcomeres, the basic contractile units of the muscle, and create the striation pattern. Two sarcomeres are schematically depicted in Figure 2-2 below.

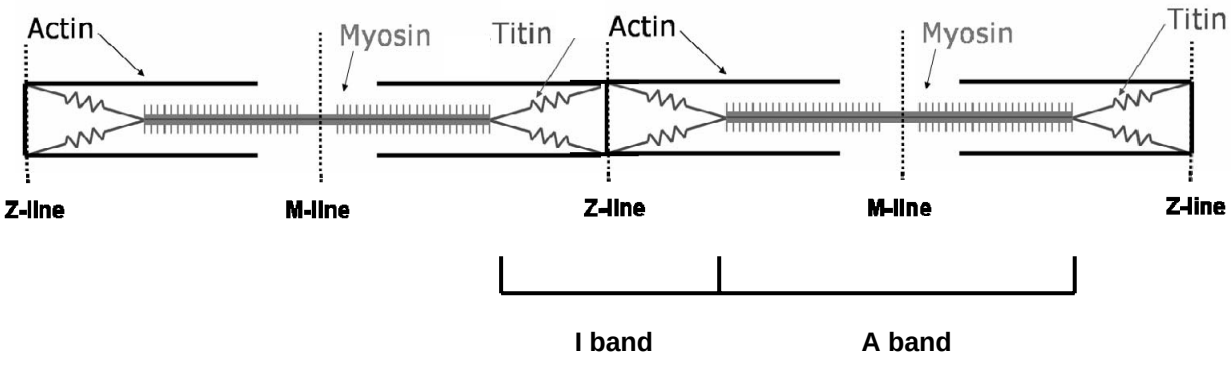

Figure 2-2 Schematic illustration of the sarcomere; reproduced and modified with permission from Brandon Hisey

In the A band, each thick filament overlaps with six thin filaments forming a perfect hexagon. The I band corresponds to the region where the thin filaments do not overlap with thick filaments. The Z lines form the extremities of the sarcomeres, and sarcomere lengths (SLs) are defined as the distance between adjacent Z lines. The physiological range of cardiac SLs has been reported to be from ~1.9 to 2.3 µm (Pollack & Huntsman, 1974) or ~1.7 - 2.4 µm (Rodriguez *et al.*, 1992). The two Z lines of a sarcomere are connected to each other by titin proteins.

Due to their composition, the thick and thin filaments are often referred to as the myosin and actin filaments respectively. A thick filament consists of several myosin molecules. Each myosin molecule is made up of two heavy chains (MHCs) (~220 kDa each), and two pairs of noncovalently bound light chains (~20 kDa each). The pairs of MHCs form a tail and a head domain consisting of two globular heads that protrude from the thick filament. A thick filament is schematically depicted in Figure 2-3 below. The heads contain an actin-binding site and an adenosinetriphosphate (ATP) hydrolysis site, and have been termed cross-bridges due to their ability to form a transient link between the thick and thin filaments.

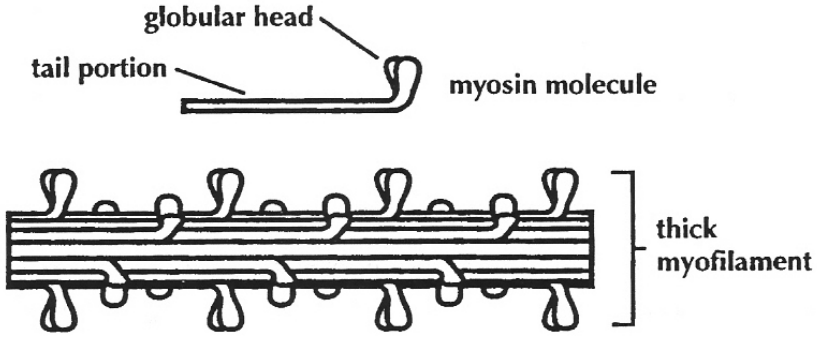

Figure 2-3 Schematic illustration of the thick filament (Herzog, 1999)

A thin filament consists of two chains of actin globules forming a helix and intertwined with long fibrous tropomyosin. Troponin is located at fixed intervals along the thin filament and is composed of three subunits: troponin C, T and I. A thin filament is schematically depicted in Figure 2-4 below.

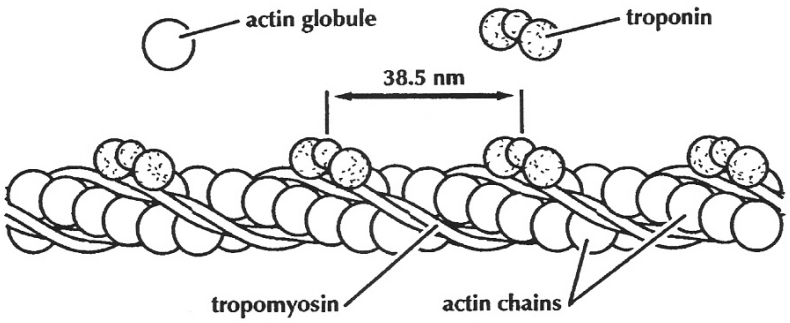

Figure 2-4 Schematic illustration of the thin filament (Herzog, 1999)

2.5 Myocardium force production

2.5.1 Active force

An action potential is induced by pacemaker cells and conducted along the external membrane and to invaginations of the cell membrane called T-tubules. Depolarization of the external membrane and of the T-tubules causes Ca^{2+} ions to flow into the cell (for a review (Ibrahim *et al.*, 2011)). These Ca^{2+} ions in turn trigger the release of Ca^{2+} ions from the sarcoplasmic reticulum, resulting in a greater intracellular Ca^{2+} concentration. The cytoplasmic Ca^{2+} ions change the configuration of tropomyosin-troponin complexes on actin filaments by binding to troponin C (for a review (Sparks, 1987)). As a result, cross-bridge attachment sites become exposed. Cross-bridges on adjacent myosin filaments attach to these binding sites. The actin filaments are pulled toward the center of the sarcomere by the cyclical action of the

cross-bridges, shortening the sarcomere. ATP molecules are also required to provide the necessary energy for contraction and to allow the cross-bridges to detach.

The Frank-Starling mechanism is a fundamental property of cardiac muscle and is considered an indicator of the (patho)physiological state of the heart. It links an increase in myocardial active force production to stretch. Accordingly, an increase in end-diastolic volume, or a greater dilation of the ventricles and a greater stretch of the fibres and sarcomeres, results in an increase in stroke volume (volume of blood ejected during systolic contraction). This mechanism regulates active force production at each beat.

Cardiac muscle activation is sub-maximal under physiological conditions (Fabiato, 1981), and the active force-SL relationship is mostly attributable to length-dependent changes in myofilament Ca^{2+} sensitivity (for a review (Allen & Kentish, 1985;Calaghan & White, 1999;De Tombe *et al.*, 2010)). For a given calcium concentration, the myofilaments produce more force when sarcomeres are stretched (Allen & Kentish, 1985;Kentish *et al.*, 1986;De Tombe *et al.*, 2010). The mechanism by which myofilament Ca^{2+} sensitivity is regulated by SL has not been fully determined (Fuchs & Martyn, 2005;De Tombe *et al.*, 2010).

2.5.2 Passive force

When a muscle is stretched passively past its resting length, it produces a measurable force that opposes the stretch and shortens the muscle after release. This passive force is an important factor in cardiac muscle. It affects the extent of filling during diastole and consequently the stroke volume (Allen & Kentish, 1985), as dictated by the Frank-Starling mechanism previously described in section 2.5.1.

In cardiac muscle, the major contributors to passive force are believed to be titin and collagen (Granzier & Irving, 1995;Granzier *et al.*, 2005). Titin was found to produce the majority of the passive force at shorter SLs, but titin and collagen produced about equal passive forces

at maximum physiological SLs (Granzier *et al.*, 2005). In an isolated cardiac myofibril, surrounding connective tissue having been removed, titin is thought to generate the majority of the passive force.

2.6 Cardiac titin

2.6.1 Structure of titin and its isoforms

Titin is the longest protein known. Each titin molecule runs from the Z-line to the M-line, thereby covering the length of the half sarcomere. It contains a molecular spring or extensible segment only located in the I-band region of the sarcomere (Trombitas *et al.*, 1995). In addition to playing a role in myocardial passive force, titin has the functions of maintaining the position of the A-band in the center of the sarcomere and SL homogeneity (Granzier & Labeit, 2007).

Titin isoforms differ between muscle types and this manifests itself, in part, by the composition of titin's extensible region. The extensible region of cardiac titin contains immunoglobulin (Ig) domains linked in tandem, a PEVK segment rich in proline (P), glutamate (E), valine (V) and lysine (K), and one or two other spring elements depending on the titin isoform (Labeit & Kolmerer, 1995). N2B and N2BA isoforms are found in cardiac muscle. The N2B isoform contains only the N2B spring element. The N2BA isoform contains both the N2B and N2A spring elements, additional Ig domains and a larger PEVK segment than the N2B isoform (Freiburg *et al.*, 2000). The N2BA isoform has a longer extensible region and a higher molecular weight (MW) than the N2B isoform, between ~3250 and ~3400 kDa compared to ~3 000 kDa (Neagoe *et al.*, 2003;Warren *et al.*, 2004). In comparison, skeletal titin isoforms are longer than cardiac isoforms and only contain N2A elements (Freiburg *et al.*, 2000). N2A skeletal isoforms of different MWs, ranging from 3300 to 3700 kDa, have been reported (Neagoe *et al.*, 2003). A schematic illustration of cardiac and skeletal titin isoforms is shown in Figure 2-5 below.

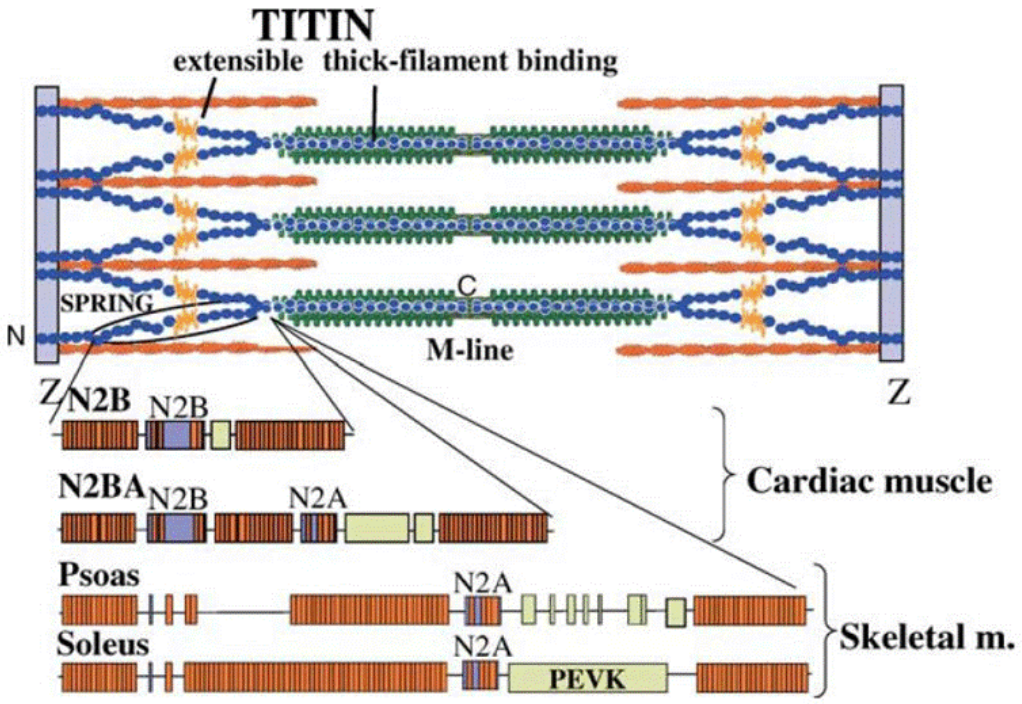

Figure 2-5 Top: Schematic illustration indicating the location of the extensible region of titin in a sarcomere. Bottom: Detailed illustration of the different extensible regions of titin for cardiac N2B, N2BA and skeletal psoas and soleus isoforms. (Orange rectangle: immunoglobin-like domains; white: PEVK domain; blue: unique sequence) Reproduced with permission from Springer (Granzier et al., 2005).

Mammalian myocardium co-expresses both the N2B and N2BA titin isoforms (Linke *et al.*, 1996;Cazorla *et al.*, 2000;Trombitas *et al.*, 2001) in the half-sarcomere (Trombitas *et al.*, 2001). The N2BA:N2B expression ratio varies greatly amongst the hearts of different mammalian species (Cazorla *et al.*, 2000;Neagoe *et al.*, 2003). N2B titin is predominantly expressed in the hearts of small mammals such as rats, but N2B and N2BA titin are co-expressed in the hearts of larger mammals. The hamster left ventricle has been reported to express 10% N2BA. Two N2BA isoforms of different MWs, 3250 and 3400 kDa, corresponding to 4 and 6% N2BA respectively, have been found (Neagoe *et al.*, 2003).

2.6.2 Mechanisms of passive force generation

During stretch, the different elements of the extensible region of titin lengthen in a sequential manner with increasing SLs due to their different bending rigidities (Watanabe *et al.*, 2002). Within physiological SLs, it is believed that the tandem Ig domains elongate first, "largely due to straightening of sequences that link Ig domains" (Granzier & Labeit, 2004), followed by the PEVK domain and N2B unique sequence, "likely due to straightening of random coil sequences" (for a review (Granzier & Labeit, 2004)). "Beyond the physiological SL range, Ig unfolding is likely to take place" (Watanabe *et al.*, 2002).

The shorter the titin isoform, the greater the passive force produced at a given SL (Linke *et al.*, 1996;Freiburg *et al.*, 2000;Cazorla *et al.*, 2000;Fukuda *et al.*, 2005a) due to the greater elongation of the elements in titin's extensible region (Cazorla *et al.*, 2000). Therefore, the N2B isoform generates a higher passive force than the N2BA isoform at a given SL.

The passive force generated by cardiac myofibrils when stretched may not be solely attributable to the extension of titin elements. Titin-actin dynamic interactions may also contribute to passive force (Stuyvers *et al.*, 1997a;Stuyvers *et al.*, 1997b;Stuyvers *et al.*, 1998;Stuyvers *et al.*, 2000), and more specifically, connections between PEVK segments from N2B isoforms and actin (Yamasaki *et al.*, 2001).

Figure 2-6 below shows passive stress-SL relations for mouse and pig left ventricular myocytes. The passive stresses produced by the intermediate filaments were subtracted from the measured values to obtain stresses produced by titin alone. The different passive stress-SL relations of the two animals reflect their different expressions of titin isoforms, the mouse predominantly expressing N2B titin, and the pig, approximately 60% N2BA.

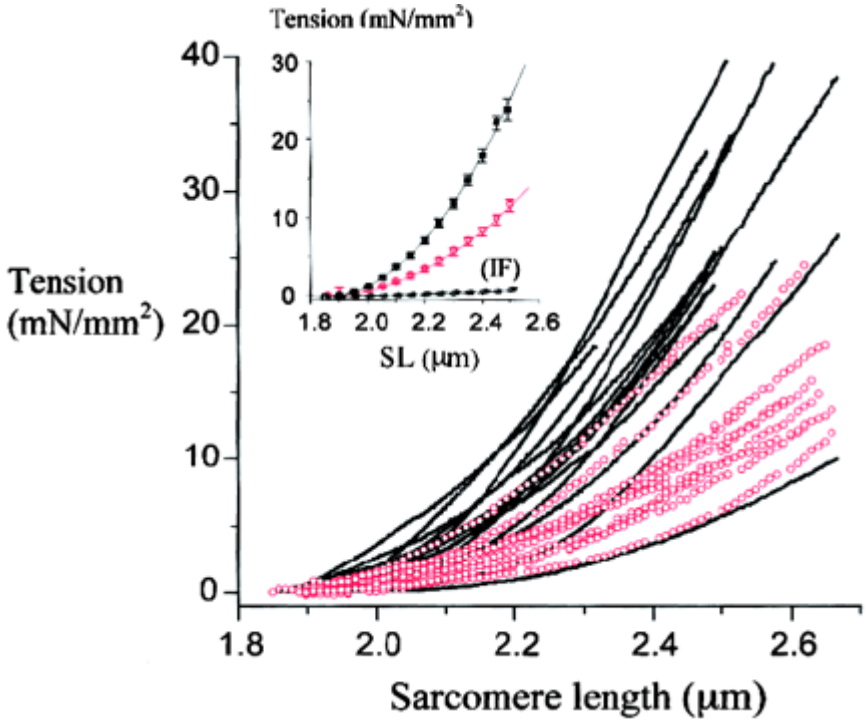

Figure 2-6 Passive stress-SL relations of 15 mouse (black lines) and 10 pig (pink circles) left ventricular myocytes. The passive stresses produced by the intermediate filaments were subtracted from the measured values to obtain stresses produced by titin alone. The means ± SEM of the cells are shown in the inset. The different passive stress-SL relations of the two animals reflect their different expressions of titin isoforms, the mouse predominantly expressing N2B titin, and the pig, approximately 60% N2BA. Reproduced with permission from the American Heart Association (Cazorla *et al.*, 2000).

2.6.3 Mechanisms of passive force modulation

The passive force generated by titin upon stretch can be modulated through various mechanisms, providing different ways of altering the diastolic properties of the heart.

1) One mechanism involves varying the co-expression ratio of titin isoforms in the myocardium. This mechanism of passive stiffness modulation is widely used even in healthy myocardium because the co-expression ratio varies in the ventricles of different species, as previously

discussed in section 2.6.1, in the different chambers of the heart (Jaber *et al.*, 2008), and across the LV wall of larger animals (Cazorla *et al.*, 2000;Neagoe *et al.*, 2003). It is also altered in disease states, which is discussed in the next section. The higher the N2BA:N2B ratio expressed, the lower the passive force produced.

2) Also, the passive force generated by the N2B and N2BA isoforms decreases with phosphorylation by protein kinase A, a protein activated in cardiac muscle by ß-adrenergic stimulation, and the effect is greater on N2B than N2BA titin (Fukuda *et al.*, 2005b). The passive force generated by the N2B and N2BA isoforms also decreases with phosphorylation by protein kinase G (Kruger *et al.*, 2009).

3) In addition, Ca^{2+} binding increases the passive force generated by the N2BA isoform, but has no effect on the N2B isoform (Fujita *et al.*, 2004). Calcium binds to the E-rich PEVK motifs that are expressed in N2BA titin but not in N2B titin and changes their conformation (Labeit *et al.*, 2003).

4) Furthermore, the N2B PEVK-actin interactions previously discussed in section 2.6.2 can be eliminated by S100A1, “a soluble calcium-binding protein found at high concentrations in the myocardium” (Yamasaki *et al.*, 2001), thereby reducing passive stiffness in cardiac muscle (Yamasaki et al., 2001).

5) Lastly, alterations in the quantity of titin expressed in cardiac muscle may be another mechanism by which the passive force generated by titin upon stretch is modulated. When measuring the passive properties of isolated myocytes from rats, cells from the endocardium layer developed higher passive forces when stretched than those from the epicardium layer (Cazorla *et al.*, 2004). No difference in the titin isoform ratio was found between the layers. However, the titin:MHC ratio was found to be lower in the epicardium than in the endocardium layer.

2.6.4 Myofibrillar stress relaxation

When a cardiac myofibril is stretched passively and maintained at a quasi constant length after stretch, it produces a stress trace that shows visocelastic behaviour (velocity-dependent). An example of an actual passive stress trace obtained is shown below in Figure 2-7.

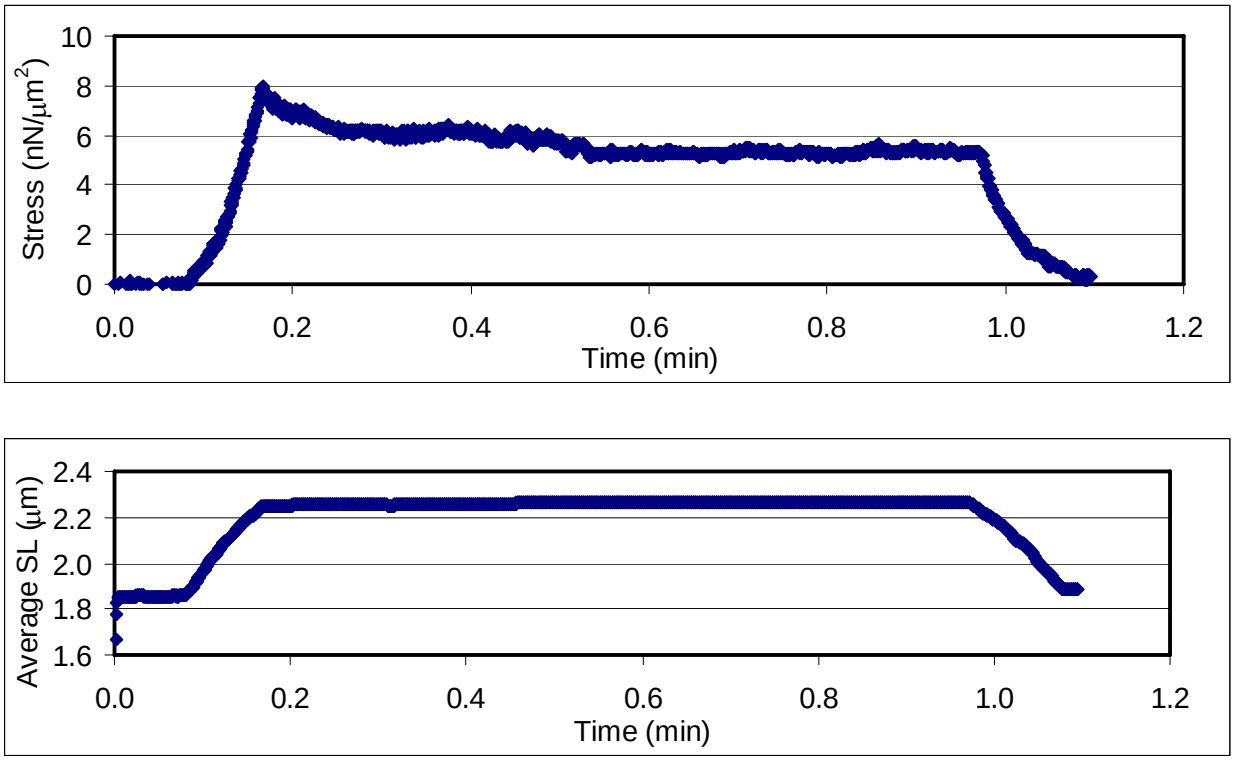

Figure 2-7 The passive stress and average SL traces of a single myofibril from the LV of a Bio F1B Syrian hamster stretched from an average SL of 1.86 to 2.24 μm and maintained at a quasi constant length after stretch for 1 minute showing stress relaxation.

The stress increases during stretch in a velocity dependent manner and reaches a peak at the end of stretch. When the stretch ends, the stress starts to fall until it reaches a quasi steady state level. The shortening of the myofibril to its initial length brings the force back to 0. The

stress decay while maintaining the final length after stretch is called stress relaxation (Linke & Leake, 2004). Some molecular mechanisms that have been suggested as possibly being involved in stress relaxation include “the unfolding of only a very small number of Ig domains per titin molecule” (Minajeva *et al.*, 2001;Linke & Leake, 2004) and “minor structural changes” (Minajeva *et al.*, 2001) in the PEVK domain. The stress-decay amplitude increases with longer lengths and the stress relaxation lasts longer (Minajeva *et al.*, 2001).

2.6.5 Effect of disease on cardiac titin

Cardiac muscle undergoes remodelling when diseased which sometimes involves changes in the titin co-expression ratio. The canine tachycardia-induced model of DCM has produced varied results of titin and collagen expressions, and LV wall stiffness. Two weeks of pacing resulted in a reduced N2BA:N2B ratio in the LV epicardium layer, but in an increased N2BA:N2B ratio in the LV endocardium layer (Bell *et al.*, 2000). Four weeks of pacing resulted in a reduced N2BA:N2B ratio in the middle of the LV wall (Wu *et al.*, 2002a). The wall stiffness was elevated in the LVs of the paced dogs as a result of increases in both the titin and collagen-based passive tensions. Five and half weeks of pacing at gradually increasing rates resulted in a reduced N2BA:N2B ratio in the LV epicardium layer but an unchanged ratio in the LV endocardium layer (Jaber *et al.*, 2008). The ratio was also reduced in the RVs, and left and right atria of the paced animals, and dilation was observed in all the chambers. The collagen content in the LVs and atria of the paced dogs was unchanged or reduced compared to the one observed in the control dogs. The LV wall stiffness was normal.

In the spontaneously hypertensive rat model (SHR) of hypertrophic cardiomyopathy, pressure overload resulted in a reduced N2BA:N2B ratio in the epicardium layer (Warren *et al.*, 2003).

Changes in titin expression associated with human cases of DCM will be discussed in chapter 3.

2.6.6 Titin's involvement in stretch sensing and signaling

Titin is believed to be involved in "length-dependent signaling processes" (Granzier & Labeit, 2004) as it contains sarcomere stretch sensing and signaling centers. The Z-disc, I-band and M-line regions of titin have been identified as those sensing and signaling centers (for a review (Granzier & Labeit, 2004)).

Some structural information is needed to understand the role of titin's Z-disc region in stretch sensing and signaling. The Z-disc consists of a lattice (Luther & Squire, 2002). "The titin filament fully penetrates the Z-disc, thereby placing the titin-caping protein T-cap (or telethonin) toward the periphery of the Z-disc lattice of the adjacent sarcomere." (Granzier & Labeit, 2004) "The Z-disc is also connected to the sarcolemma at T-tubules […] and costameres." (Granzier & Labeit, 2004) Costameres are sub-membranous structures that have been implicated in the "transmission of force from the sarcomere to the sarcolemma and extracellular matrix, maintaining mechanical integrity of the sarcolemma, and orchestrating mechanically related signalling" (Peter *et al.*, 2011).

The Z-disc signaling center probably senses titin-based tension arising from sarcomere stretch, tension produced by actin-myosin cross-bridges, and tension transmitted from the sarcolemma through the costameres. By altering the Z-disc lattice spacing, which could modify the binding abilities of the T-cap and Z-disc proteins, these tensions could affect signaling. The T-cap and Z-disc may be involved in myogenesis and myogenic differentiation**. "**Exposure to nonphysiological biomechanical signals" (Granzier & Labeit, 2004) has been reported to contribute to the progression of DCM, and "the Z-disc region of titin and its various ligands" (Granzier & Labeit, 2004) appear to be implicated.

The I-band signaling center probably senses titin-based tension only. Considering that all the ligands that bind to the I-band region of titin have also been reported to be present in the nucleus, this signaling center may be involved in regulating transcription, cell cycle and gene expression. There is also evidence suggesting that the N2B element in the I-band region of titin is involved in protecting titin from structural damage, and that the N2A element plays a role in protein degradation.

The M-line signaling center probably senses titin-based tension and tension produced by actin-myosin cross-bridges. This region of titin may also be involved with the regulation of gene expression and protein degradation.

In healthy cardiac muscle, several mechanisms of passive stiffness adjustment which involve altering titin's stiffness have been reported. In a variety of cardiac diseases, the same mechanisms of titin-based stiffness regulation have been reported, but resulted in an altered stiffness in the diseased myocardium compared to normal. Titin may be involved in sensing chronic "nonphysiological biomechanical signals" (Granzier & Labeit, 2004) and in initiating "length-dependent signalling processes" (Granzier & Labeit, 2004).

CHAPTER THREE: DILATED CARDIOMYOPATHY IN HUMANS

3.1 Introduction

This chapter contains background information on the epidemiology of DCM in humans, criteria used to diagnose the disease, and the mechanisms of systolic and diastolic dysfunctions.

3.2 Epidemiology

According to statistics from the American Heart Association (Lloyd-Jones et al., 2010), approximately 5.8 million US citizens suffered from heart failure in 2010. DCM is responsible for at least half of the cases of heart failure in the US. The majority of the cases of DCM in the US are caused by ischemic heart disease due to coronary artery disease. Approximately 35 to 40% of DCM cases are idiopathic. A genetic cause has been reported for approximately 30 to 35% of idiopathic cases (Hershberger et al., 2010). Mutations in 33 different genes that encode nuclear membrane, sarcomeric, cytoskeletal, sarcolemmal and extra cellular proteins have now been found to be linked to DCM (Hershberger & Siegfried, 2011). A mutation in the SGCD gene which affects the delta-sarcoglycan (δ-SG) protein has been associated with human cases of familial DCM (Karkkainen et al., 2003;Tsubata et al., 2000;Sylvius et al., 2003) at an estimated frequency of 0.003 (Hershberger et al., 2010).

More than 75 specific diseases of the heart muscle can produce DCM. It appears to be the end result of myocardial damage originating from a variety of causes (Hershberger et al., 2010), and initiating cardiac remodelling. A non exhaustive list of causes of DCM is provided here. Some of the causes are still unknown.

- ischemic conditions,
- structural heart disease,

- toxins, such as alcohol, carbon monoxide, cigarette smoke, chemotherapeutic agents, cocaine, iron, and chest radiation,
- metabolic abnormalities, such as nutritional deficiencies in thiamine, selenium and carnitine,
- endocrinal abnormalities,
- inflammatory conditions, infectious (caused by viral, bacterial, protozoal and fungal agents, to name a few), and non-infectious myocarditis,
- infiltrative diseases, and
- genetic factors.

3.3 Diagnosis of DCM

DCM is characterized by dilation, left ventricular and sometimes right ventricular and atrial, and systolic dysfunction. The heart becomes heavier and larger, and the dilated walls become thin and extended, resulting in impaired contraction (Luk et al., 2009). Symptoms of congestive heart failure develop toward the end stages of the disease (Wynne & Braunwald, 2005). Some criteria that have been developed to diagnose DCM are as follows (Mestroni et al., 1999;Luk et al., 2009;Hershberger et al., 2010):

1. LV ejection fraction less than 45-50% and/or fractional shortening less than 25-28%.

$$\text{ejection fraction} = \frac{\text{stroke volume}}{\text{end-diastolic volume}} = \frac{\text{end-diastolic volume} - \text{end-systolic volume}}{\text{end-diastolic volume}}$$

$$\text{fractional shortening} = \frac{\text{end diastolic dimension} - \text{end systolic dimension}}{\text{end diastolic dimension}}$$

2. “LV end-diastolic diameter greater than 117% of the predicted value corrected for age and body surface area” (Mestroni *et al.*, 1999) using the formula:

$$= (45.3 \times (\text{body surface area})^{1/3} - (0.03 \times \text{age}) - 7.2) \pm 12\%)$$

The following histological findings are also involved: increased apoptosis, reduced number of myocytes and interstitial fibrosis (Schaper et al., 1991;Luk et al., 2009).

3.4 Systolic dysfunction

In human hearts failing due to DCM, the Frank-Starling mechanism has been found to sometimes be preserved but impaired, and sometimes absent. Vahl et al. found a reduction in the length-dependent increase in active force in electrically stimulated LV muscle strips from human myocardium failing due to DCM compared to the one developed by muscle strips from normal hearts (Vahl et al., 1997;Vahl et al., 1998). However, Schwinger et al. found an absence of the Frank-Starling mechanism or no increase in force with length in electrically stimulated DCM ventricular papillary muscles and skinned fibres (Schwinger et al., 1994). The mechanisms at the origin of the deterioration of cardiac function include a reduction in the number of functional myocytes, development of fibrosis, remodeling of LV chamber and possibly of other chambers, and diminished myocyte function. Alterations in calcium handling, in myofilament function, and in the cytoskeleton of cardiac myocytes have been suggested as contributing to the decrease in myocyte function (de Tombe, 1998).

In the case of familial DCM, some of the mutations have been found to impair force generation in the myocardium because they 1) affect the integrity of the sarcomere unit or 2) affect the transmission of the force generated by the sarcomere to the extracellular matrix (for a review (Luk et al., 2009)). Mutations affecting β-cardiac MHC and cardiac troponin T are in the first group, whereas mutations affecting cardiac actin at the site of actin–cytoskeleton interaction, α-tropomyosin, strophin, desmin, δ-SG, plakoglobin and desmoplakin are in the second group.

3.5 Diastolic dysfunction

Passive stiffness is typically increased in human hearts failing due to DCM. This has been attributed to an increase in collagen expression as well as an increase in cross-linking of collagen fibres (Burlew & Weber, 2002). Two studies have looked at the contribution of titin to the total passive forces generated by muscle strips (Nagueh et al., 2004) and cardiomyofibrils (Makarenko et al., 2004) extracted from the LVs of human hearts failing due to non-ischemic DCM. The latter study reported a reduced contribution of titin to the total passive stiffness, and both studies reported increased N2BA:N2B titin ratios in the LVs of the failing hearts compared to the control donor hearts. The titin to MHC ratio was unchanged between the failing and control hearts in the first study, and the titin per unit tissue was reduced in some of the failing hearts in the second study due to the loss of myocytes and the development of fibrosis. In the second study, the passive stress generated by the LV myofibrils isolated from the failing hearts was reported to be lower on average by 25 to 30% than the one generated by the control myofibrils. Also, the expression of collagen was increased in the DCM hearts in this study.

The N2BA:N2B isoform ratio was also increased in the LVs of human hearts failing due to ischemic DCM caused by coronary artery disease, compared to the one in control donor hearts (Neagoe et al., 2002). Accordingly, the passive stress measured on isolated LV myofibrils from the human hearts failing due to ischemic DCM was also found to be reduced compared to the one measured on control myofibrils. Also, the expression of collagen was increased in the DCM hearts.

Considering the decreased contribution of titin to the total passive tension found in DCM human hearts, this study was aimed at examining titin's contribution to the progression of the remodelling process in the Bio TO-2 animal model of DCM.

CHAPTER FOUR: BIO TO-2 ANIMAL MODEL

4.1 Introduction

This chapter contains background information relating to the Bio TO-2 hamster model of DCM, more specifically, on its genetic defect, the progression of the cardiac hemodynamic and contractile indices in its heart, and results of mechanical testing previously performed on its myocardium.

4.2 Genetic defect of the Bio TO-2 hamster

For many years, specific strains of Syrian hamsters have been used as genetic models of cardiomyopathy and congestive heart failure. There are two sublines of cardiomyopathic hamsters which descend from the same ancestor, the Bio 1.50. The first one is characterized by cardiac hypertrophy, and it comprises "the Bio 14.6, UM-X7.1, CHF 146, and CHF 147 strains" (Goineau *et al.*, 2001). The second, which includes "the Bio 53.58 and Bio TO-2 strains" (Goineau *et al.*, 2001), exhibits dilation of the ventricles. Both sublines have a defect in the δ-SG gene (Sakamoto *et al.*, 1997). The Bio TO-2 hamster lacks the α-, β-, γ- and δ-SG proteins (Sakamoto *et al.*, 1997;Kawada *et al.*, 1999), and shows a partial loss of the α- and β-dystroglycan proteins (Sakamoto *et al.*, 1997). The α-, β-, γ- and δ-SG proteins link Dys to the extracellular matrix via α- and β-dystroglycan (Holt *et al.*, 1998). These protein complexes are involved in "transmitting the force developed through the actin-myosin cross-bridges to the extracellular matrix" (Kawada *et al.*, 2005) and in providing some "mechanical resistance to the over-expansion of the sarcolemma" (for a review (Kawada *et al.*, 2005)).

4.3 Clinical course of the Bio TO-2 hamster

The Bio TO-2 strain is a good animal model to study the progression of dilated cardiomyopathy because its clinical course evolves fairly gradually before the development of symptoms of congestive heart failure. The progression of the cardiac hemodynamic and contractile indices, determined by cardiac catheterization and echocardiography respectively, of the Bio TO-2 and Bio F1B hamsters have been reported for the duration of life of the Bio TO-2 hamster, which is approximately 43 weeks (Goineau *et al.*, 2001;Kawada *et al.*, 2005;Kato *et al.*, 2006;Ichihara *et al.*, 2006). Goineau et al. tested the animals at 20, 26, 31, 37 and 43 weeks of age. The normal Bio F1B hamster displayed growth-dependent changes, while the Bio TO-2 strain showed progressive systolic and diastolic dysfunctions. Compared with controls, a decrease in cardiac output averaging -34% from 20 to 43 weeks of age was found in the Bio TO-2 strain, accompanied by a decrease in stroke volume averaging -36%. A cardiac hypertrophy progressively developed in the atria and RV, but at 20 weeks of age, the LV already displayed dilation with thinning of the LV wall. Increases in LV and RV collagen content were first detected around 26 weeks of age. The Bio TO-2 strain showed a decrease in fractional shortening (Kawada *et al.*, 2005;Kato *et al.*, 2006;Ichihara *et al.*, 2006) and LV ejection fraction (Kawada *et al.*, 2005).

Kawada et al., who tested the animals at 5, 15, 25 and 40 weeks, also reported a close correlation between the progression of the hemodynamic indices and a cleavage of Dys in the Bio TO-2 hearts. The content of intact Dys started to decline at about 15 weeks and was clearly reduced at the advanced stage of heart failure. In contrast, normal F1B hearts did not lose Dys content. The disruption of Dys has also been observed in human hearts failing due to DCM (Vatta *et al.*, 2002;Toyo-oka *et al.*, 2004).

4.4 Previous results of mechanical studies on Bio TO-2 myocardium

Two studies have previously reported on the mechanical properties of myocardium from the Bio TO-2 hamster compared to those of the Bio F1B hamster. Mancinelli et al. studied papillary muscles from 4 month old animals (Mancinelli et al., 2005). They observed a reduction of muscle stiffness in the Bio TO-2 hamsters. Also, the active stress-length and force-frequency relations, and peak rates of tension rise and fall were decreased. Following the functional experiments, the papillary muscles were fixed at the length at which they produced maximum active force during twitch contractions, sliced, and the SLs were determined using electron microscopy. A minimum of 20 SL measurements were made per papillary muscle and averaged. The average SLs of the DCM papillary muscles ranged from about 0.9 to 3.0 µm, whereas the average SLs of the control papillary muscles ranged from about 1.85 to 2.2 µm. Seven DCM papillary muscles studied showed a shorter average SL, and three showed a longer average SL, compared to the average SLs of the ten control muscles. Also, larger SL standard deviations were measure on some of the DCM papillary muscles compared to the control ones.

Nishimura et al. studied cardiomyocytes from the LVs of 2 month old Bio TO-2 and F1B hamsters (Nishimura *et al.*, 2005). The passive stress-SL relations obtained in the presence of BDM (2,3-butanedione monoxime, used to inhibit the formation of cross-bridges) were similar for the DCM and control myocytes. However, the maximum shortening velocity, isometric peak force, and external work were decreased compared to normal in the DCM myocytes. Neither of these studies included an analysis of the titin isoforms.

The Bio TO-2 hamster was selected for this study for the following reasons:

- It is considered to be a good animal model of human DCM. Its genetic defect on the gene encoding δ-SG causes the myocardial damage that leads to cardiac remodelling and the

development of DCM in its heart, just like DCM in human hearts appears to be the end result of myocardial damage caused by a multitude of diseases. Also, it shows systolic and diastolic dysfunctions, and pathophysiological features replicating human cases of DCM (Kawada *et al.*, 2005). Furthermore, human cases of DCM have also been attributed to a mutation in the gene encoding δ-SG.

- Although its passive properties were not found to be altered in myocytes from 2 month old animals, it showed reduced stiffness in papillary muscles from 4 month old animals. It was hypothesised that the myocytes from 2 month old animals were too young to show impairment of passive properties, and that the reduced stiffness in the papillary muscles from 4 month old animals reflected a change in the expression of titin not yet hidden by the development of fibrosis.

CHAPTER FIVE: CARDIAC MYOFIBRIL ISOLATION PROTOCOL

5.1 Introduction

This document gives a detailed description of the methodology developed to isolate single myofibrils from the LV wall of the Bio TO-2 hamster model of DCM which develops significant fibrosis, and of its control animal the Bio F1B hamster. The methodology was taken from Stehle et al. 2002 (Stehle *et al.*, 2002a;Stehle *et al.*, 2002b) and modified as required. It takes 5 to 6 hours to prepare the tissue up to the point where it can be homogenized to break it down into myofibrils. Therefore, the tissue was usually prepared on Mondays and the experiments with isolated myofibrils performed from Tuesdays to Fridays. The methodology is broken down into chronological steps, assuming the same use of the days of the week.

5.2 Preparation of solutions

The rigor solution required to perform a retrograde perfusion of the heart, and the solutions used to dissect, skin, rinse and store the LV wall tissue are prepared on Monday morning. The relaxing and activating solutions are prepared on the days of experimentation with myofibrils. Stock solutions are prepared in advance but some of the components have to be added daily. Also, due to the price of sodium creatine phosphate, it was not included in the stock solutions in order to not waste it. Attached in Appendix A in Table A-1 are the compositions of the stock solutions given in mass of each chemical for solution volumes of 500 and 1000 ml.

5.2.1 Rigor solution to perfuse the heart

A rigor solution is required to perform a retrograde perfusion of the heart. Its composition is given in Table 5.1 below.

		MW	mM
Stock solution kept in fridge	Tris	121.1	10
	NaCl	58.4	132
	KCl	74.6	5
	$MgCl_2 \cdot 6H_2O$	203.3	1
	NaN_3	65.0	1
pH adjusted to 7.0 at 20ºC	EGTA	380.4	5
To be added the day of tissue preparation	Glucose monohydrate	180.2	7
	DTT	154.3	2

Table 5-1 Rigor solution molar composition

A volume of 80 ml of rigor solution is needed to perform the retrograde perfusion of one heart. On Monday morning, this volume of stock rigor solution of which the pH was previously adjusted to 7.0 at 20ºC is warmed up. Glucose monohydrate and dithiothreitol (DTT) are then added to the stock solution. They do not change the solution's pH. This solution is prepared at room temperature to prevent a thermal shock to the heart so that it can keep beating as long as possible. Table A-2 in Appendix A details the composition of the rigor solution given in mass or volume of each component.

5.2.2 Solutions to dissect, skin, rinse, store and homogenize the tissue

One solution is used to dissect the LV wall tissue, rinse it after skinning and then store it. It is called the "storage solution" in this document. Also, triton is added to this solution to skin the tissue. On the days of experimentation with myofibrils, the storage solution is also used during the homogenization of the tissue. Its composition is given in Table 5-2 below.

			MW	mM in stock sol'n	mM in whole sol'n
1	Stock solution kept in fridge	K_2HPO_4	174.2	10	5
		NaN_3	65.0	10	5
		Mg-acetate·$4H_2O$	214.5	6	3
2	K_4Cl_2EGTA solution frozen in aliquots	EGTA	380.4	250	5
	pH adjusted to 7.0 at 20ºC with KOH	KCl	74.6	500	10
3		Na_2CrP	327.1		47
4	Protease inhibitor tablets (Complete EDTA-free)		Quantity: 1 per 50 ml of solution		
5		DTT	154.3		2
6	Cl_2Na_2MgATP solution frozen in aliquots	Na_2ATP	551.1	50	3
		$MgCl_2$·$6H_2O$	203.3	50	3
Adjust pH to 7 at 10ºC.					

Table 5-2 Storage solution molar composition

To save time during the week, a solution containing components 1, 2 and 3 (refer to Table 5-2) is prepared on Monday morning in a volume large enough to meet the requirements for the week, and kept in the fridge. Table 5-3 below lists the volumes of storage solution needed to dissect, skin, rinse, store and homogenize the tissue for each day of the week. These volumes are based on the dissection of one heart and on the use of one storage container. The remaining tissue is disposed of on Friday, so no volume is needed on that day for storing. Note that the total volumes for each day of the week add up to a factor of 25 ml so that either half or full protease inhibitor tablets can be added (one per 50 ml of solution).

(ml)	Monday	Tuesday	Wednesday	Thursday	Friday	Total
Dissecting	80					
Skinning	20					
Rinsing	30					
Storing	20	20	20	20		
Homogenizing		30	30	30	25	
Total	150	50	50	50	25	325

Table 5-3 Volumes of storage solution needed throughout the week

To the volume of solution containing components 1,2 and 3 needed for Monday, components 4 and 5, namely the protease inhibitor tablets and DTT, are added. Once the protease inhibitor tablets and DTT have dissolved, the solution is placed in the fridge for one hour. The protease inhibitors make the pH of the solution fluctuate for approximately one hour. Component 6 is then added to the solution and its pH adjusted to 7 at 10ºC. The required volume of skinning solution is prepared by adding 1% triton to some of the storage solution.

The storage and skinning solutions are then put on ice to keep them cold in preparation for the collection of the cardiac tissue. Tables A-3, A-4 and A-5 in Appendix A detail how the required volumes of storage and skinning solutions are prepared each day of the week.

5.2.3 Relaxing and activating solutions

On the days of experimentation with myofibrils, a relaxing and/or activation solution is needed. After the tissue is homogenized in storage solution and the resulting myofibril suspension is placed on top of the cover slip and left to settle, the storage solution is either replaced with a relaxing solution to perform passive stretches or an activating solution for active contractions. More details on the homogenization and mechanical testing procedures are given in sections 5.8 and 6.2.2 respectively. The compositions of the relaxing and activating solutions are given in Tables 5-4 and 5-5 below.

			MW	mM in stock sol'n	mM in whole sol'n
1	Stock solution kept in fridge	Imidazole	68.08	20	10
		$MgCl_2 \cdot 6H_2O$	203.3	6	3
2		Na_2CrP	327.14		47.7
3		DTT	154.26		2
4	K_4Cl_2EGTA solution frozen in aliquots	EGTA	380.4	250	3
	pH adjusted to 7.0 at 20ºC with KOH	KCl	74.6	500	6
5	Cl_2Na_2MgATP solution frozen in aliquots	Na_2ATP	551.1	50	1
		$MgCl_2 \cdot 6H_2O$	203.3	50	1
Adjust pH to 7 at room temperature.					

Table 5-4 Relaxing solution

			MW	mM in stock sol'n	mM in whole sol'n
1	Stock solution kept in fridge	Imidazole	68.08	20	10
		$MgCl_2 \cdot 6H_2O$	203.3	6	3
2		Na_2CrP	327.14		47.7
3		DTT	154.26		2
4	$K_4Cl_2CaEGTA$ solution frozen in aliquots	EGTA	380.4	250	3
	pH adjusted to 7.0 at 20ºC with KOH	$CaCl_2 \cdot 2H_2O$	74.6	250	3
5	Cl_2Na_2MgATP solution frozen in aliquots	Na_2ATP	551.1	50	1
		$MgCl_2 \cdot 6H_2O$	203.3	50	1
Adjust pH to 7 at room temperature.					

Table 5-5 Activating solution

To save time during the week, a solution of components 1 and 2 (refer to Tables 5-4 and 5-5) is prepared on Tuesday morning in a volume large enough to meet the requirements for the week, and kept in the fridge. These components are the same for both the relaxing and activating solutions. 45 ml of this solution is prepared per half day of experimentation, which allows for enough relaxing and activating solutions to perform 2 experiments per day. Then, component 3 is added to approximately 45 ml of the solution containing components 1 and 2. Approximately 20 ml of this solution is used to make the relaxing solution by adding the corresponding components 4 and 5, and another 20 ml is used to make the activation solution by adding the corresponding components 4 and 5. In this way, components 3, 4 and 5 are never older than half a day, which corresponds to the shelf life of ATP at room temperature. The pH of the relaxing and activating solutions are then adjusted to 7 at room temperature. Tables A-6 and A-7 in Appendix A detail how the required volumes of relaxing and activating solutions are prepared each day of the week.

5.3 Excision of the heart

The animal is placed in a plastic box and a mixture of isoflurane and air is fed to the box. When the animal is deeply asleep, its head is cut off using a guillotine. The skin covering the rib cage is cut off, as well as the rib cage in order to expose the heart. The aorta, which is the artery closest to the sternum, is found and clamped so that it can easily be located to perform a retrograde perfusion of the heart.

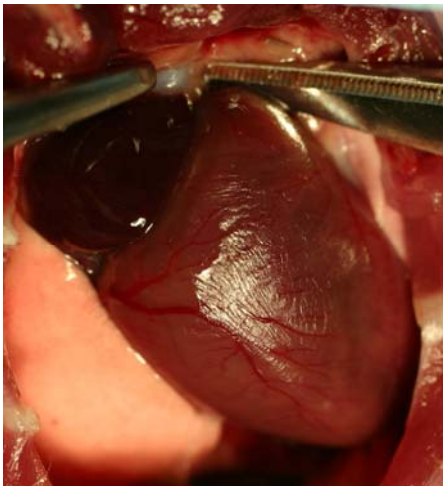

Figure 5-1 Picture of a hamster heart showing the location of the aorta

The veins and arteries coming into and leaving the heart are cut off above the clamp to excise the heart, leaving enough of the aorta to perform the perfusion. The heart is then placed in a small volume of the rigor solution previously prepared and maintained at room temperature, just enough to cover it.

5.4 Perfusion of the heart

The retrograde perfusion of the heart is done to evacuate the blood from the heart as blood contains enzymes that can degrade the muscle tissue. It is performed under a magnifying lamp. The heart is transferred to a Petri dish filled with rigor solution at room temperate. Pins are then inserted through the heart into a layer of silicone elastomer placed at the bottom of the Petri dish to maintain the heart in place. The needle of a syringe filled with rigor solution is then placed into the aorta.

Figure 5-2 Picture of the tools and equipment needed to perfuse a heart

The aorta is kept in place around the needle using tweezers. The plunger is compressed to move the rigor solution through the heart. As a result, the blood leaves the heart and the coronary arteries become invisible.

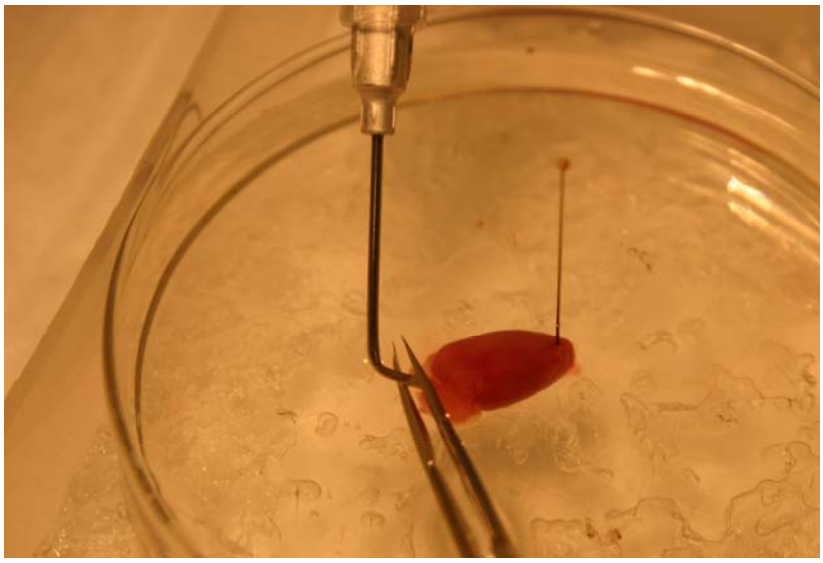

Figure 5-3 Picture showing how the aorta is kept in place around the needle using tweezers

5.5 Dissection of the LV wall

The heart is then transferred to a Petri dish filled with cold storage solution (0-4ºC), and placed on ice. The bottom of the Petri dish is covered with a layer of silicone elastomer to aid in the dissection.

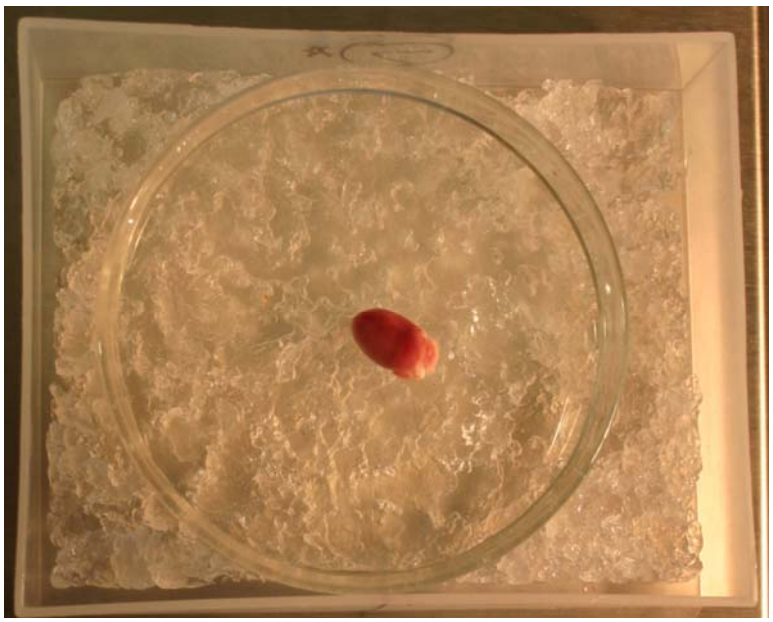

Figure 5-4 Picture of a heart in a Petri dish on ice

The atria are removed first. The RV wall, which can be differentiated from the LV wall because it is thinner, is then cut away from the heart. Pinning the heart down with one or two pins facilitates dissection of the ventricular wall.

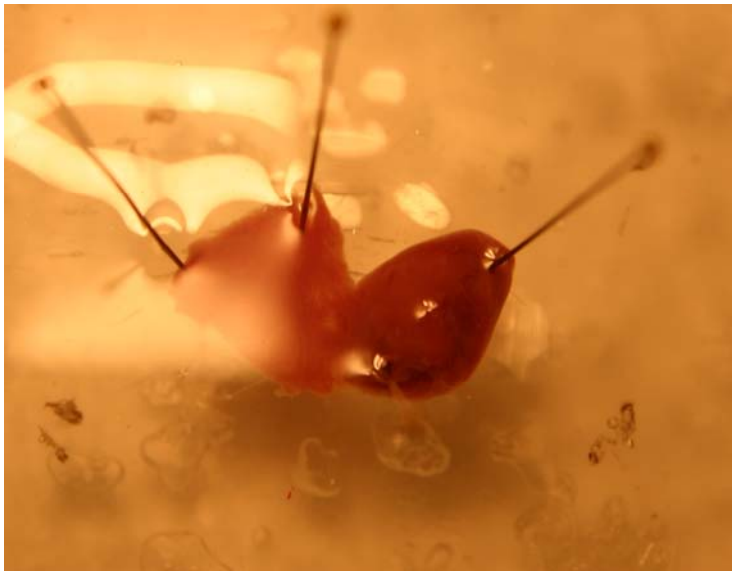

Figure 5-5 Picture showing how the RV is dissected

A cut is then made on one side of the LV wall where it meets the septum. The LV wall, still attached on one side to the septum, and the septum are pinned down so that the inside of the LV cavity is exposed. The 2 papillary muscles, which look like tubular structures extending out from the LV wall, are cut off at the wall.

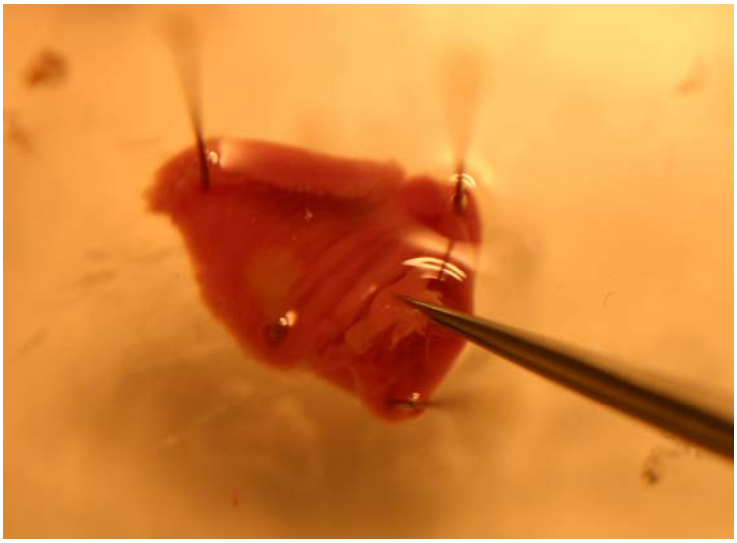

Figure 5-6 Picture showing how the papillary muscles are dissected

The LV wall and septum grouping is then flipped over to see where the LV wall should be separated from the septum.

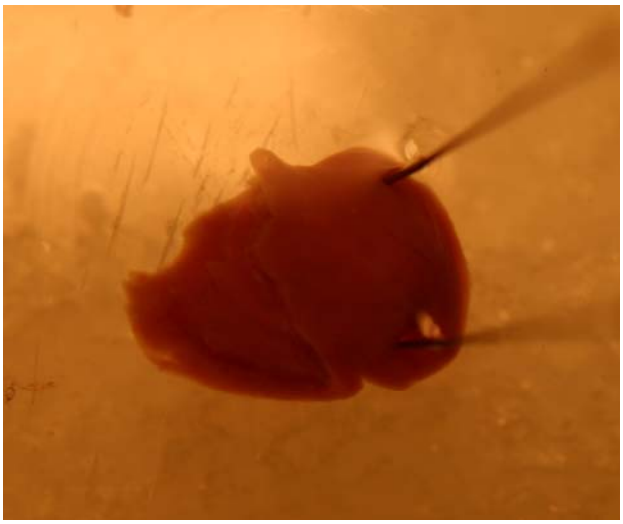

Figure 5-7 Picture showing how the LV is dissected

The LV wall is then cut away from the septum. Thin strips are sliced across the LV wall with a blade starting at the apex and moving up toward the superior portion of the wall. Since the cardiac fibres change direction from the endocardium to the epicardium, it is not possible to follow the direction of the fibres when dissecting the wall.

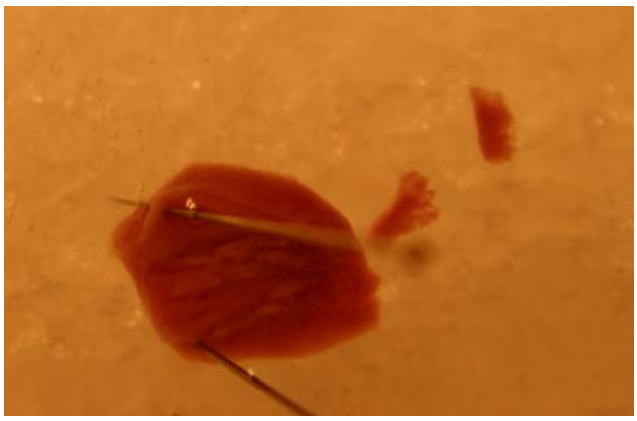

Figure 5-8 Picture showing how the LV is sliced

5.6 Skinning of the LV muscle strips

The muscle strips are then transferred to a plastic receptacle containing some cold skinning solution (0-4ºC), and placed over ice. The muscle strips are pinned at slack length to the silicone elastomer at the bottom of the dish, and remain in the skinning solution for two hours. The container is kept in the fridge over ice for that duration. After two hours, the pinned muscle strips are rinsed three times with the storage solution.

Figure 5-9 Picture showing how the LV strips are skinned and stored

5.7 Preservation of the LV muscle strips

The pinned muscle strips are preserved in storage solution in the fridge over ice for a maximum of 4 days. The storage solution needs to be replaced daily during this period to ensure that the tissue is always exposed to fresh ATP, DTT and protease inhibitors.

5.8 Blending protocol

On the morning of an experiment, some storage solution is prepared with fresh protease inhibitors, DTT and Cl_2Na_2MgATP solution, and its pH is adjusted to 7 at room temperature. Half a muscle strip is homogenized in some of the storage solution at a speed of 24 000 RPM for 7 seconds to separate single myofibrils. Myofibrils from the LV wall do not separate as easily as those from papillary muscles or from some skeletal muscles. However, a few single myofibrils are normally present on the cover slip after the suspension is allowed to settle, even with LV walls of Bio TO-2 hamsters which develop fibrosis.

CHAPTER SIX: PASSIVE PROPERTIES OF DCM AND NORMAL HAMSTER MYOFIBRILS

6.1 Introduction

This study was aimed at comparing the passive mechanical properties of LV experimental myofibrils to those of LV control myofibrils at two time points during the life span of the Bio TO-2 hamster, and at relating the myofibrillar passive mechanical properties to the expression of titin (N2BA:N2B and titin:MHC ratios) in the LVs of the experimental and control hearts. This chapter contains the methodology followed to perform the passive mechanical testing and the results obtained, which were:

1. the peak and steady state passive stress–SL relations,
2. the SL standard deviation-SL relations at peak stress and steady state,
3. the stress decay magnitude-SL relations, and
4. the quadratic coefficient-SL relations for quadratic equations fitted to the stress relaxation curves starting at the end of stretch.

6.2 Methods

6.2.1 Animal age groups

Aged matched male Bio TO-2 and Bio F1B hamsters were euthanized at two different stages of the disease following a protocol approved by the University of Calgary's Animal Care and Ethics Committee. The reproductive system of the Bio TO-2 hamster matures at around 7 weeks of age. The body weight of both strains levels off at 12 to 13 weeks. Sometime between 5 and 15 weeks, the hemodynamic properties of both strains become significantly different (Kawada *et al.*, 2005). At 20 weeks or before, the Bio TO-2 LV wall shows visible dilation and

thinning (Goineau *et al.*, 2001). Between 20 and 26 weeks, an increase in collagen density is detectable. Between 37 and 43 weeks, symptoms of pulmonary congestion and congestive heart failure develop (Kawada *et al.*, 2005;Goineau *et al.*, 2001). The experiments were performed at approximately 17 weeks of age, when the animals are adults and the hemodynamic properties of both strains differ significantly, but before fibrosis develops, and approximately 38 weeks of age, at the beginning of the development of heart failure.

6.2.2 Single myofibril passive mechanical testing

6.2.2.1 Testing setup

The experimental setup and methodology used to perform the mechanical testing of the cardiac myofibrils are detailed elsewhere (Rassier *et al.*, 2003;Joumaa *et al.*, 2007). Approximately 2 ml of the myofibril suspension prepared as described in Chapter 5 is placed into a cover slip chamber on top of an inverted microscope (Zeiss Axiovert 200 M, Germany). The cardiac myofibrils take approximately 30 minutes to settle onto the cover slip. A relaxing solution is then pushed into the chamber through a syringe to flush it and simultaneously removed on the other side of the chamber with a second syringe, thereby removing the majority of the debris. Some relaxing solution is left in the chamber to bath the single myofibrils that remained attached to the cover slip. A great deal of care then needs to be taken to select a single myofibril with a good striation pattern. One end of a myofibril is attached to a glass needle that is fixed to a motor controlled by a computer for stretching. The other end is glued to a silicon-nitride cantilever of known stiffness for force measurements. Light is sent vertically through the myofibril and the associated dark/white (myosin/actin) striation pattern captured for SL determination. The cantilever also changes the light intensity so its deflection induced by passive stretching is also captured.

6.2.2.2 Testing protocol

Each myofibril was subjected to a series of ramp stretches starting at slack length (approximately 1.9 μm). The stretches increased by increments of 0.1 μm/sarcomere up to an average SL of ~2.2 μm, then by increments of 0.2 μm/sarcomere up to a maximum average SL of ~3.0 μm. For each stretch, the following protocol was followed:

1) The myofibril was stretched at a speed of 0.1 μm/sarcomere/second.

2) It was maintained at the final length for 1 minute to reach steady state.

3) It was shortened to its initial length at the same speed.

4) A 5 minute waiting period followed prior to the next stretch to allow the myofibril to return to its initial slack length.

At the end of the passive mechanical testing, the relaxing solution was replaced with an activating solution to verify that the myofibril was viable and could contract.

6.2.3 Data analysis

Two methods were used to record the myofibril striation pattern and the deflection of the cantilever during the myofibril experiments:

1) The light intensity variation along the longitudinal direction of the myofibril was imaged with a linear high-density photodiode array consisting of 10680 individual elements and stored to binary files for future processing. The resolution at a magnification of 250x was 6.7 nm/pixel (unpublished tests, Herzog and Leonard, 2007).

2) Video recordings were created by a camera coupled to a video recorder. The experiments were recorded onto a VHS tape in the highest quality NTSC mode (SP) and then digitized to an AVI format preserving the full resolution. The vertical and horizontal resolutions were

determined using a calibrated slide imaged at a magnification of 250x and were found to be 78 and 71 nm/pixel, respectively.

A custom-built software program was developed by Dr. Appaji Panchangam using Matlab® which accepted the binary files from the photodiode array or the AVI video files as input. The software was used to obtain the following data:

- force-time traces for each stretch from the photodiode array and video files after processing and smoothing of the data as described below,
- measurements of the myofibrils' diameters from the video files,
- measurements of individual SLs from the video files.

The binary files from the photodiode array were parsed into an *n* x 10680 matrix, where *n* was the number of time points. Each row of this matrix represented a line scan of the light intensity variation along the myofibril at a particular time point with successive rows corresponding to the time evolution of the intensity variation along the myofibril. Due to the exposure and read out limitations on the photodiode array, scans were obtained at a frequency of approximately 5 Hz.

The AVI video files were de-interlaced into individual frames of size 720 x 480 containing the light intensity information, which were rasterized for further analysis. The experiments were represented in an *n* x 720 matrix, where *n*, once again, was the number of time points. Successive rows represent the time evolution of the intensity variation along the myofibril at NTSC video rates (approximately 29 frames per second).

The light intensity data from the matrices was then processed further. Each pixel was initially attributed a light intensity number between 0 and 255. A value of zero was then assigned to the average light intensity, which resulted in the dark pixels being assigned a negative intensity value, and the light pixels, a positive one. The negative intensity values were then converted to positive ones, and the positive values, to negative ones. The peak intensity

(local maxima) corresponding to a prominent location on the cantilever was tracked over time by a tracking algorithm in a semi-automated manner. The light intensity data from the video files was interpolated.

Force-time traces were obtained from the photodiode array and video files by multiplying the displacement of the cantilever by its stiffness. The cantilevers used for this study had a stiffness of either 21.5 or 68 nN/μm. For each stretch, the displacement of the cantilever from zero force to peak force was first measured visually on the video recording and a peak force was obtained. Either the force-time trace obtained from the photodiode array or video was selected, depending on which one gave a peak force closest to the one obtained by visually determining the displacement of the cantilever. Force was normalized to myofibril cross-sectional area to obtain stress for comparison across myofibrils. An example of an actual stress-time trace is displayed in Figure 2-7. From the resulting stress-time trace, the peak stress at the end of stretch and the steady-state stress after holding the stretch for 58.5 seconds were determined. This is depicted in Figure 6-1 below. The steady state stress was corrected when the cantilever did not return exactly to its initial position by subtracting the stress after shortening from it. The peak and steady state stresses obtained for each stretch were plotted against the corresponding average SLs, which were determined by measuring the distance from Z-line to Z-line of individual sarcomeres and taking an average. Sarcomeres for which the Z-lines were not visible were not measured. The peak and steady state stress-SL relations obtained for each myofibril, each date corresponding to one myofibril, are reported in sections 6.3.1 and 6.3.3 respectively. For comparison purposes, passive stress-SL relations obtained on rabbit psoas myofibrils during continuous stretches also performed at a speed of 0.1 μm/sarcomere/second are given in Figures 6-11 and 6-12 (Leonard & Herzog, 2010). The SL standard deviation was calculated at the time points corresponding to peak and steady state stresses for each stretch. The SL standard deviation-SL relations are given in sections 6.3.2

and 6.3.4 respectively. The stress decay magnitude was calculated by subtracting the steady state stress from the peak stress. The stress decay magnitudes-SL relations are shown in section 6.3.5. For some of the stretches performed on each myofibril, a quadratic equation was fitted to the section of the stress-time trace starting at the time point corresponding to the peak stress and covering approximately 9 seconds to match approximately the duration of the stress relaxation. The quadratic coefficient-SL relations are displayed in section 6.3.6.

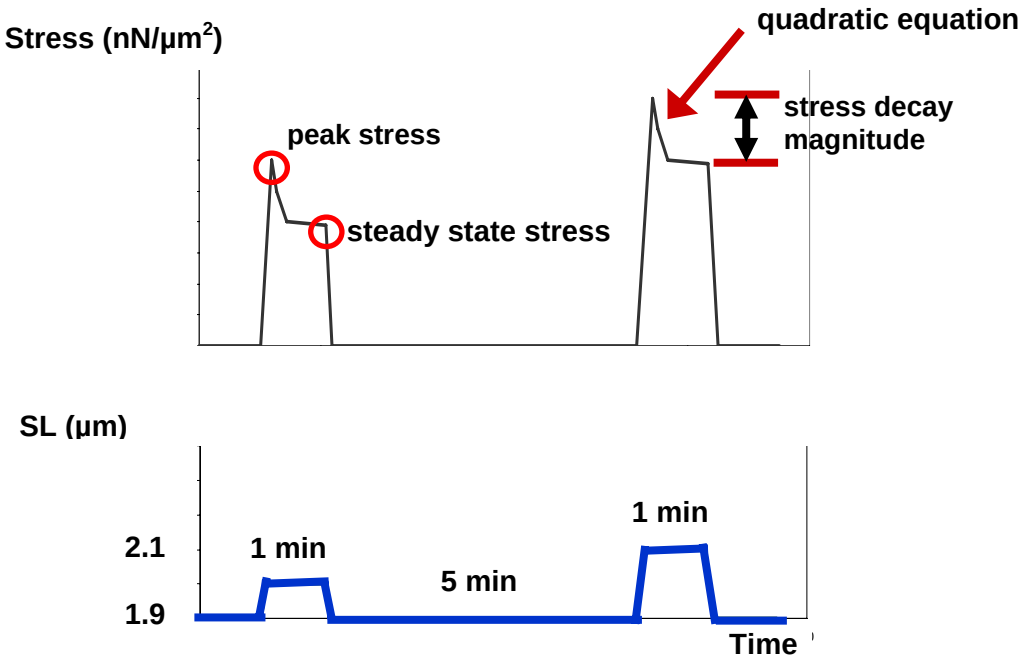

Figure 6-1 Illustration of the stretching protocol and resulting stress-time traces. The location of the peak and steady state stresses are shown on a stress-time trace. The stress decay magnitude is the difference between the peak and steady state stresses. The quadratic coefficient for the decay of stress is obtained from a best fit quadratic equation to the stress-time trace starting at the end of stretch plus approximately 9 seconds.

6.2.4 Statistical analysis

In order to perform the statistical analysis, the passive mechanical properties were binned in SL ranges. The peak and steady state stresses were binned in the following SL ranges: 1.9 to 2.09, 2.1 to 2.19, 2.2 to 2.29, 2.3 to 2.39, 2.4 to 2.49, 2.5 to 2.59, 2.6 to 2.69, and 2.7 to 3.0 µm. The average peak and steady state stress versus average SL relations were then interpolated to obtain values corresponding to SLs of 2.0, 2.1, 2.2, 2.3, 2.4, 2.5, 2.6 and 2.7 µm. The SL standard deviations and magnitudes of stress decay were binned in the following SL ranges: 1.9 to 2.09, 2.1 to 2.29, 2.3 to 2.49, 2.5 to 2.69, and 2.7 to 2.99 µm. For the stress decay quadratic coefficients, only the SL bins ranging from 2.3 to 2.39 µm and 2.4 to 2.49 µm were analyzed. The SL standard deviation, magnitude of stress decay and quadratic coefficient versus SL relations were not interpolated. But as shown below in figures 6-14, 6-18, 6-32, 6-36, 6-41, 6-45 and 6-49, lines fitted through the averaged control and experimental data overlap. If there were more than one value in a bin for a myofibril, the values were averaged so that the myofibrils were weighed equally. Not all of the bins had at least one value per myofibril.

For the majority of the data, ANCOVA parametric analysis was used to compare the passive mechanical properties of the two animal and two age groups (17 (n=3) and 38 (n=9) week old experimental myofibrils, and 17 (n=6) and 38 (n=8) week old control myofibrils). The covariate used at each SL (or SL bin) was the value of the passive mechanical property at the preceding smaller SL. 2-way ANOVA parametric analysis was performed to compare the passive mechanical properties at the shortest SLs, and at the SLs at which the use of an ANCOVA analysis was found to be inappropriate. Mann Whitney-U non-parametric testing was also carried out for comparisons between groups with low sample sizes. A significance level of $\alpha=0.05$ was used for all statistical tests.

6.3 Passive behaviour results

6.3.1 Peak stresses

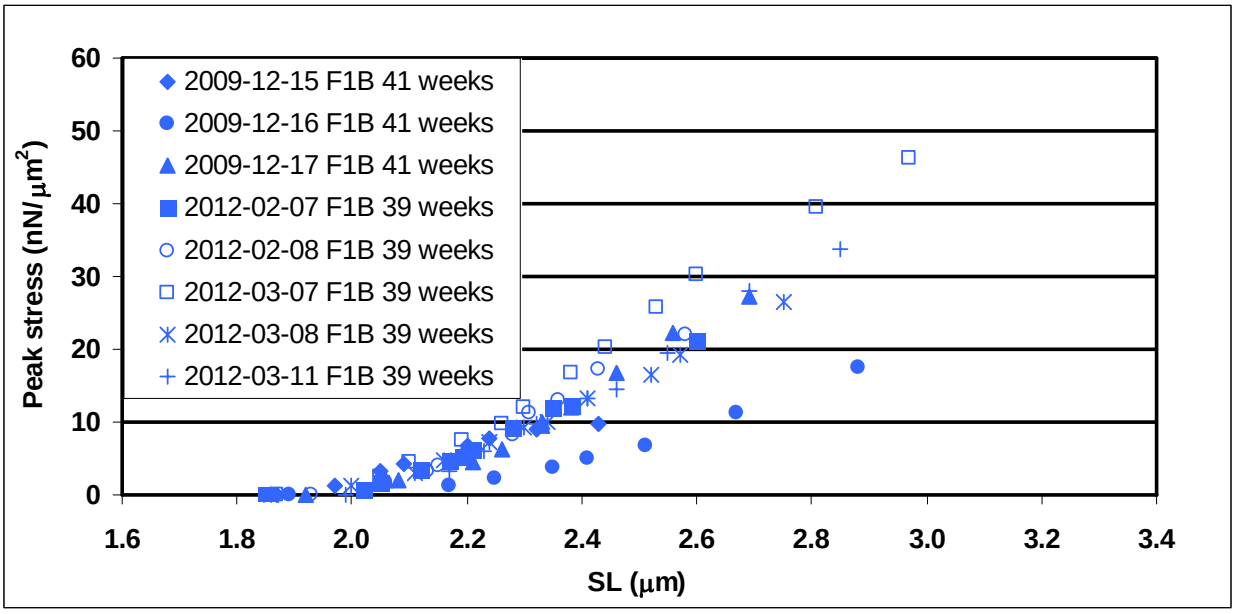

Figure 6-2 Peak passive stress-SL relations for control myofibrils at 38 weeks of age

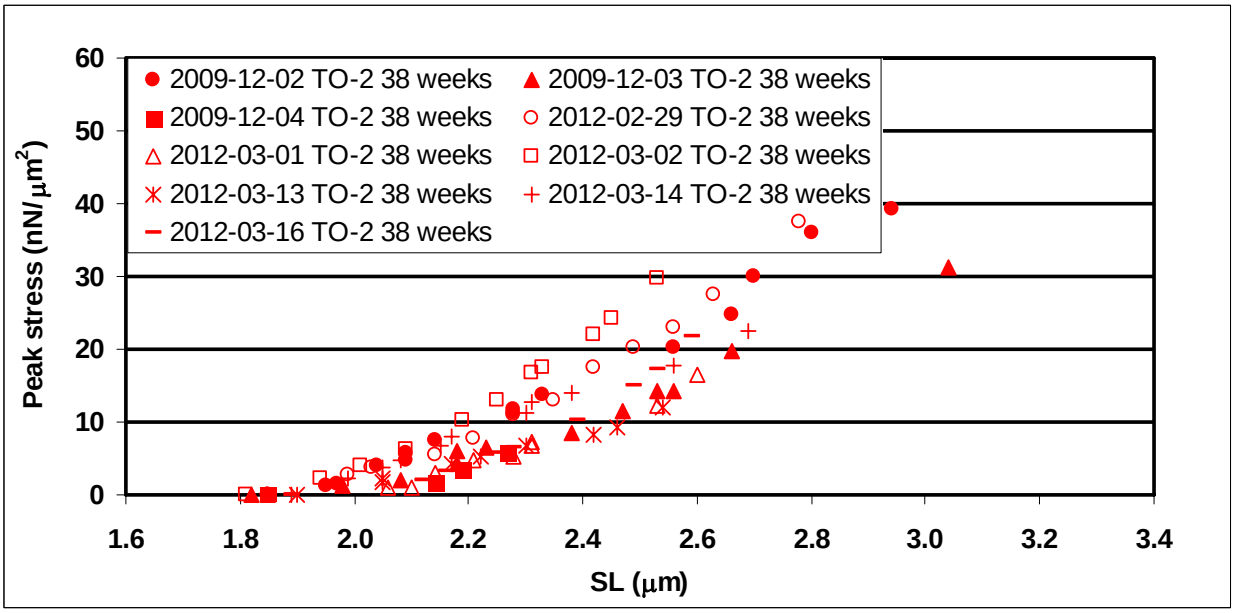

Figure 6-3 Peak passive stress-SL relations for experimental myofibrils at 38 weeks of age

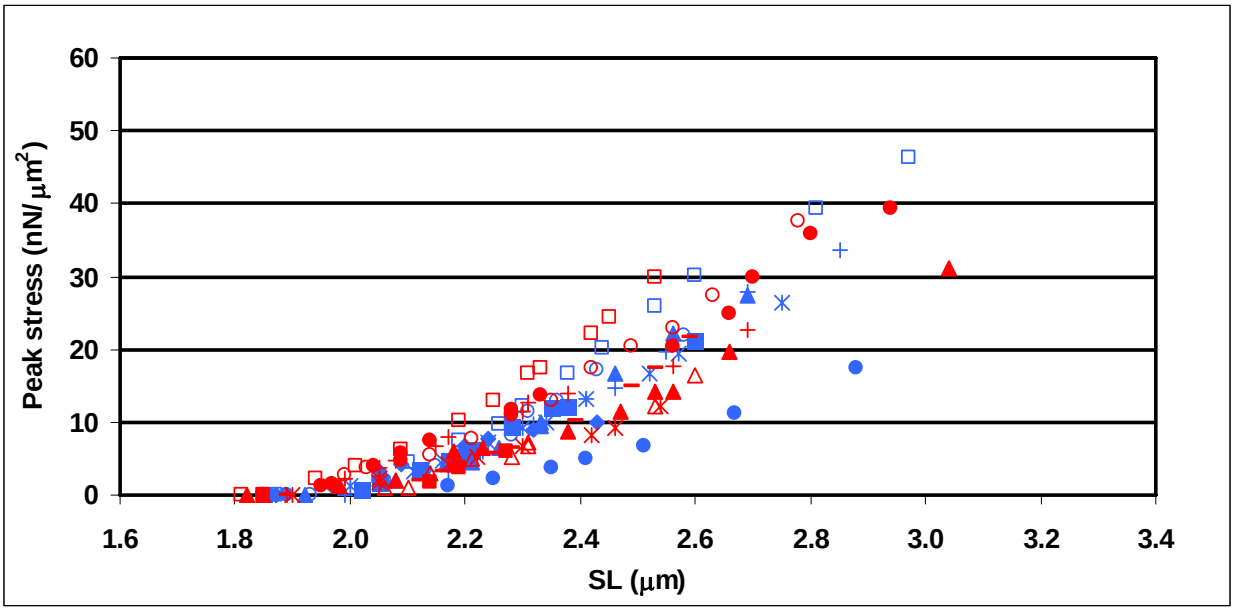

Figure 6-4 Peak passive stress-SL relations at 38 weeks of age (blue: control myofibrils, n=8; red: experimental myofibrils, n=9)

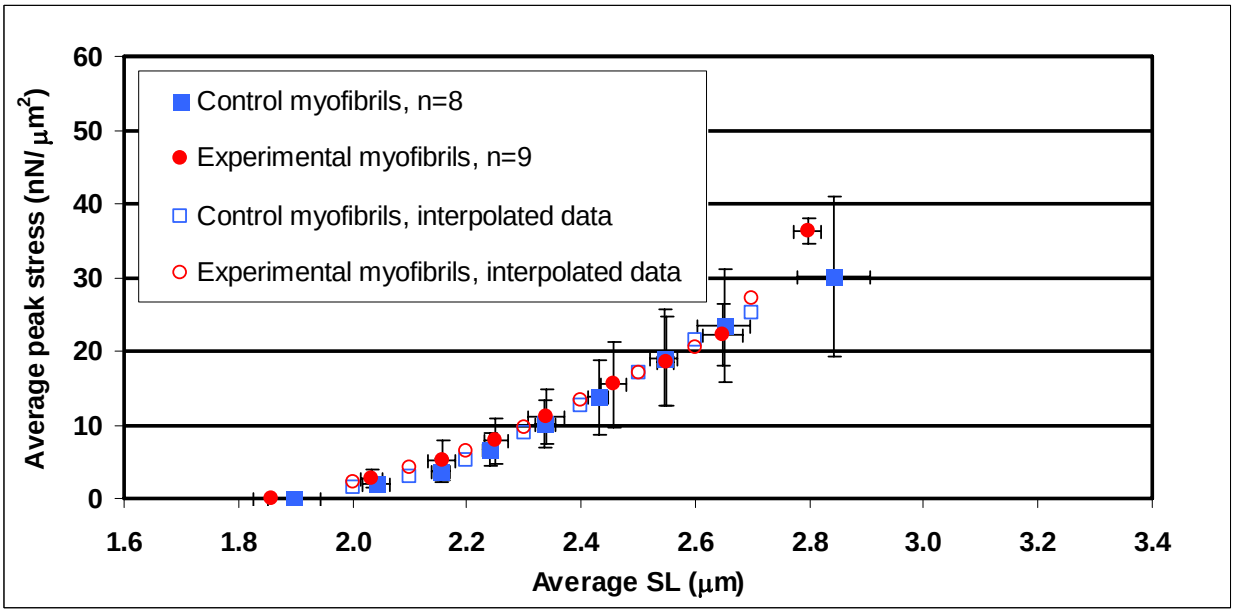

Figure 6-5 Average and interpolated peak passive stress-average SL relations at 38 weeks of age (vertical and horizontal lines correspond to standard deviations)

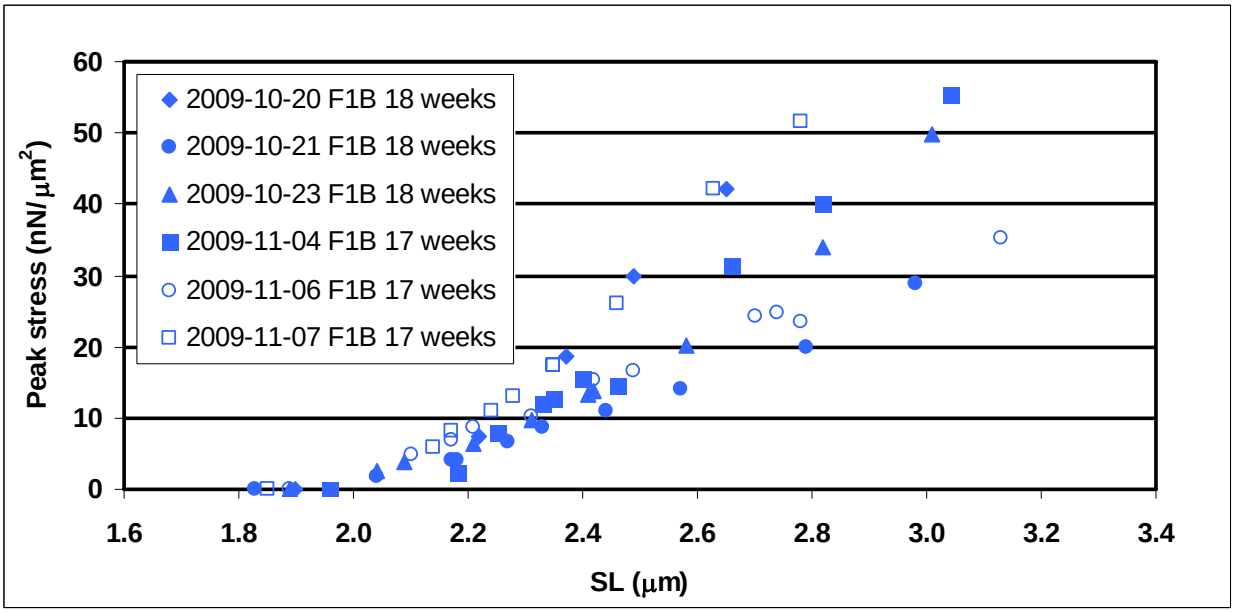

Figure 6-6 Peak passive stress-SL relations for control myofibrils at 17 weeks of age

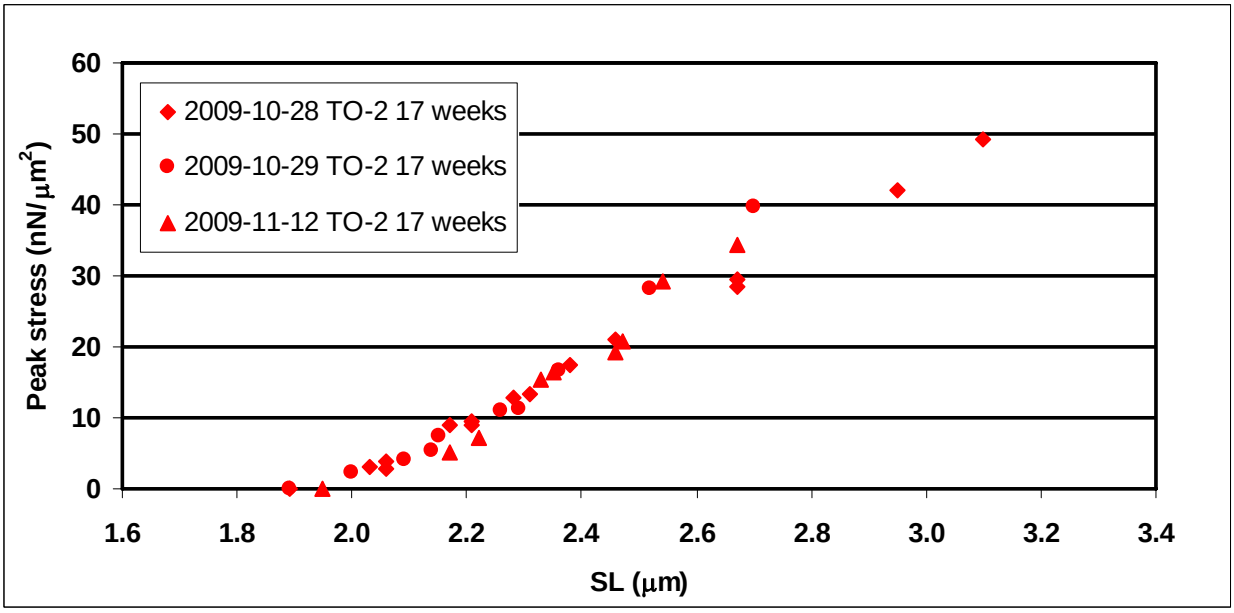

Figure 6-7 Peak passive stress-SL relations for experimental myofibrils at 17 weeks of age

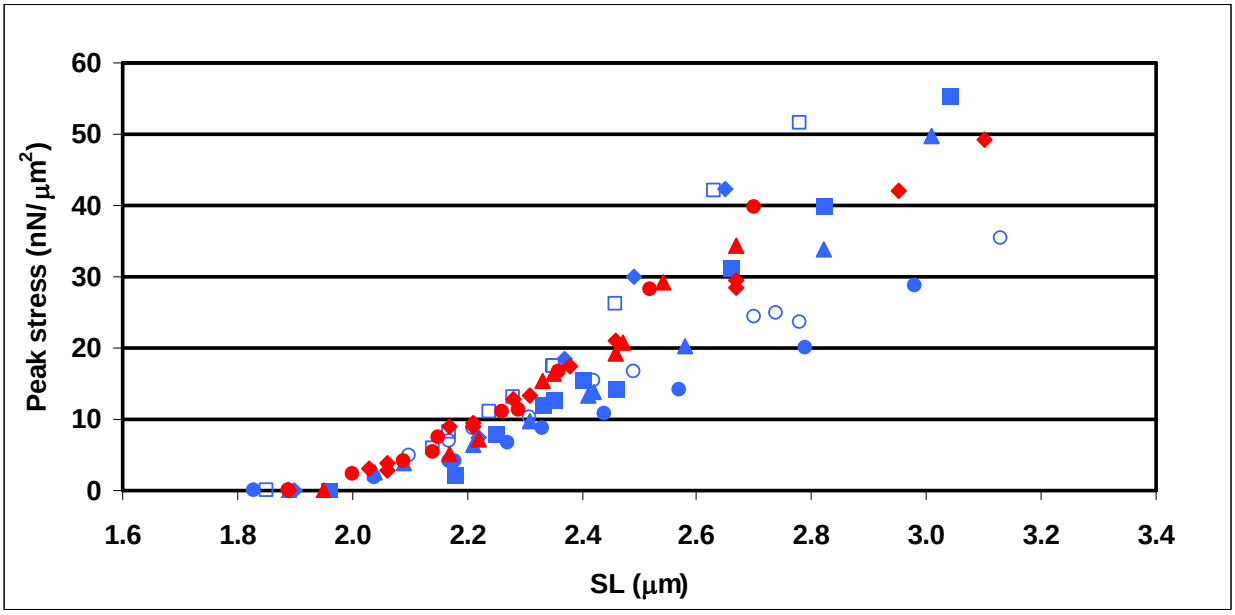

Figure 6-8 Peak passive stress-SL relations at 17 weeks of age (blue: control myofibrils, n=6; red: experimental myofibrils, n=3)

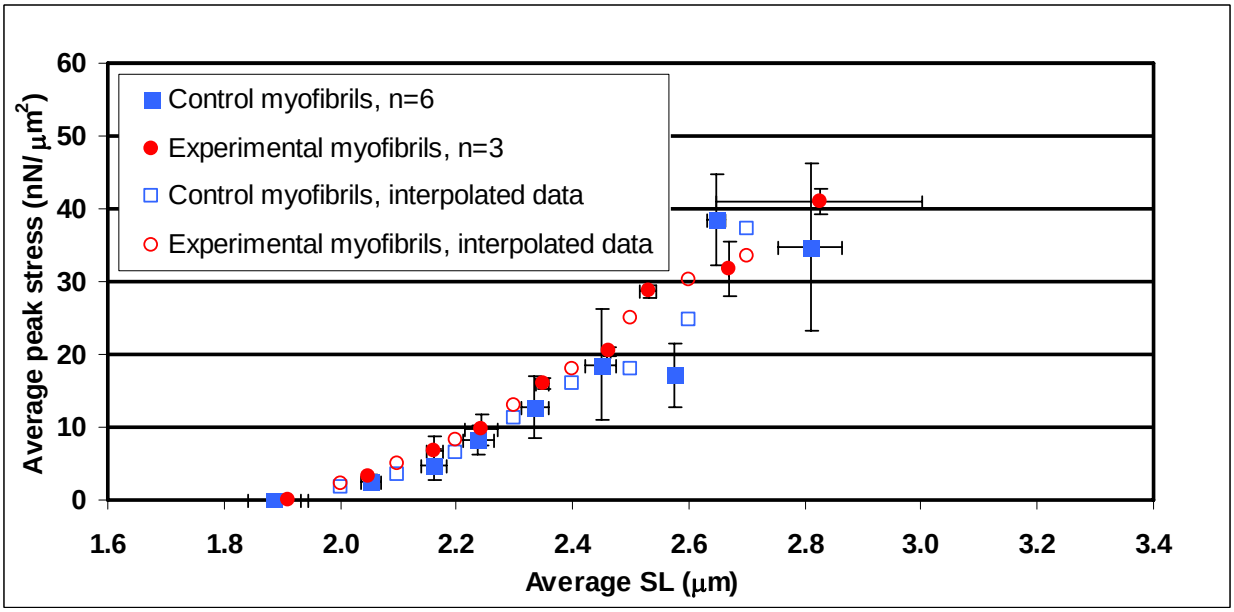

Figure 6-9 Average and interpolated peak passive stress-SL relations at 17 weeks of age (vertical and horizontal lines correspond to standard deviations)

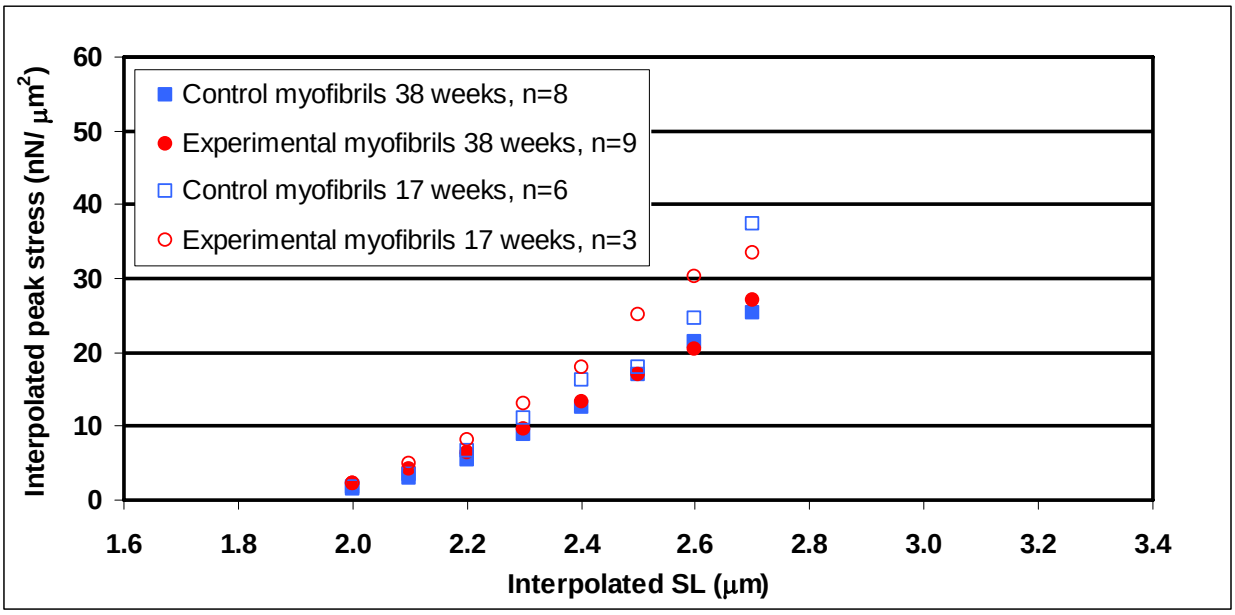

Figure 6-10 Interpolated peak passive stress-SL relations

The appropriateness of performing an ANCOVA analysis was tested at all SLs greater than 2.0 μm. Only at a SL of 2.3 μm was the ANCOVA analysis found to be inapplicable. Using ANCOVA parametric tests, statistically significant interaction effects were found at SLs of 2.1 and 2.2 μm. The estimated marginal mean peak stress, or the mean peak stress adjusted for the covariate, decreased with age for the experimental myofibrils, but increased with age for the control myofibrils at these two SLs. Furthermore, at a SL of 2.1 μm only, the following animal group and age statistically significant differences were found: the adjusted mean peak stress of the 17 week old experimental myofibrils was found to be greater than the one of the 17 week old control myofibrils, and the adjusted mean peak stress of the 17 week old experimental myofibrils was found to be greater than the one of the 38 week old experimental myofibrils.

At a SL of 2.3 μm, a statistically significant age effect was found using a 2-way ANOVA parametric test. However, no statistically significant age difference was found between the peak

stresses of the 17 and 38 week old experimental myofibrils and between the 17 and 38 week old control myofibrils due to the smaller group sizes.

Using Mann Whitney-U non-parametric tests for comparisons between groups with low sample sizes, a statistically significant age effect was found at a SL of 2.6 μm only. The peak stresses of the 17 week old experimental myofibrils were found to be greater than those of the 38 week old experimental myofibrils.

Therefore, statistically significant differences were found between the adjusted mean peak stresses of the 17 week old experimental and control myofibrils at a SL of 2.1 μm, the adjusted mean peak stresses of 17 and 38 week old experimental myofibrils at a SL of 2.1, and the mean peak stresses of 17 and 38 week old experimental myofibrils at a SL of 2.6 μm.

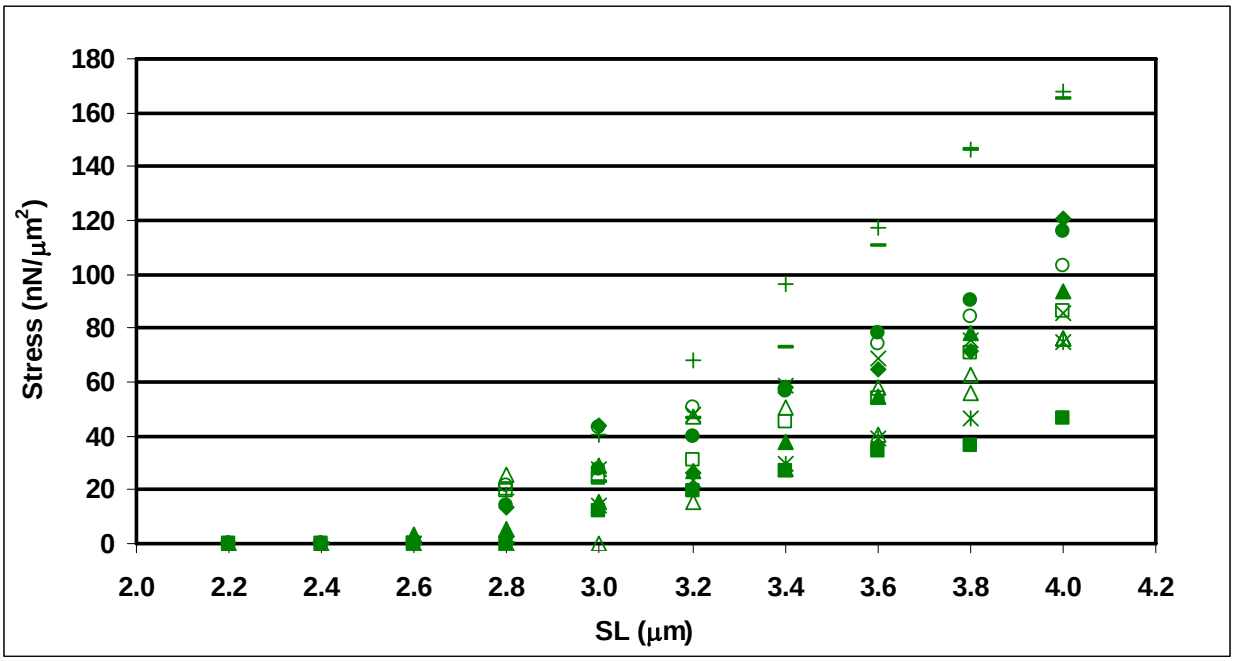

Figure 6-11 Passive stress-SL relations of rabbit psoas myofibrils (Leonard & Herzog, 2010)

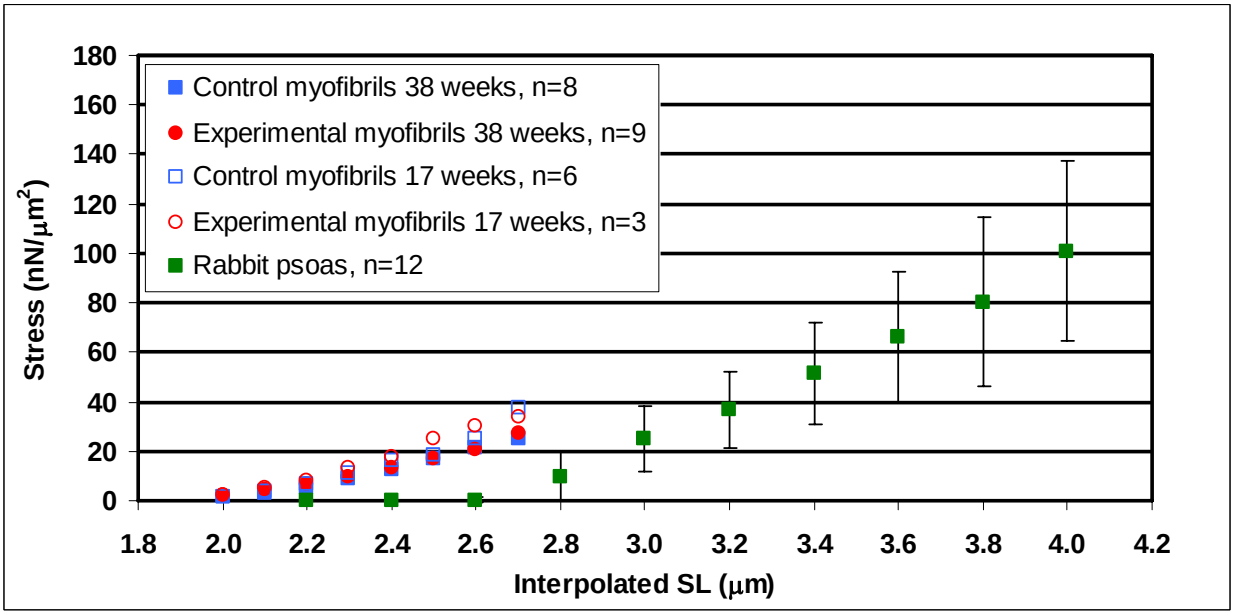

Figure 6-12 Interpolated peak passive stress-SL relations of control Bio F1B and experimental Bio TO-2 hamsters myofibrils at 38 and 17 weeks, and passive stress-SL relations of rabbit psoas myofibrils (vertical lines correspond to standard deviations)

6.3.2 SL standard deviations at peak stress

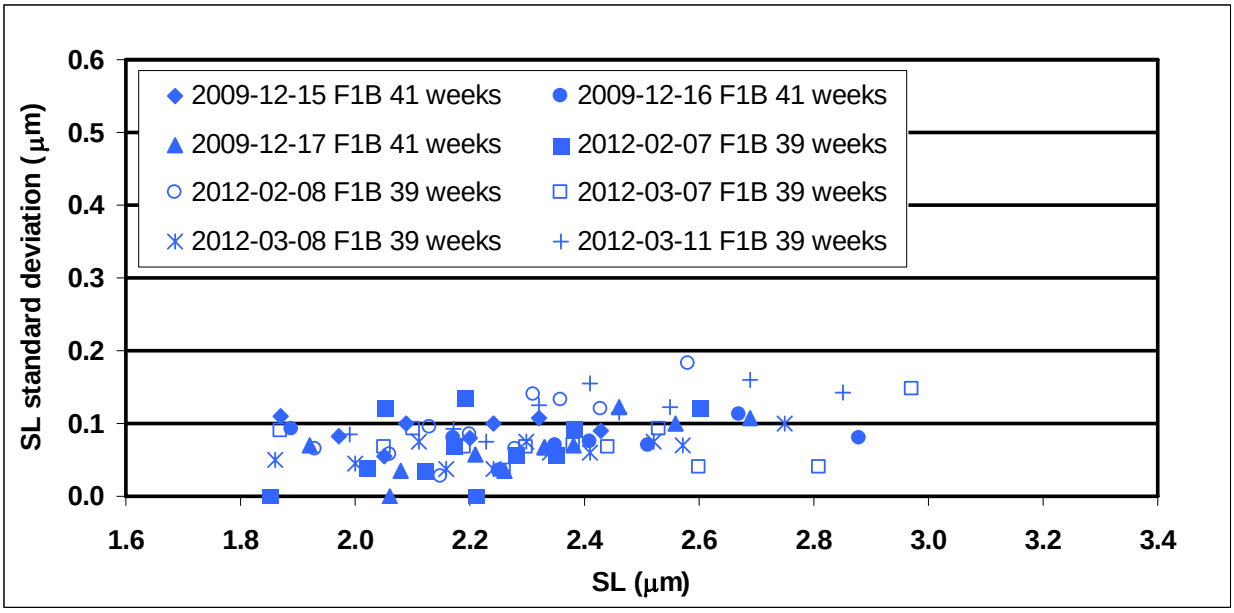

Figure 6-13 SL standard deviation-SL relations at peak stress and 38 weeks of age, for control myofibrils

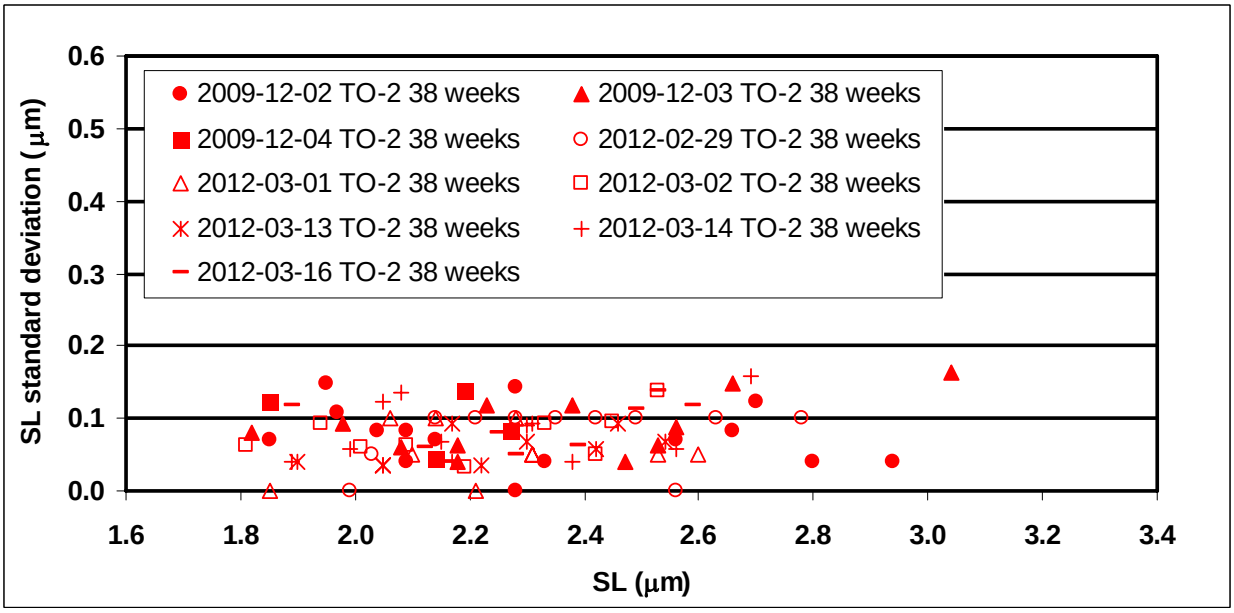

Figure 6-14 SL standard deviation-SL relations at peak stress and 38 weeks of age, for experimental myofibrils

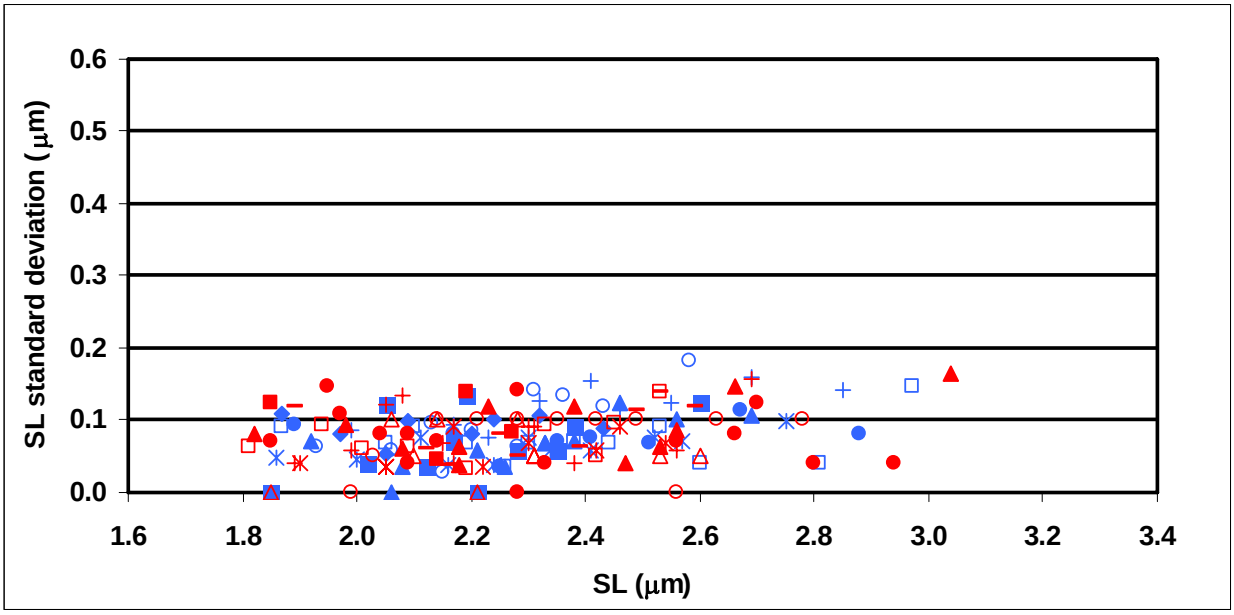

Figure 6-15 SL standard deviation-SL relations at peak stress and 38 weeks of age (blue: control myofibrils, n=8; red: experimental myofibrils, n=9)

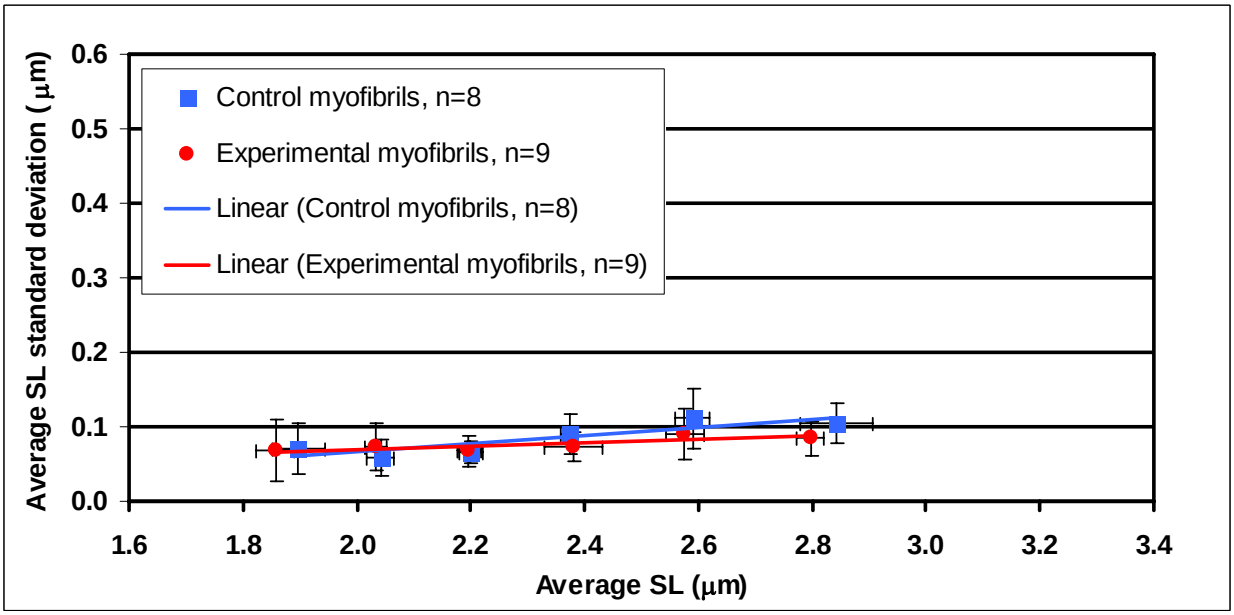

Figure 6-16 Average SL standard deviation-average SL relations at peak stress and 38 weeks of age (vertical and horizontal lines correspond to standard deviations)

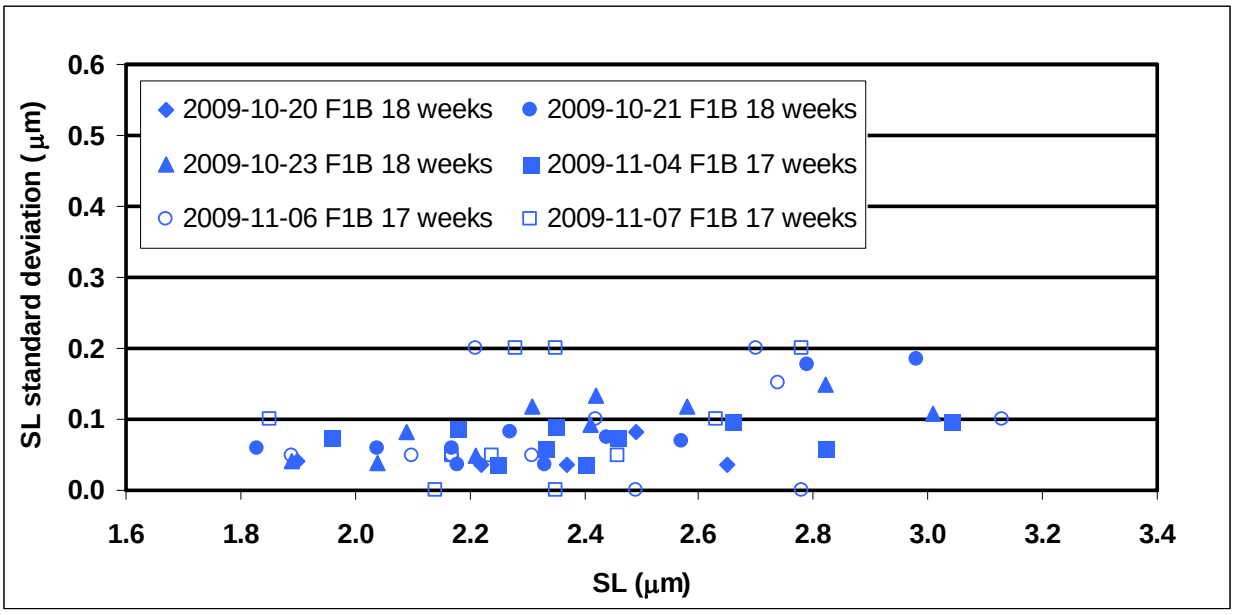

Figure 6-17 SL standard deviation-SL relations at peak stress and 17 weeks of age, for control myofibrils

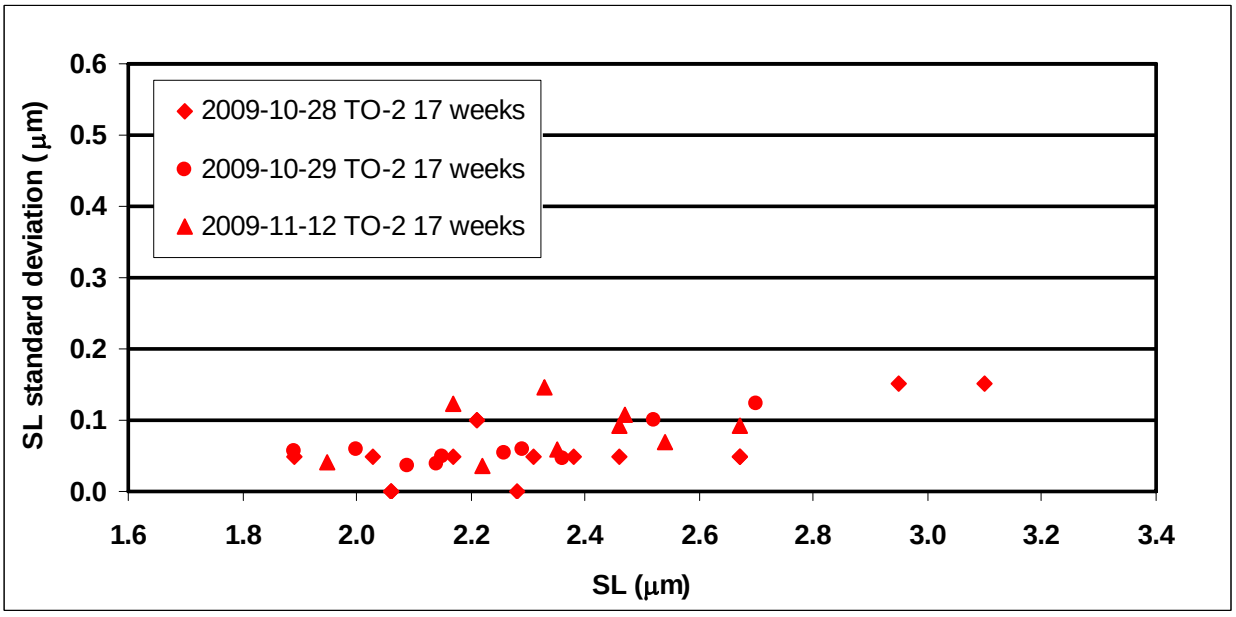

Figure 6-18 SL standard deviation-SL relations at peak stress and 17 weeks of age, for experimental myofibrils

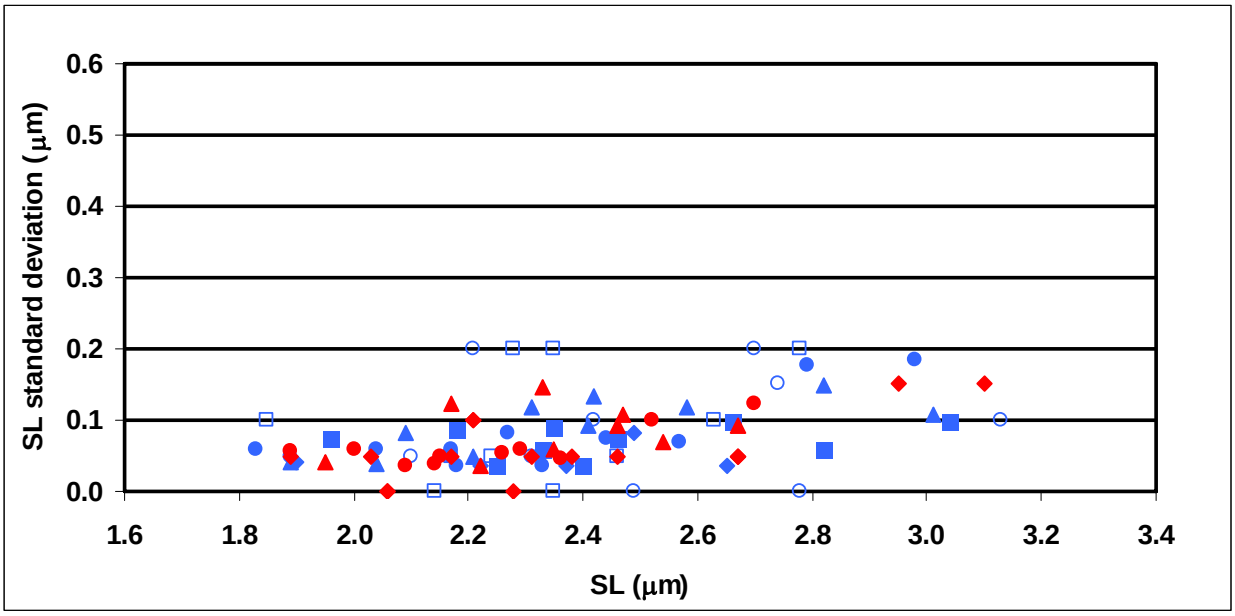

Figure 6-19 SL standard deviation-SL relations at peak stress and 17 weeks of age (blue: control myofibrils, n=6; red: experimental myofibrils, n=3)

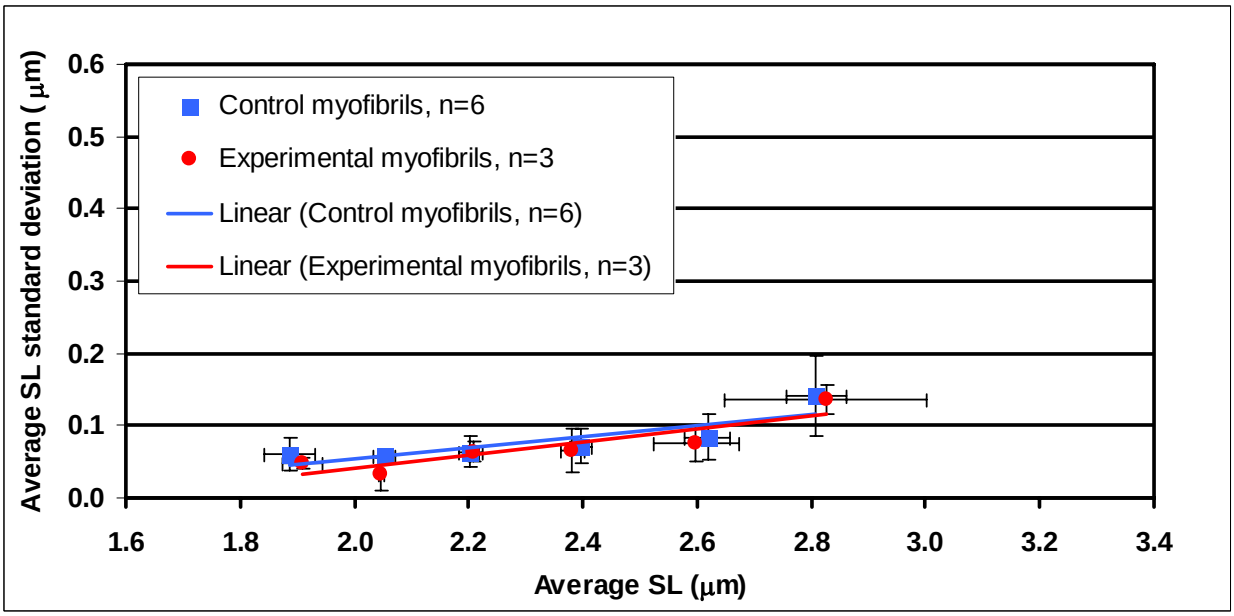

Figure 6-20 Average SL standard deviation-average SL relations at peak stress and 17 weeks of age (vertical and horizontal lines correspond to standard deviations)

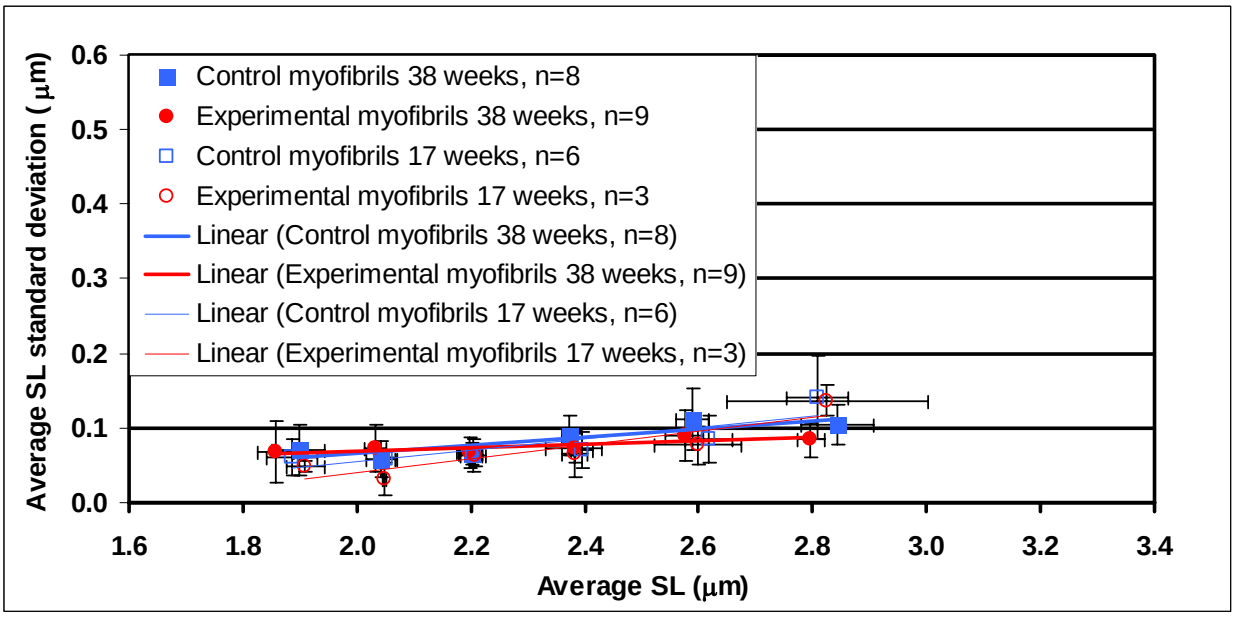

Figure 6-21 Average SL standard deviation-average SL relations at peak stress (vertical and horizontal lines correspond to standard deviations)

The appropriateness of performing an ANCOVA analysis was tested for all SL bins greater than the one ranging from 1.9 to 2.1 μm. Only at the SL bin ranging from 2.3 to 2.5 μm was an ANCOVA analysis found to be inapplicable. Using ANCOVA and 2-way ANOVA parametric analysis when applicable, and Mann Whitney-U non-parametric tests for comparisons between groups with low sample sizes, no statistically significant difference was found between the adjusted mean and mean SL standard deviations at peak stress of the myofibrils from the two animal and two age groups.

6.3.3 Steady state stresses

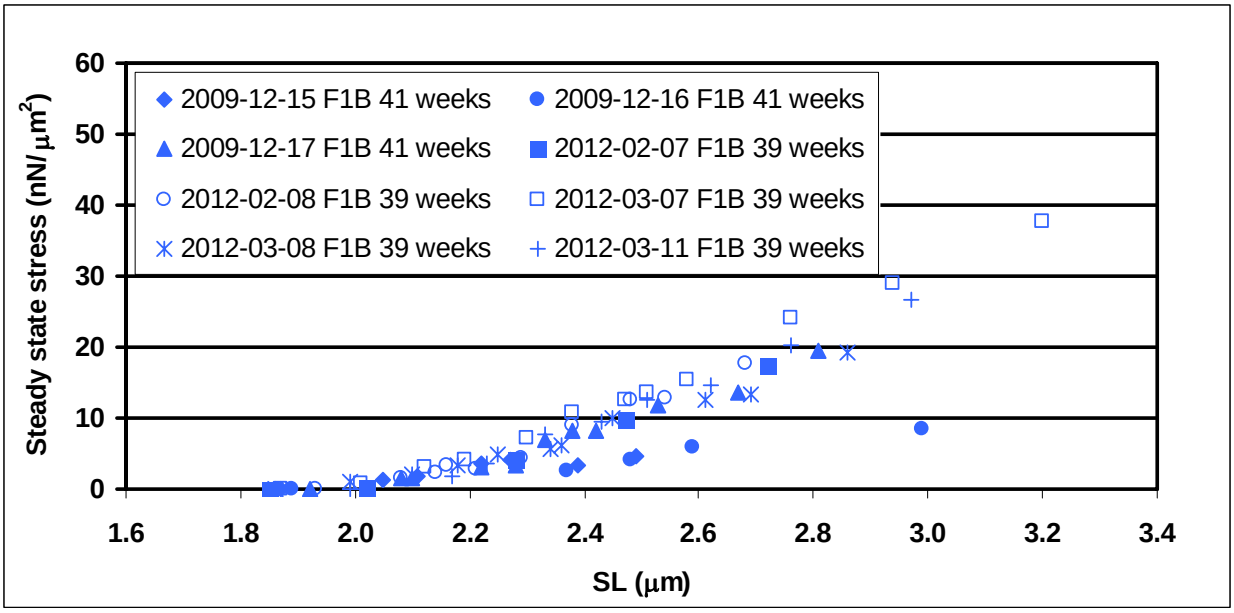

Figure 6-22 Steady state passive stress-SL relations for control myofibrils at 38 weeks of age

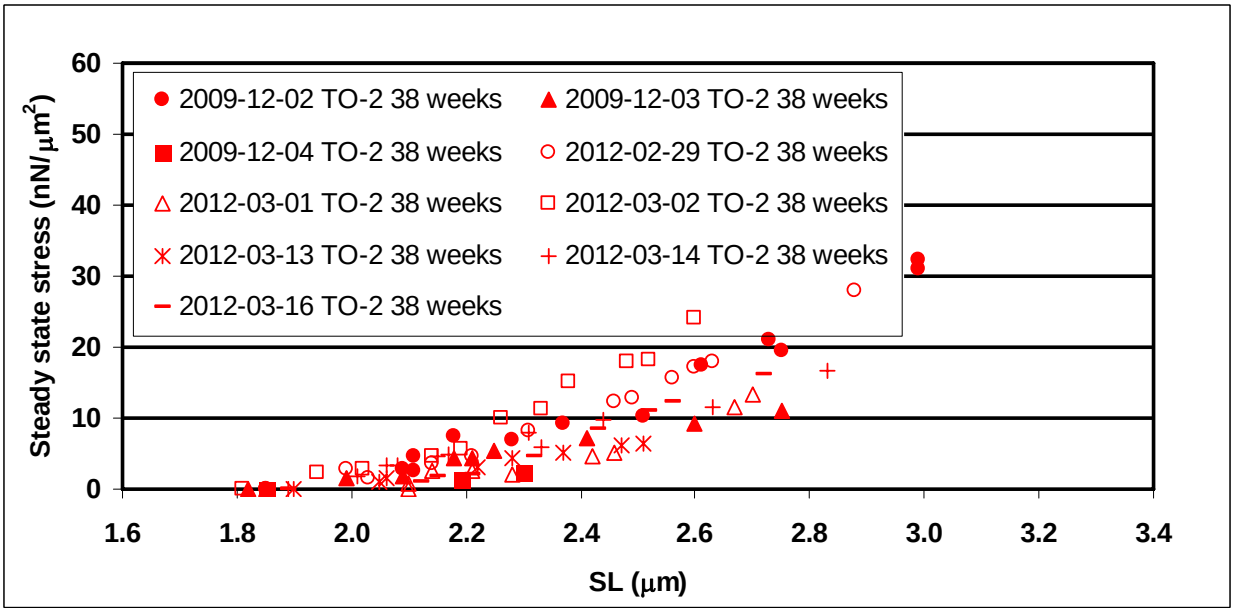

Figure 6-23 Steady state passive stress-SL relations for experimental myofibrils at 38 weeks of age

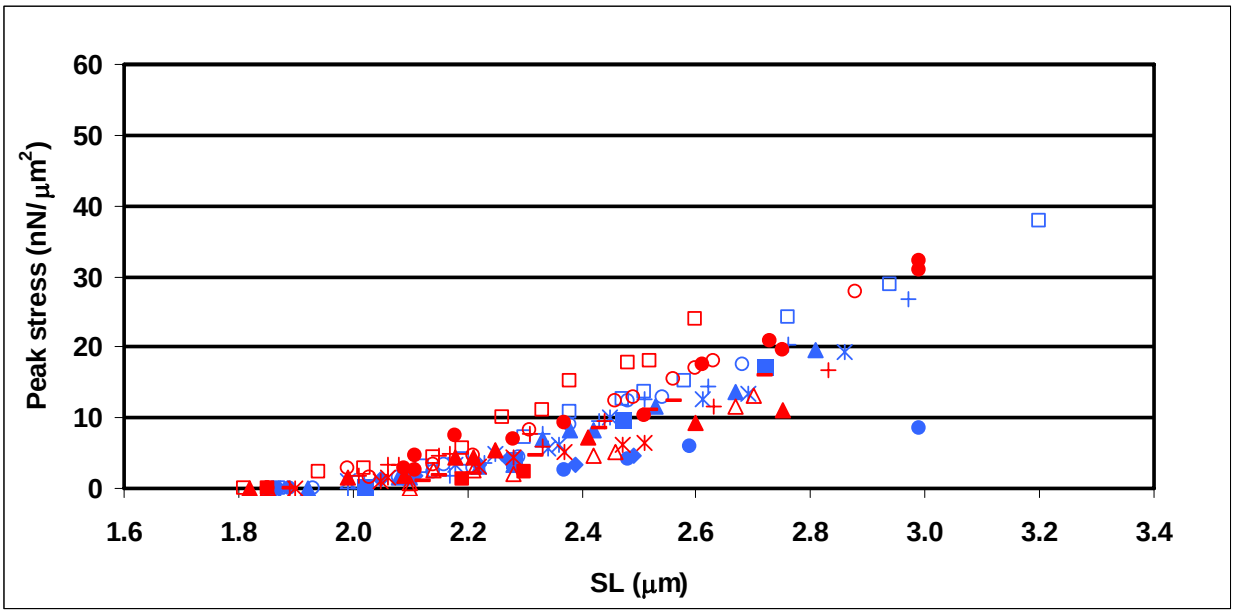

Figure 6-24 Steady state passive stress-SL relations at 38 weeks of age (blue: control myofibrils, n=8; red: experimental myofibrils, n=9)

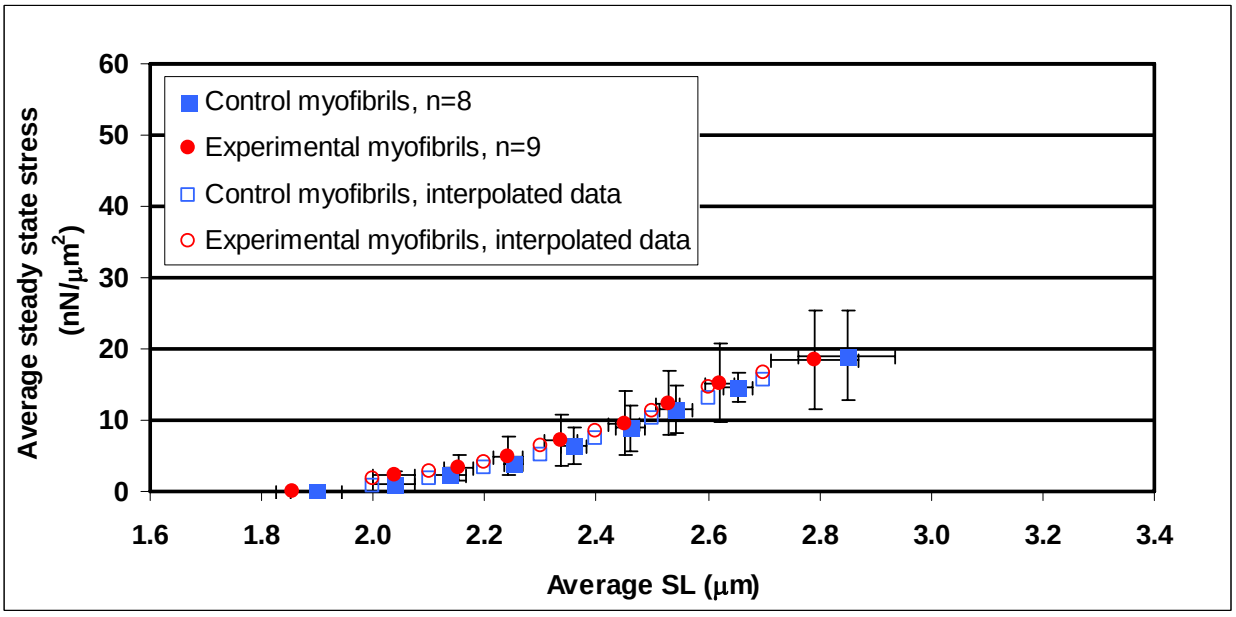

Figure 6-25 Average and interpolated steady state passive stress-SL relations at 38 weeks of age (vertical and horizontal lines correspond to standard deviations)

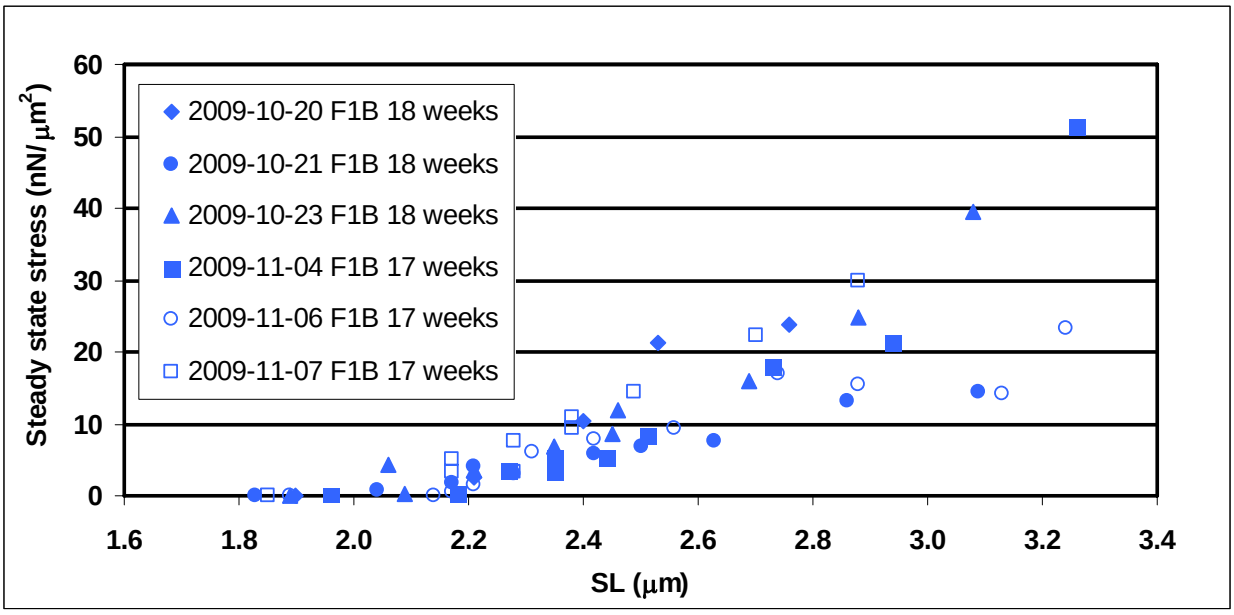

Figure 6-26 Steady state passive stress-SL relations for control myofibrils at 17 weeks of age

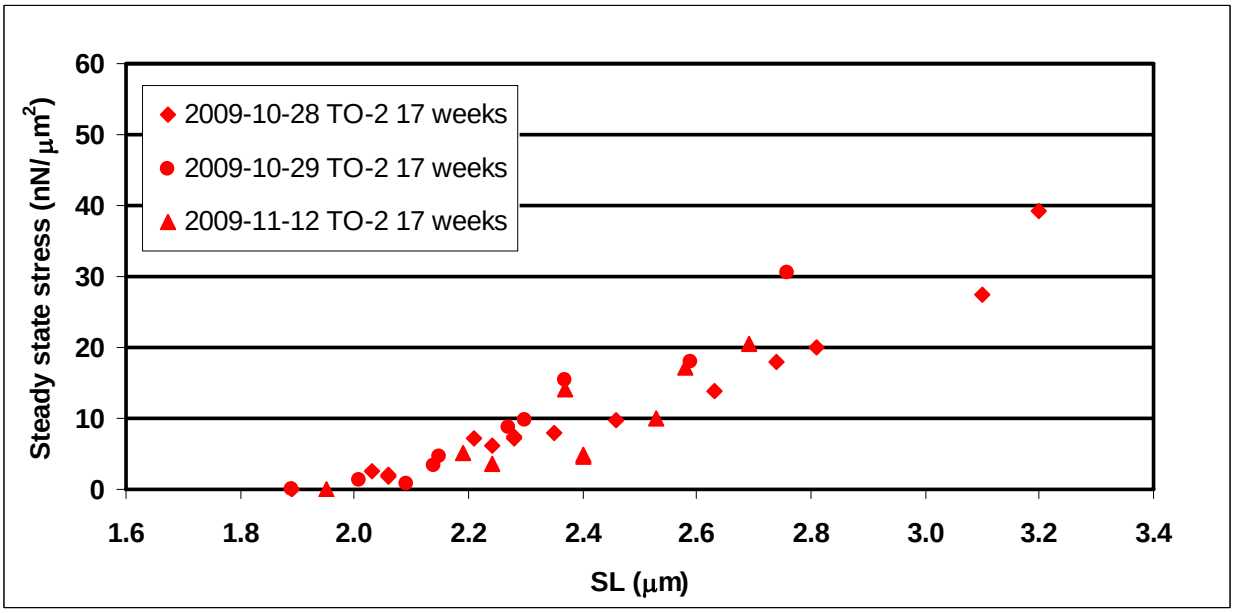

Figure 6-27 Steady state passive stress-SL relations for experimental myofibrils at 17 weeks of age

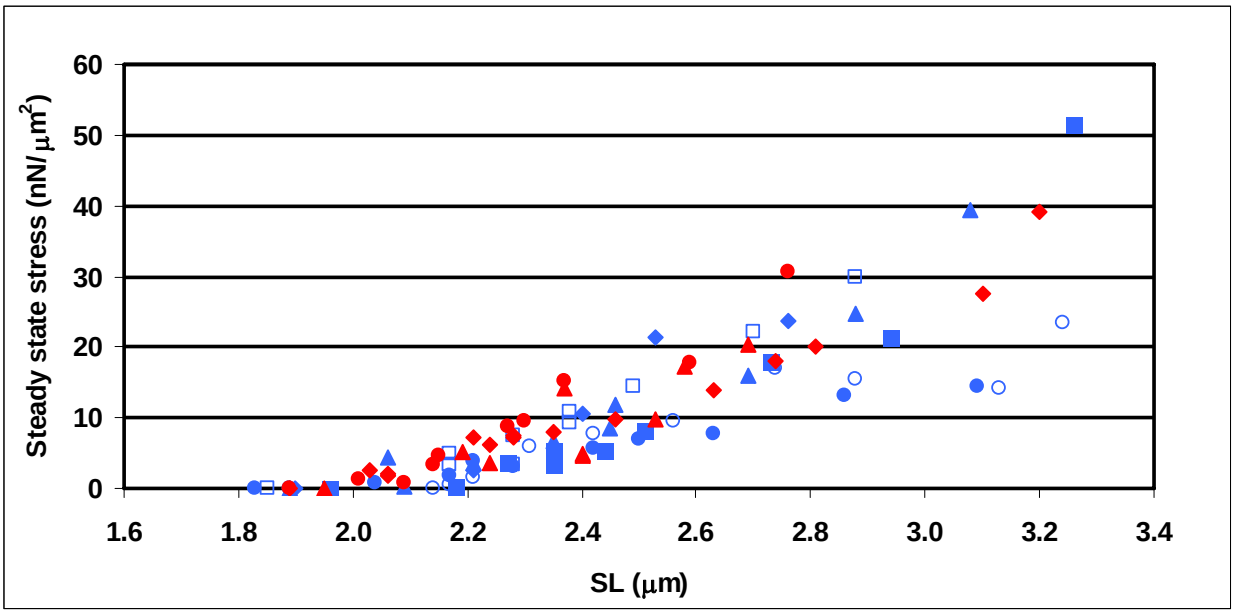

Figure 6-28 Steady state passive stress-SL relations at 17 weeks of age (blue: control myofibrils, n=6; red: experimental myofibrils, n=3)

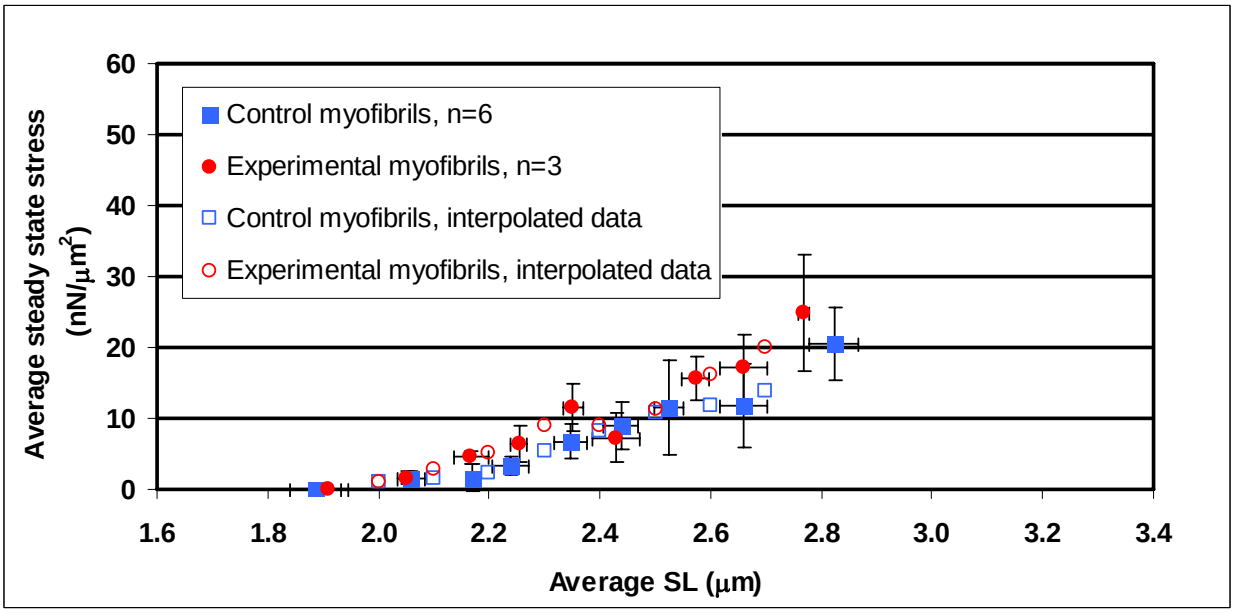

Figure 6-29 Average and interpolated steady state passive stress-SL relations at 17 weeks of age (vertical and horizontal lines correspond to standard deviations)

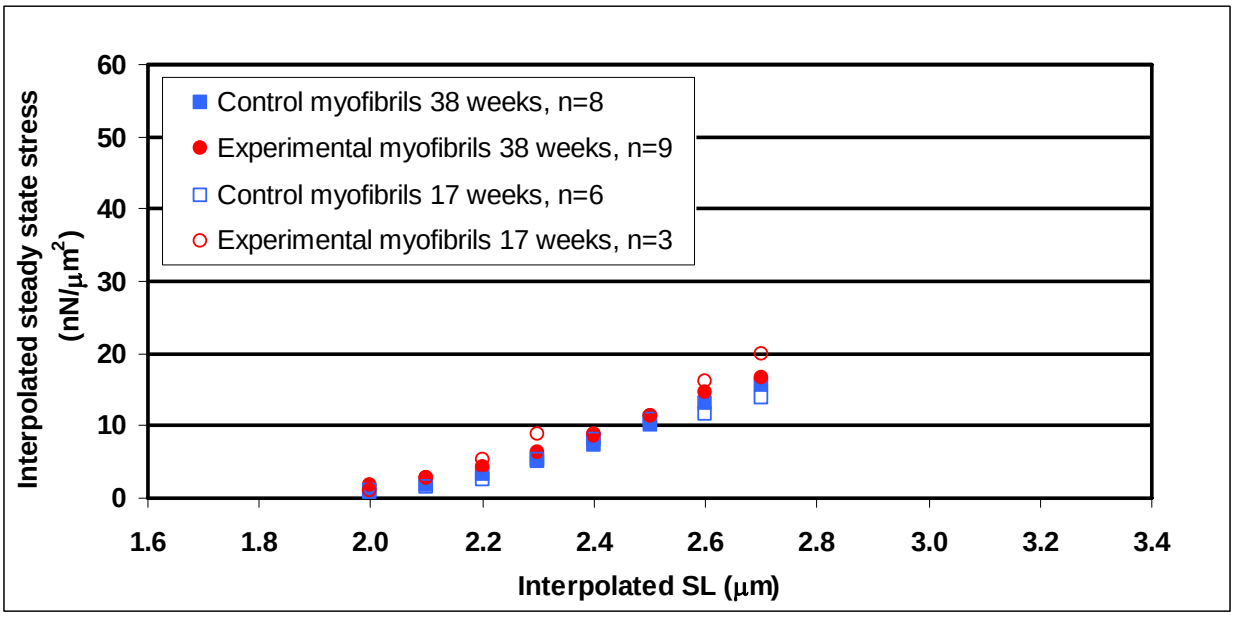

Figure 6-30 Interpolated steady state passive stress-SL relations

The appropriateness of performing an ANCOVA analysis was tested at all SLs greater than 2.0 μm. An ANCOVA analysis was found to be inapplicable at SLs of 2.2, 2.5 and 2.7 μm. Using ANCOVA parametric tests, statistically significant interaction effects were found at SLs of 2.1 and 2.4 μm. At a SL of 2.1 μm, the adjusted mean steady state stress decreased with age for the experimental myofibrils, but increased with age for the control myofibrils. Furthermore, the following animal group and age statistically significant differences were found at this SL: the adjusted mean steady state stress of the 17 week old experimental myofibrils was found to be greater than the one of the 17 week old control myofibrils, the adjusted mean steady state stress of the 17 week old experimental myofibrils was found to be greater than the one of the 38 week old experimental myofibrils, and the adjusted mean steady state stress of the 17 week old control myofibrils was found to be smaller than the one of the 38 week old control myofibrils. At a SL of 2.4 μm, the adjusted mean steady state stress increased with age for the experimental myofibrils, but decreased with age for the control myofibrils. Moreover, the following animal

group and age statistically significant differences were found at this SL: the adjusted mean steady state stress of the 17 week old experimental myofibrils was found to be smaller than the one of the 17 week old control myofibrils, and the adjusted mean steady state stress of the 17 week old experimental myofibrils was found to be smaller than the one of the 38 week old experimental myofibrils.

Using a 2-way ANOVA parametric test and a Mann Whitney-U non-parametric test, a statistically significant animal group effect was found at a SL of 2.2 μm. The steady state stresses of the 17 week old experimental myofibrils were found to be greater than those of the 17 week old control myofibrils. Using a Mann Whitney-U non-parametric test, a statistically significant animal group effect was also found at a SL of 2.3 μm, again the steady state stresses of the 17 week old experimental myofibrils were found to be greater than those of the 17 week old control myofibrils.

Therefore, statistically significant differences were found between the adjusted mean steady state stresses of the 17 week old experimental and control myofibrils at SLs of 2.1, 2.3 and 2.4 μm, the mean steady state stresses of the 17 week old experimental and control myofibrils at a SL of 2.2 μm, the adjusted mean steady state stresses of the 17 and 38 week old experimental myofibrils at SLs of 2.1 and 2.4 μm, and the adjusted mean steady state stresses of the 17 and 38 week old control myofibrils at a SL of 2.1 μm.

6.3.4 SL standard deviations at steady state

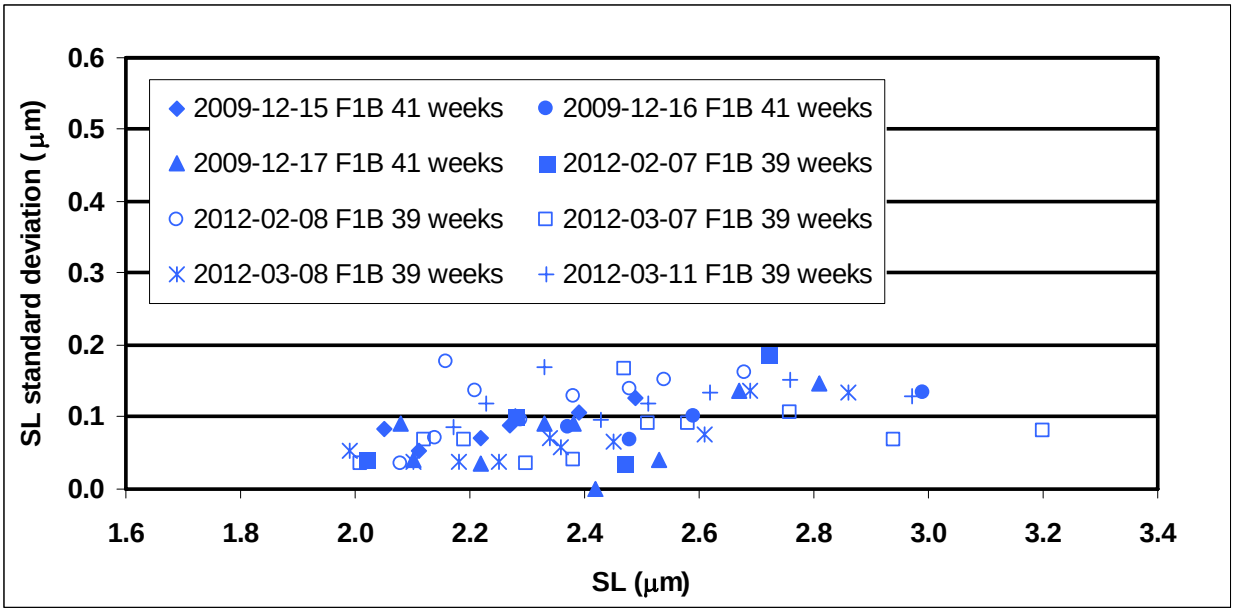

Figure 6-31 SL standard deviation-SL relations at steady state and 38 weeks of age, for control myofibrils

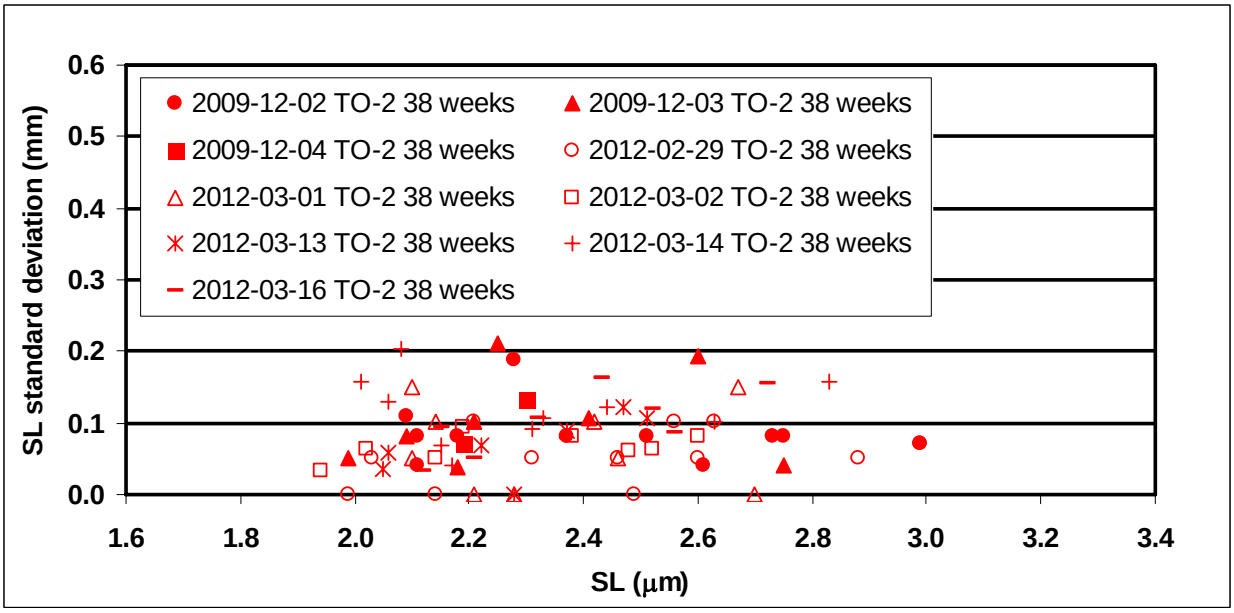

Figure 6-32 SL standard deviation-SL relations at steady state and 38 weeks of age, for experimental myofibrils

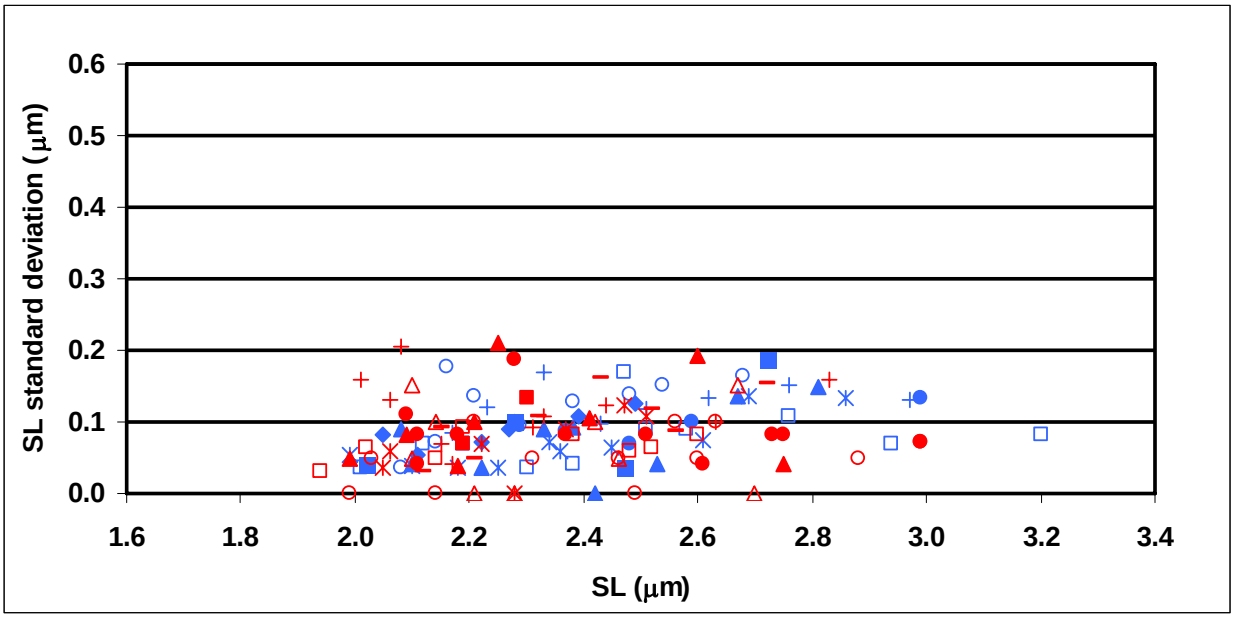

Figure 6-33 SL standard deviation-SL relations at steady state and 38 weeks of age (blue: control myofibrils, n=8; red: experimental myofibrils, n=9)

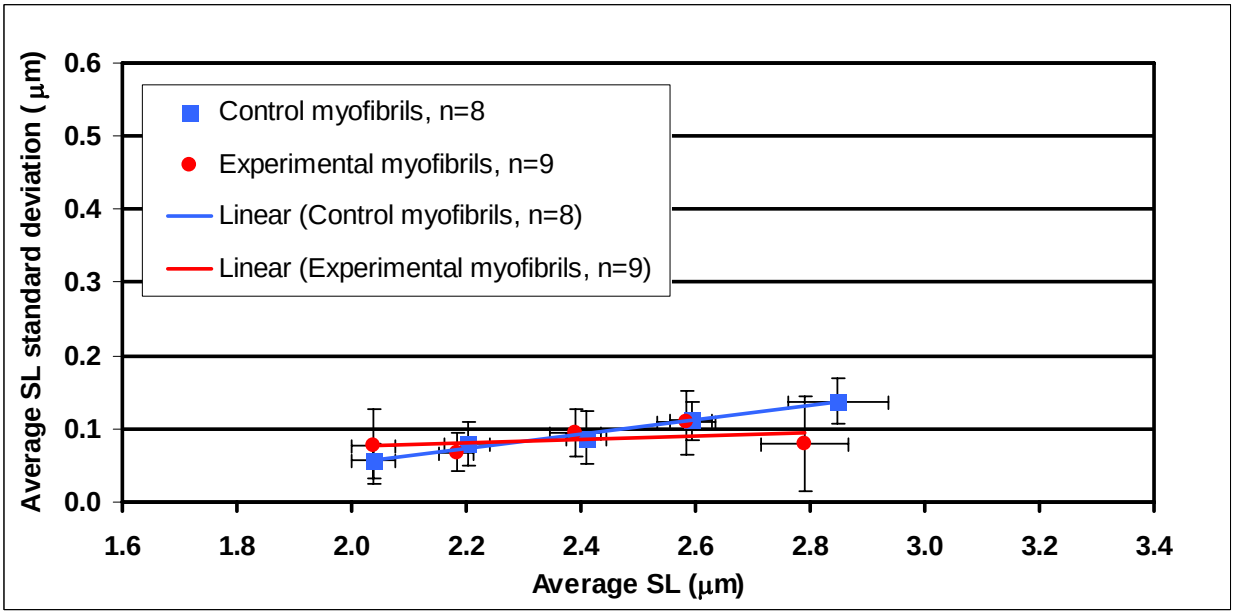

Figure 6-34 Average SL standard deviation-average SL relations at steady state and 38 weeks of age (vertical and horizontal lines correspond to standard deviations)

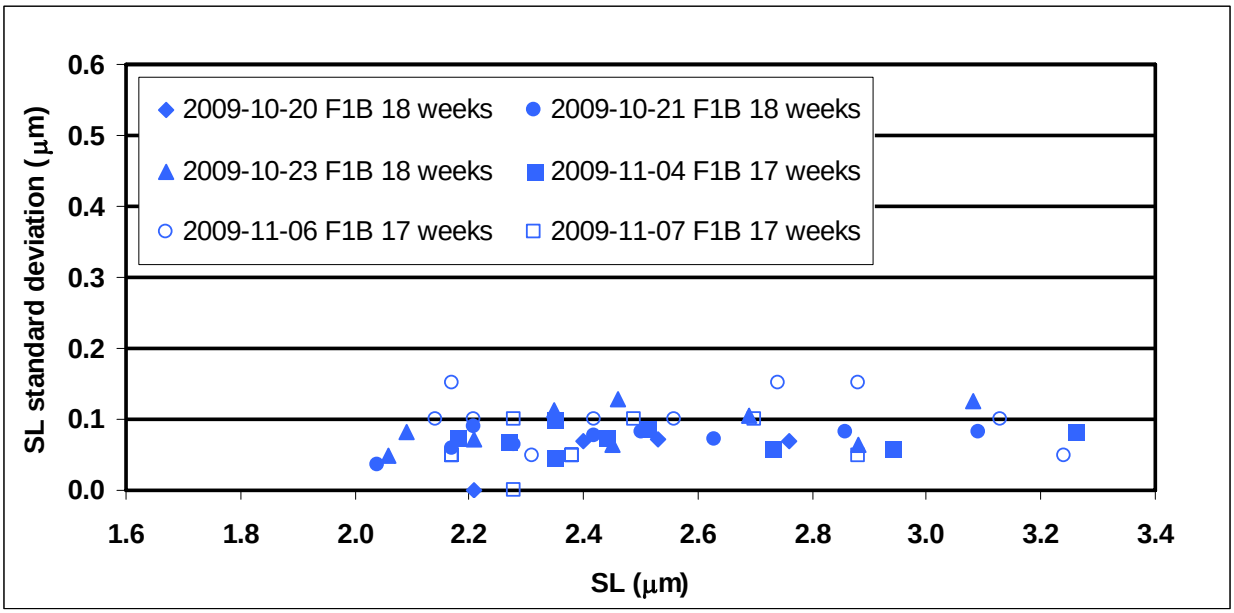

Figure 6-35 SL standard deviation-SL relations at steady state and 17 weeks of age, for control myofibrils

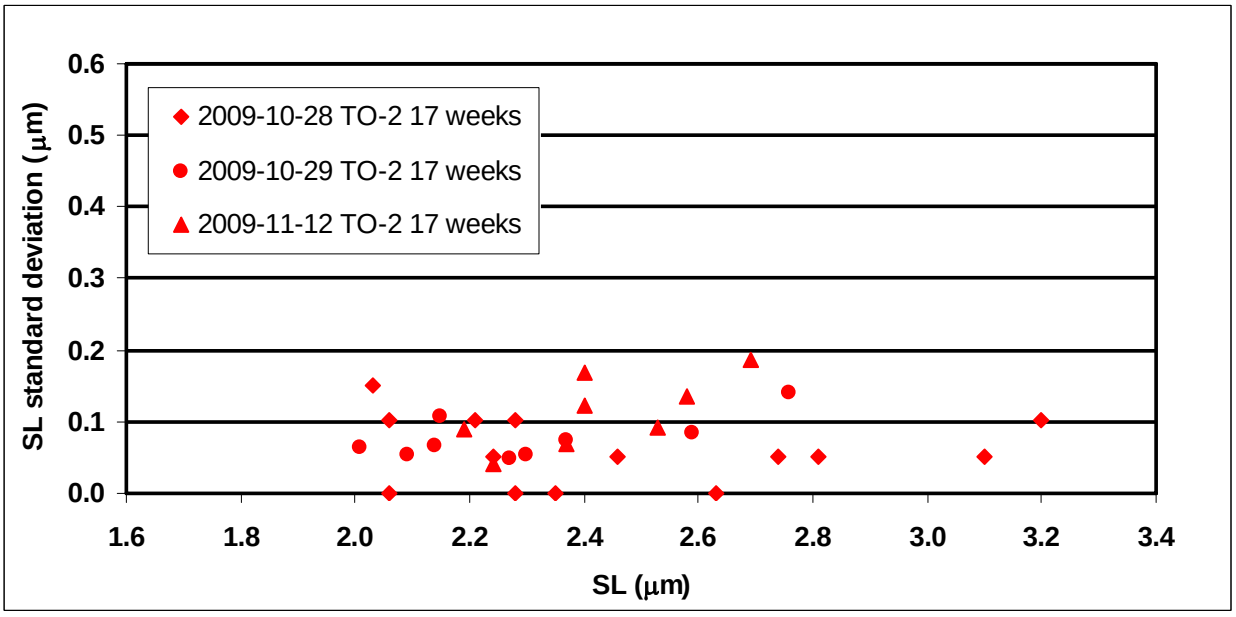

Figure 6-36 SL standard deviation-SL relations at steady state and 17 weeks of age, for experimental myofibrils

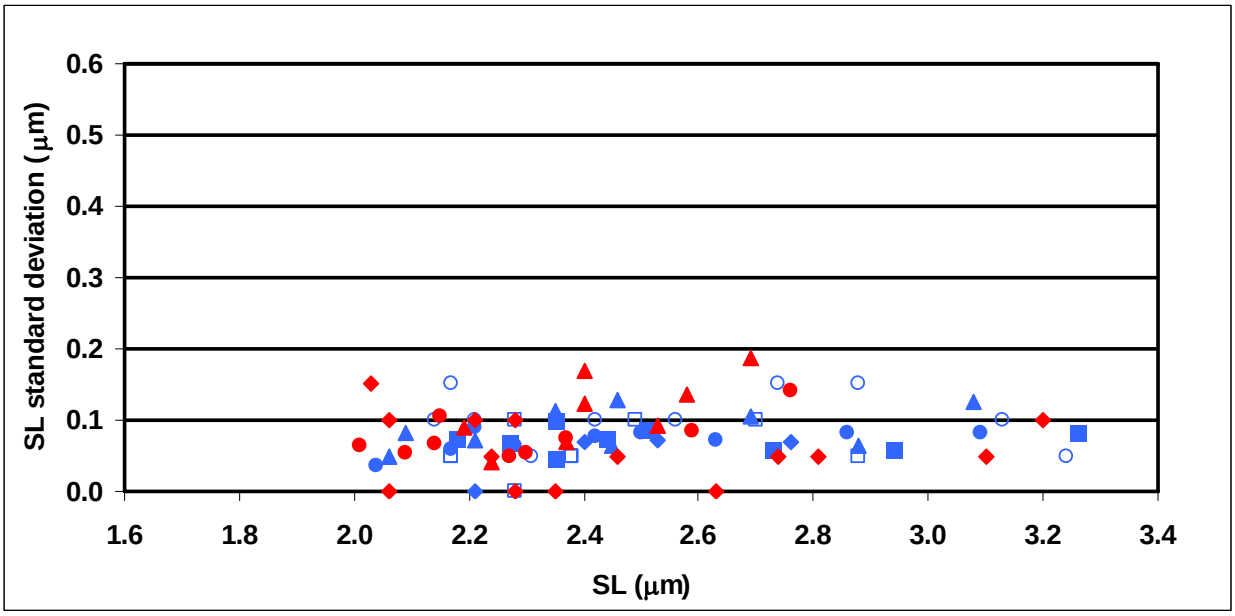

Figure 6-37 SL standard deviation-SL relations at steady state and 17 weeks of age (blue: control myofibrils, n=6; red: experimental myofibrils, n=3)

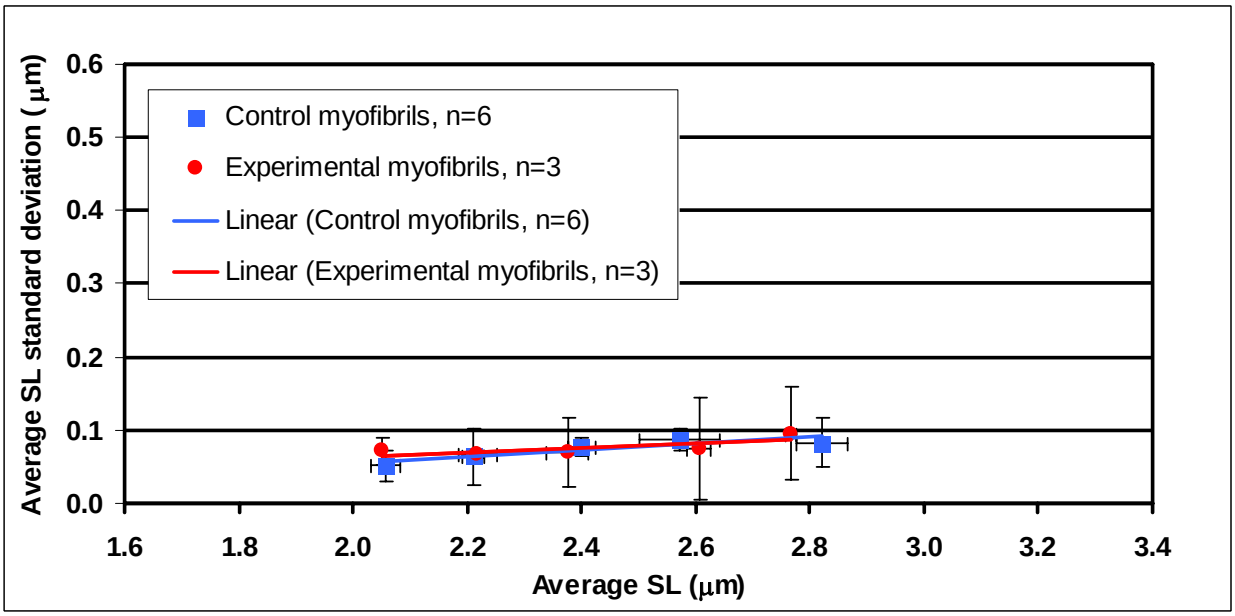

Figure 6-38 Average SL standard deviation-average SL relations at steady state and 17 weeks of age (vertical and horizontal lines correspond to standard deviations)

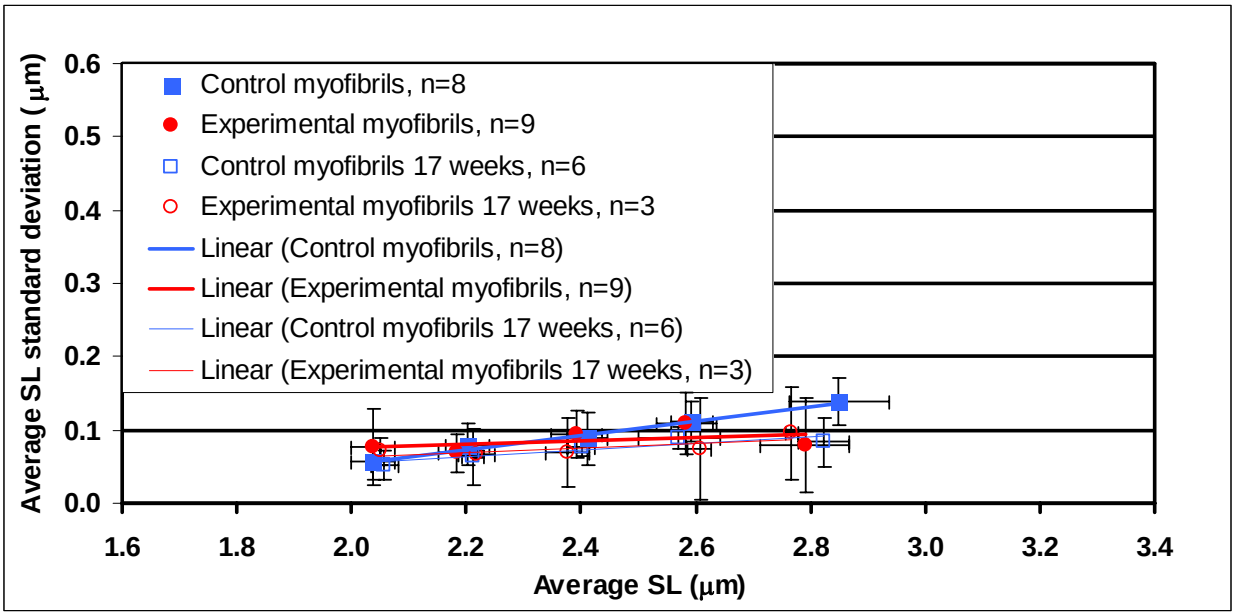

Figure 6-39 Average SL standard deviation-average SL relations at steady state (vertical and horizontal lines correspond to standard deviations)

The appropriateness of performing an ANCOVA analysis was tested for all SL bins greater than the one ranging from 1.9 to 2.1 μm. An ANCOVA analysis was found to be applicable at all these SL bins. Using ANCOVA and 2-way ANOVA parametric analysis when applicable, and Mann Whitney-U non-parametric tests for comparisons between groups with low sample sizes, no statistically significant difference was found between the adjusted mean and mean SL standard deviations at steady state stress of the myofibrils from the two animal and two age groups.

6.3.5 Stress decay magnitudes

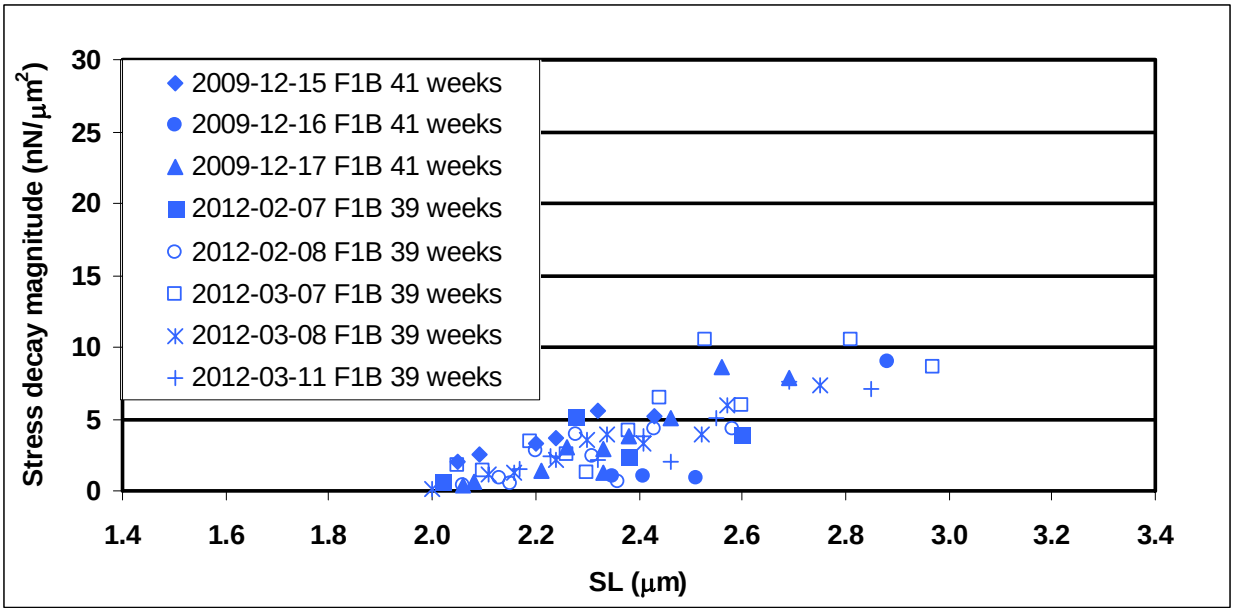

Figure 6-40 Stress decay magnitude-SL relations for control myofibrils at 38 weeks of age

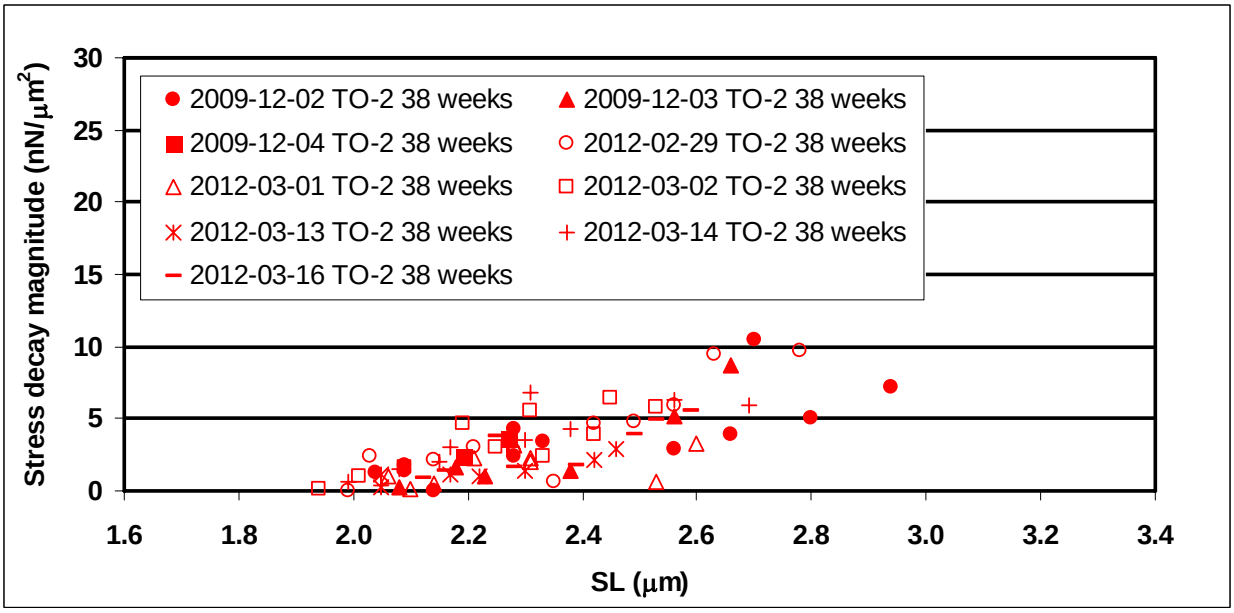

Figure 6-41 Stress decay magnitude-SL relations for experimental myofibrils at 38 weeks of age

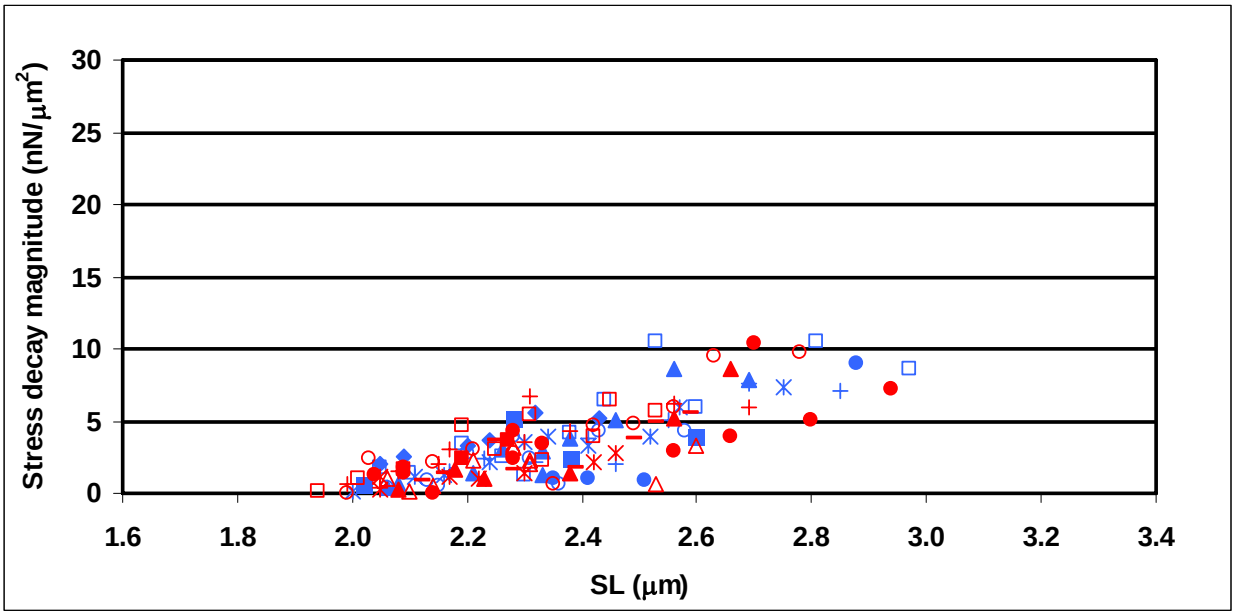

Figure 6-42 Stress decay magnitude-SL relations at 38 weeks of age (blue: control myofibrils, n=8; red: experimental myofibrils, n=9)

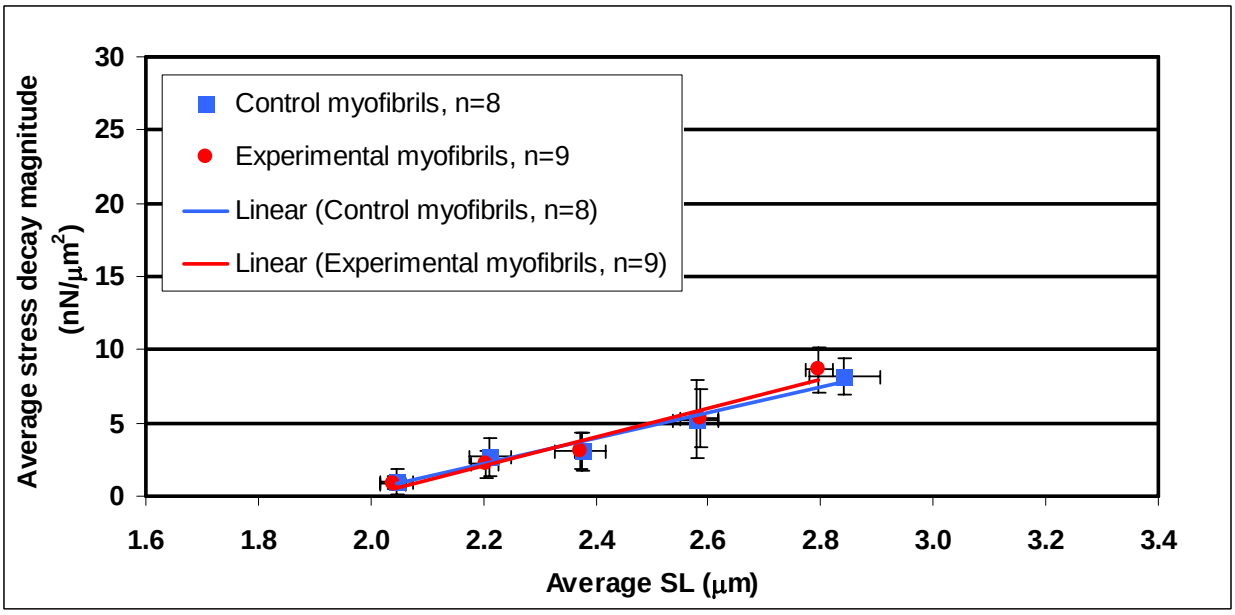

Figure 6-43 Average stress decay magnitude-average SL relations at 38 weeks (vertical and horizontal lines correspond to standard deviations)

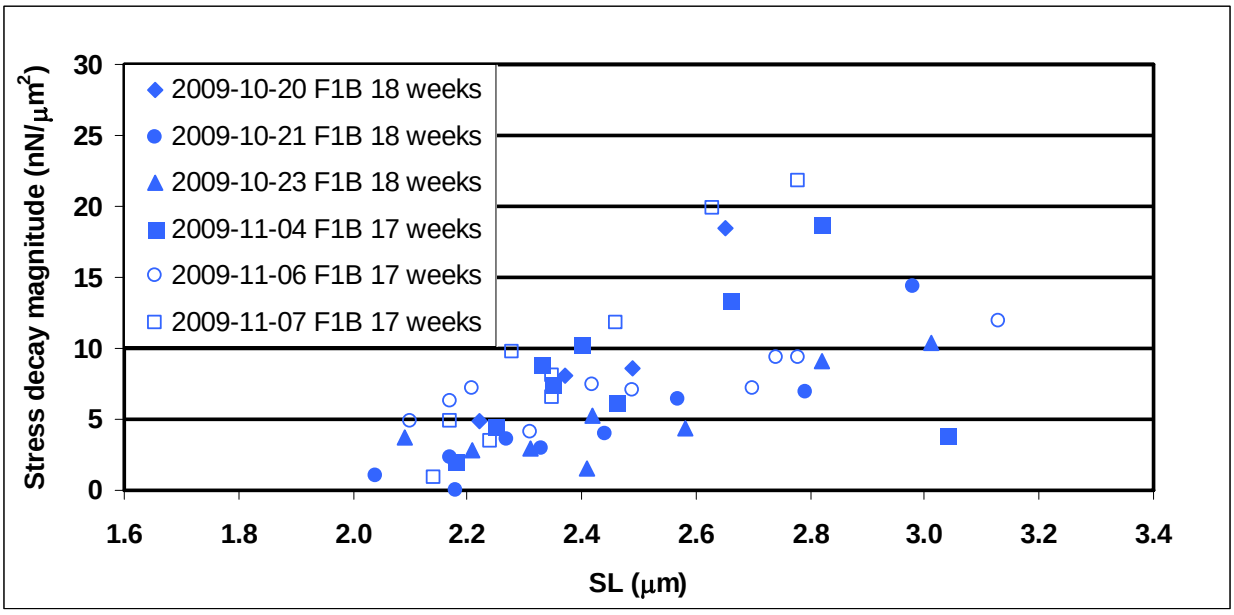

Figure 6-44 Stress decay magnitude-SL relations for control myofibrils at 17 weeks of age

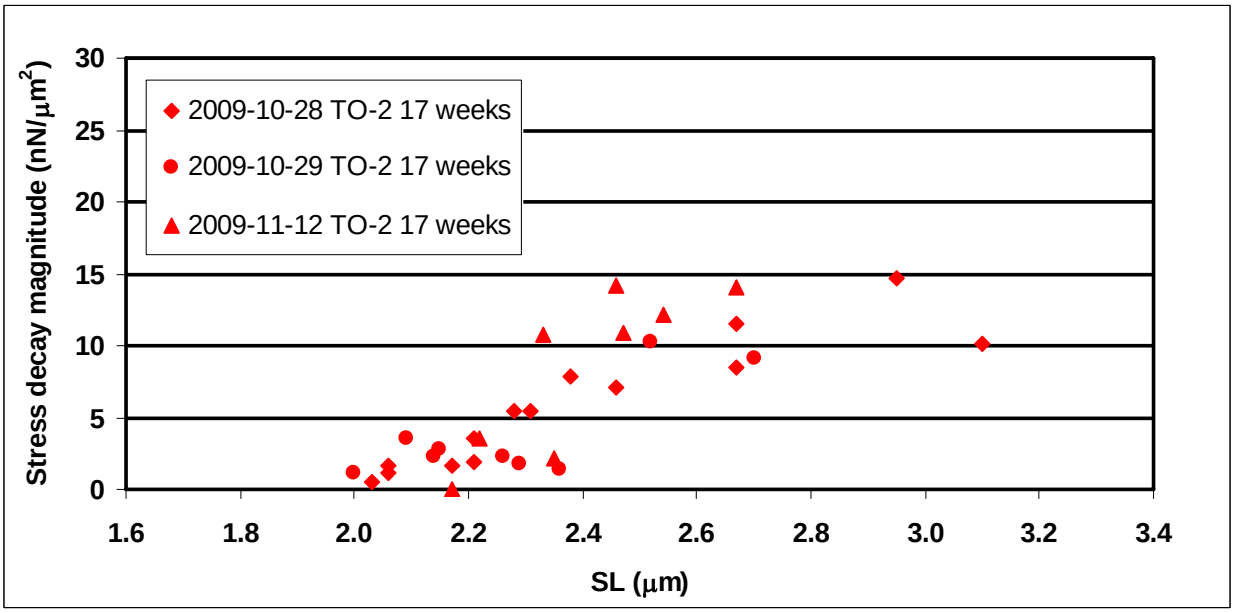

Figure 6-45 Stress decay magnitude-SL relations for experimental myofibrils at 17 weeks of age

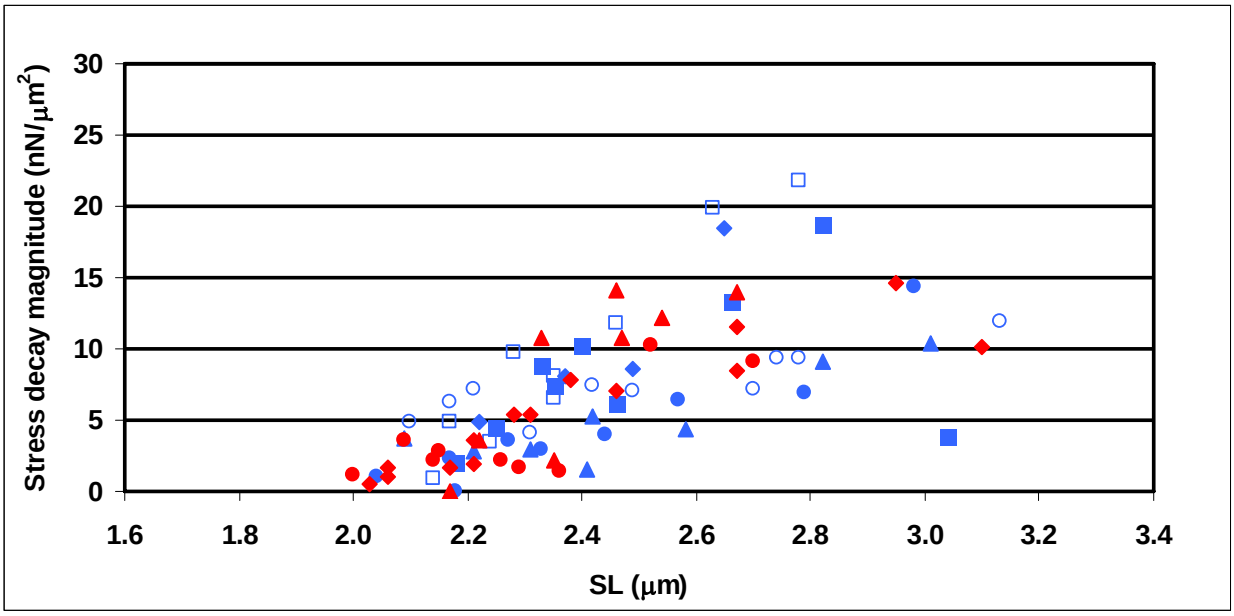

Figure 6-46 Stress decay magnitude-SL relations at 17 weeks of age (blue: control myofibrils, n=6; red: experimental myofibrils, n=3)

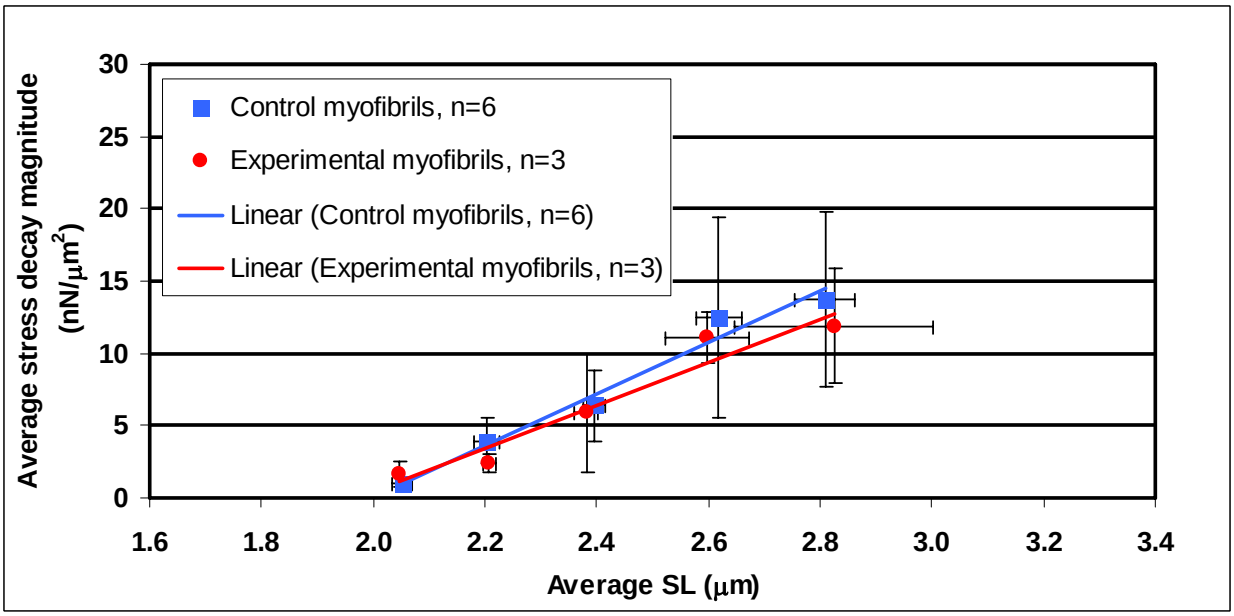

Figure 6-47 Average stress decay magnitude-average SL relations at 17 weeks of age (vertical and horizontal lines correspond to standard deviations)

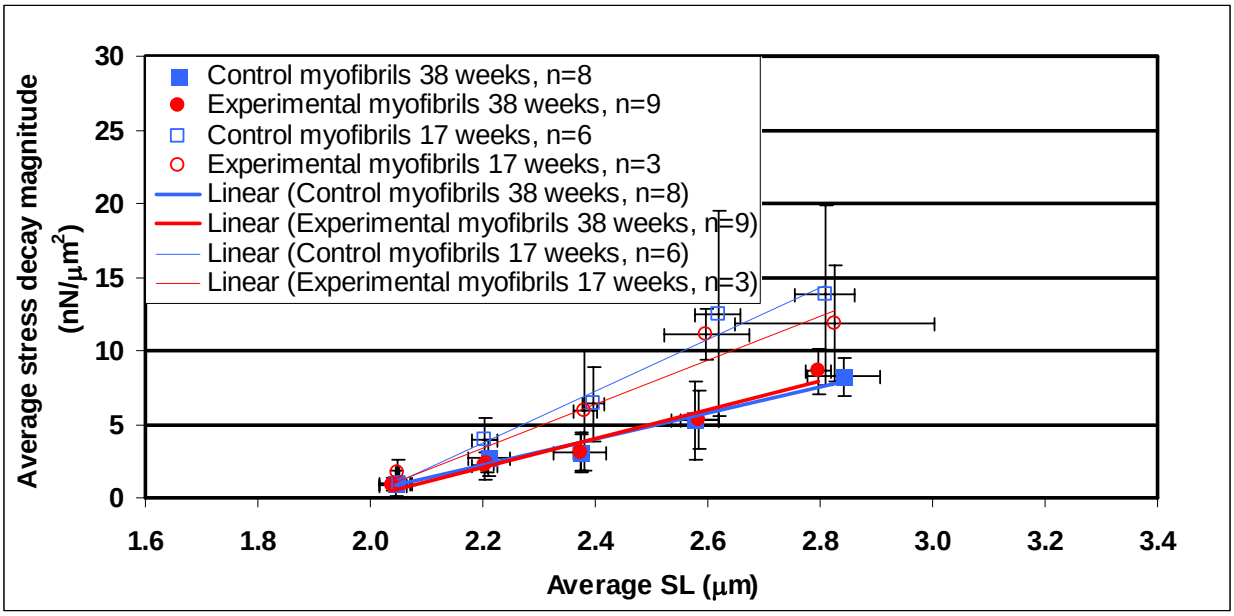

Figure 6-48 Average stress decay magnitude-average SL relations (vertical and horizontal lines correspond to standard deviations)

The appropriateness of performing an ANCOVA analysis was tested for all SL bins greater than the one ranging from 1.9 to 2.1 μm. An ANCOVA analysis was found to be inapplicable at the SL bins ranging from 2.5 to 2.7 and 2.7 to 3.0 μm. Using an ANCOVA parametric test, a statistically significant age effect was found at the SL bin ranging from 2.3 to 2.5 μm. However, no statistically significant age difference was found between the 17 and 38 week old experimental myofibrils and between the 17 and 38 week old control myofibrils due to the smaller group sizes.

Using a 2-way ANOVA parametric test and a Mann-Whitney-U non-parametric test, a statistically significant age effect was found at the SL bin ranging from 2.5 to 2.7 μm. The stress decay magnitudes of the 17 week old experimental myofibrils were found to be greater than those of the 38 week old experimental myofibrils. Using a 2-way ANOVA parametric test, another statistically significant age effect was found at the SL bin ranging from 2.5 to 2.7 μm.

The stress decay magnitudes of the 17 week old control myofibrils were found to be greater than those of the 38 week old control myofibrils.

Therefore, statistically significant differences were found between the mean stress decay magnitudes of the 17 and 38 week old experimental myofibrils, and between those of the 17 and 38 week old control myofibrils at the SL bin ranging from 2.5 to 2.7 μm.

6.3.6 Stress decay coefficients

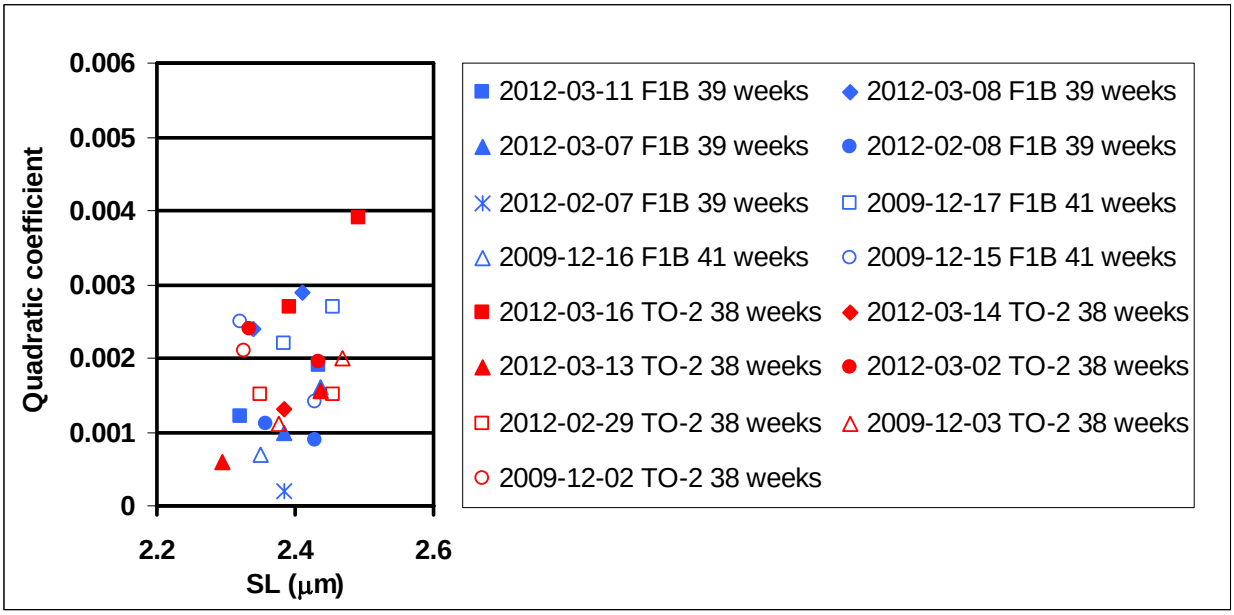

Figure 6-49 Quadratic coefficient-SL relations at 38 weeks (blue: control myofibrils, n=8; red: experimental myofibrils, n=7)

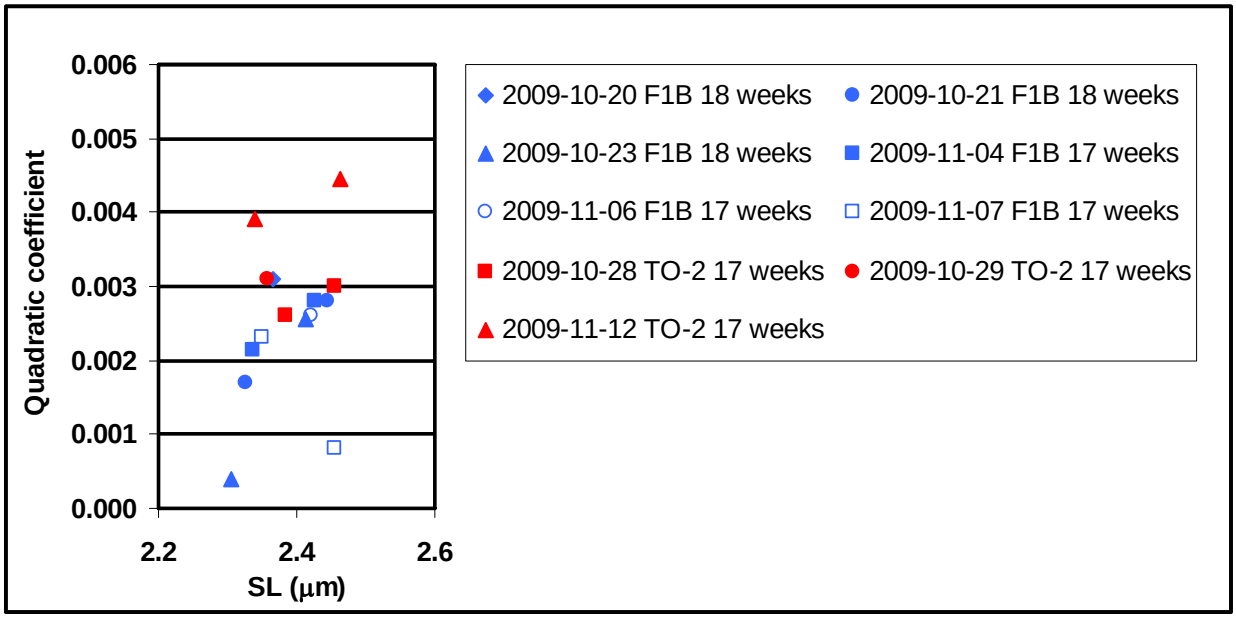

Figure 6-50 Quadratic coefficient-SL relations at 17 weeks (blue: control myofibrils, n=6; red: experimental myofibrils, n=3)

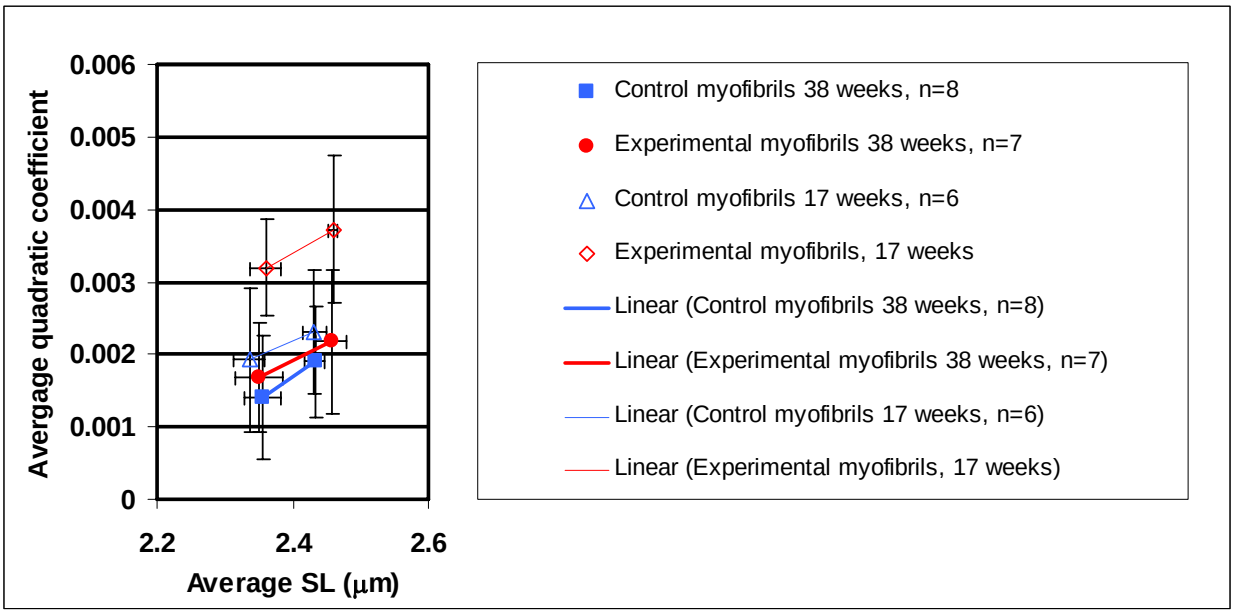

Figure 6-51 Quadratic coefficient-SL relations (vertical and horizontal lines correspond to standard deviations)

The appropriateness of performing an ANCOVA analysis was tested for the SL bin ranging from 2.4 to 2.5 μm. An ANCOVA analysis was found to be applicable at this SL, and no statistically significant difference was found between the stress decay quadratic coefficients of the two animal and two age groups.

Using a 2-way ANOVA parametric test and a Mann Whitney-U non-parametric test, an age effect was found at the SL bin ranging from 2.3 to 2.4 μm. The stress decay quadratic coefficients of the 17 week old experimental myofibrils were found to be greater than those of the 38 week old experimental myofibrils.

Therefore, a statistically significant difference was found between the mean stress decay quadratic coefficients of the 17 and 38 week old experimental myofibrils at the SL bin ranging from 2.3 to 2.4 μm.

Here is a summary of the differences between the passive mechanical properties of the myofibrils from the two animal and two age groups:

1) Peak stresses: an animal group difference was found at a SL of 2.1 μm, and age differences were found at SLs of 2.1 and 2.6 μm. Namely, statistically significant differences were found between the adjusted mean peak stresses of the 17 week old experimental and control myofibrils at a SL of 2.1 μm, the adjusted mean peak stresses of 17 and 38 week old experimental myofibrils at a SL of 2.1, and the mean peak stresses of 17 and 38 week old experimental myofibrils at a SL of 2.6 μm.
2) SL standard deviations at peak stress: no statistically significant difference was found.
3) Steady state stresses: animal group differences were found at SLs of 2.1, 2.2, 2.3 and 2.4 μm, and age differences were found at SLs of 2.1 and 2.4 μm. Namely, statistically significant differences were found between the adjusted mean steady state stresses of the 17 week old experimental and control myofibrils at SLs of 2.1, 2.3 and 2.4 μm, the mean steady state stresses of the 17 week old experimental and control myofibrils at a SL of 2.2 μm, the adjusted mean steady state stresses of the 17 and 38 week old experimental myofibrils at SLs of 2.1 and 2.4 μm, and the adjusted mean steady state stresses of the 17 and 38 week old control myofibrils at a SL of 2.1 μm.
4) SL standard deviations at steady state stress: no statistically significant difference was found.
5) Stress decay magnitudes: only age differences were found at the SL bin ranging from 2.5 to 2.7 μm. Namely, statistically significant differences were found between the mean stress decay magnitudes of the 17 and 38 week old experimental myofibrils, and between those of the 17 and 38 week old control myofibrils.

6) Stress decay quadratic coefficients: only an age difference was found at the SL bin ranging from 2.3 to 2.4 μm. Namely, a statistically significant difference was found between the mean stress decay quadratic coefficients of the 17 and 38 week old experimental myofibrils.

The validity and significance of these results will be discussed in Chapter 8.

CHAPTER SEVEN: TITIN EXPRESSION IN DCM AND NORMAL HAMSTERS

7.1 Introduction

One of the goals of this study was to relate the passive mechanical properties of the experimental and control myofibrils to the expression of titin in the LV walls that they were isolated from. This chapter contains the methodology followed to determine the expression of titin in the experimental and control LV walls, and the results obtained, which were:

1. the N2BA:N2B ratios,
2. the titin:MHC ratios,
3. the N2BA:N2B ratios in the endocardium and epicardium layers,
4. the titin:MHC ratios in the endocardium and epicardium layers,
5. the MWs of the N2BA and N2B isoforms, and
6. the N2BA:N2B ratios as a function of an indicator of the progression of DCM (the weights of the hearts filled with solution divided by body weight).

7.2 Method

7.2.1 Gel electrophoresis protocol

The weights of the Bio TO-2 and Bio F1B hamsters were recorded just before they were euthanized. After the hearts were excised and perfused, they were kept in solution at all times to prevent degradation of the tissue, and the weights of the hearts filled with solution were recorded. The animal weights and the weights of their hearts filled with solution are given in section 7.3.5. Each dissected LV wall was divided in two parts. The inferior part was sliced and used for mechanical testing, and the superior part was frozen for titin expression analysis. For some of the LV superior parts, the endocardium and epicardium layers were tested separately to check for transmural differences in the expression of titin. There are some LV walls for which

the titin expression was tested, but no mechanical result could be obtained. In the result section, each date represents a LV wall.

Two different types of gels were prepared by Dr. Venus Joumaa. The first type of gel was used to separate the titin isoform bands and find the N2BA:N2B ratios, and the second type of gel was used to obtain total titin and MHC bands and find the titin:MHC ratios. The frozen muscle samples were homogenized and added to a solubilization buffer (26 µl/1 mg muscle sample). To determine the N2BA:N2B ratios, 2% acrylamide gels were run at a constant voltage of 22 V overnight and then stained using Coomassie blue. To determine the titin:MHC ratios, 2.8% acrylamide gels were run at a constant current of 4 mA for 16 to 17 hours and then stained using Coomassie blue. The titin isoforms do not separate in a 2.8% gel. Rat LV muscle (N2B MW ~ 3 000 kDa (Neagoe *et al.*, 2003)) and rabbit psoas (two N2A titin isoforms of MW ~ 3300 kDa and 3400 kDa (Prado *et al.*, 2005)) were included on the gels. The corresponding titin isoform and myosin bands were used as standard markers to identify the titin isoform and myosin bands from the control and experimental LVs. An example is given in Figure 7-1 below.

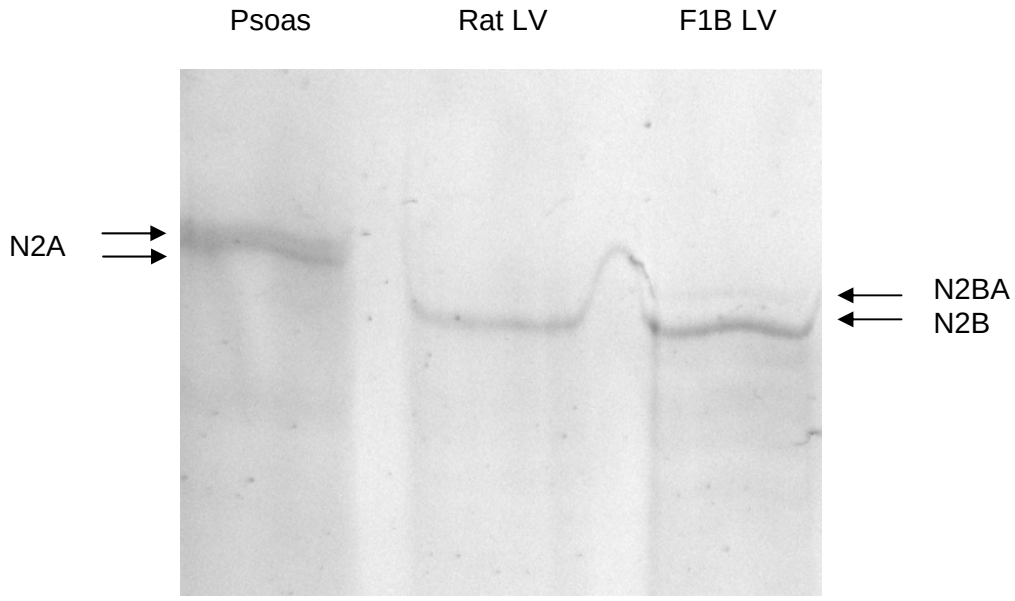

Figure 7-1 2% acrylamide gel showing the two N2A titin bands of rabbit psoas, the one N2B titin band of rat LV myocardium, and the N2BA (top) and N2B (bottom) titin bands of Bio F1B hamster myocardium

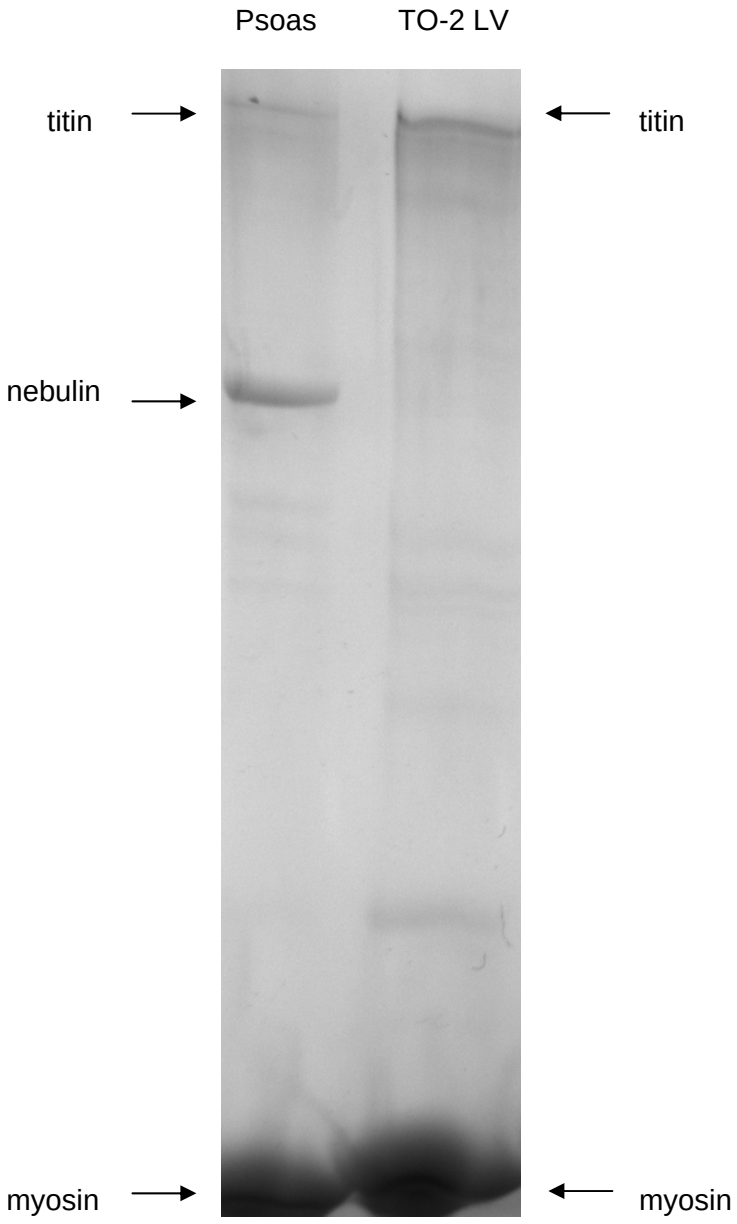

Figure 7-2 2.8% acrylamide gel showing the total titin (top) and MHC (bottom) bands of rabbit psoas and Bio TO-2 hamster LV myocardium

7.2.2 Data analysis

The gels were scanned and analyzed using GeneSnap 6.05 and Genetools 3.06 from SynGene. Integrated optical density values were obtained for the N2BA and N2B bands from the 2% acrylamide gels, and the titin and MHC bands from the 2.8% acrylamide gels. To determine the N2BA:N2B ratio of each LV wall, the integrated optical density value of the N2BA band was divided by the integrated optical density value of the N2B band. Averages were calculated for repeated gels. The N2BA:N2B ratios for all the LV walls and the endocardium and epicardium layers tested are reported in sections 7.3.1 and 7.3.3.1, and the titin:MHC ratios obtained the same way from the optical density values of the titin and MHC bands, are reported in sections 7.3.2 and 7.3.3.2. The N2BA:N2B ratios were then plotted as a function of an indicator of the progression of DCM, i.e. the weights of the hearts filled with solution divided by body weight, as displayed in Figure 7-3 in section 7.3.6. This ratio was used as an indicator of the progression of DCM because: 1) the weights of hearts from Bio TO-2 hamsters normalized to body weight have been reported to gradually increase as the animals aged from 20 to 26, 31, 37 and 43 weeks (Goineau *et al.*, 2001), 2) this increase was associated with increased normalized atria and RV weights, but not with increased normalized LV weights, and 3) DCM is characterized by dilation of the LV wall, so adding the weight of the solution filling the hearts to the heart weights before normalizing to body weight should provide a stronger indicator of the progression of the LV dilation then the normalized heart weights alone.

The MWs of the titin isoforms from the Bio TO-2 and Bio F1B hamsters were also determined. Since the N2B bands from the hamsters' control and experimental LVs lined up with the rat LV N2B band on the gels, except for when the bands in the different wells shifted diagonally along the gel, a MW of 3000 kDa was assigned to this isoform. The known MWs of the rabbit psoas and rat LV titin isoforms were used to develop a linear relationship between log MW and migration distance, which was then used to determine the MWs of N2BA titin from the

control and experimental LVs. When the N2BA and N2B bands in the different wells shifted diagonally along the gel, the migration distance of each N2BA band was corrected. The MWs of the N2BA isoforms are given in section 7.3.4.

7.2.3 Statistical analysis

The N2BA:N2B and titin:MHC ratios, N2BA isoform MWs, animal weights and weights of solution filled hearts for the two animal and two age groups were compared by performing 2-way ANOVA parametric analysis, and Mann Whitney-U non-parametric testing for comparisons between groups with low sample sizes. Due to the limited number of LVs that were separated into endocardium and epicardium layers and tested for transmural differences in their N2BA:N2B and titin:MHC ratios, the four groups were not tested separately. T-tests and Mann Whitney-U tests were performed on two groups that either included the 17 and 38 week old control and experimental LV walls, or just the 17 and 38 week old experimental LV walls. A significance level of $\alpha=0.05$ was used for all statistical tests, unless otherwise specified.

7.3 Results

7.3.1 N2BA:N2B ratios

38 week age group							
Control		Age (weeks)	Ratio	**Experimental**		Age (weeks)	Ratio
2009-06-22	Endo	36	0.121	2009-06-17	Endo	37	0.087
2009-06-22	Epi	36	0.105	2009-06-17	Epi	37	0.084
	Average		0.113		Average		0.085
2009-08-31		36	0.216	2009-07-06	Endo	38	0.096
2009-09-21		44	0.106	2009-07-06	Epi	38	0.094
2009-12-14		41	0.091		Average		0.095
				2009-09-08		37	0.092
				2009-09-14		36	0.057
				2009-11-30		38	0.068
Average			0.132	Average			0.080

17 week age group							
Control		Age (weeks)	Ratio	**Experimental**		Age (weeks)	Ratio
2009-05-11	Endo	17	0.072	2009-05-05	Endo	17	0.080
2009-05-11	Epi	17	0.093	2009-05-05	Epi	17	0.095
	Average		0.083		Average		0.088
2009-10-19		18	0.121	2009-05-25	Endo	18	0.114
2009-11-03		17	0.090	2009-05-25	Epi	18	0.133
					Average		0.123
				2009-10-27		17	0.099
				2009-11-09		17	0.070
Average			0.098	Average			0.095

Table 7-1 N2BA:N2B titin isoform ratios in the LVs of Bio TO-2 and Bio F1B hamsters at 17 and 38 weeks of age

Using a Mann Whitney-U non-parametric test, a slightly statistically significant difference was found between the N2BA:N2B ratios of the 38 week old experimental and control LVs ($p<0.1$, 2-tailed; $p<0.05$, 1-tailed), the experimental N2BA:N2B ratios being lower than the control ratios.

The statistical analysis was repeated after the exclusion of an outlier N2BA:N2B ratio, the value of 0.121 obtained from the 38 week old control LV labelled 2009-08-31. The slightly statistically significant difference between the N2BA:N2B ratios of the 38 week old experimental and control LVs became not statistically significant.

The N2BA:N2B ratios found are comparable to previously reported values in the LVs of hamsters (Neagoe *et al.*, 2003). However, Neagoe et al. found two N2BA bands using Coomassie blue staining, but only one N2BA band was observed in this study.

7.3.2 Titin:MHC ratios

38 week age group							
Control		Age (weeks)	Ratio	**Experimental**		Age (weeks)	Ratio
2009-06-22	Endo	36	0.188	2009-06-17	Endo	37	0.169
2009-06-22	Epi	36	0.146	2009-06-17	Epi	37	0.117
	Average		0.167		Average		0.143
2009-08-31		36	0.174	2009-07-06	Endo	38	0.078
2009-09-21		44	0.080	2009-07-06	Epi	38	0.144
2009-12-14		41	0.121		Average		0.111
				2009-09-08		37	0.165
				2009-09-14		36	0.108
				2009-11-30		38	0.128
Average			0.136	Average			0.131

17 week age group							
Control		Age (weeks)	Ratio	**Experimental**		Age (weeks)	Ratio
2009-05-11	Endo	17	0.111	2009-05-05	Endo	17	0.150
2009-05-11	Epi	17	0.145	2009-05-05	Epi	17	0.120
	Average		0.128		Average		0.135
2009-11-03		17	0.147	2009-05-25	Endo	18	0.144
				2009-05-25	Epi	18	0.128
					Average		0.136
				2009-11-09		17	0.117
Average			0.138	Average			0.129

Table 7-2 Titin:MHC ratios in the LVs of Bio TO-2 and Bio F1B hamsters at 17 and 38 weeks of age

No statistically significant difference was found between the titin:MHC ratios of the two animal and two age groups.

The titin:MHC ratios found are not consistently comparable to previously reported values. They differed from the ratio of 0.29 previously reported by (Cazorla *et al.*, 2000) in the LVs of mice, but are similar the ratio of 0.09 previously reported by (Neagoe *et al.*, 2002) in the

RVs of rats. Cazorla et al. used a different technique to determine the amount of titin relative to MHC. They ran a series of gels on the same muscle, varying the amount of muscle loaded in each gel. They then developed a relation of integrated optical density as a function of loading for the titin and MHC bands. The titin:MHC ratio was calculated as the slope of the linear range of the relation for titin divided by the slope of the linear range of the relation for MHC. For a given muscle, the techniques used by Cazorla et al. and by Dr. Joumaa should yield the same titin:MHC ratio for a constant loading, unless saturation of a band (most likely the MHC band) occurred. According to Dr. Joumaa, if saturation of a band had occurred, it would have become shiny. None of the bands became shiny.

7.3.3 Titin expression in the LV endocardium and epicardium layers

7.3.3.1 N2BA/N2B ratios

Endocardium layer						
38 week age group						Average
Control	Age (weeks)	Ratio	**Experimental**	Age (weeks)	Ratio	
2009-06-22	36	0.121	2009-06-17	37	0.087	
			2009-07-06	38	0.096	
17 week age group						
Control	Age (weeks)	Ratio	**Experimental**	Age (weeks)	Ratio	
2009-05-11	17	0.072	2009-05-05	17	0.080	
			2009-05-25	18	0.114	
Average		0.097	Average		0.094	0.095

Epicardium layer						
38 week age group						Average
Control	Age (weeks)	Ratio	**Experimental**	Age (weeks)	Ratio	
2009-06-22	36	0.105	2009-06-17	37	0.084	
			2009-07-06	38	0.094	
17 week age group						
Control	Age (weeks)	Ratio	**Experimental**	Age (weeks)	Ratio	
2009-05-11	17	0.093	2009-05-05	17	0.095	
			2009-05-25	18	0.133	
Average		0.099	Average		0.101	0.101

Table 7-3 N2BA:N2B ratios in the LV endocardium and epicardium layers of Bio TO-2 and Bio F1B hamsters at 17 and 38 weeks of age

No statistically significant difference was found between the N2BA:N2B ratios in the endocardium and epicardium layers of the two groups, whether the groups included the 17 and 38 week old control and experimental LV walls, or just the 17 and 38 week old experimental LV walls.

7.3.3.2 Titin:MHC ratios

Endocardium layer						
38 week age group						Average
Control	Age (weeks)	Ratio	**Experimental**	Age (weeks)	Ratio	
2009-06-22	36	0.188	2009-06-17	37	0.169	
			2009-07-06	38	0.078	
17 week age group						
Control	Age (weeks)	Ratio	**Experimental**	Age (weeks)	Ratio	
2009-05-11	17	0.111	2009-05-05	17	0.150	
			2009-05-25	18	0.144	
Average		0.150	Average		0.136	0.140

Epicardium layer						
38 week age group						
Controls	Age (weeks)	Ratio	**Experimental**	Age (weeks)	Ratio	
2009-06-22	36	0.146	2009-06-17	37	0.117	
			2009-07-06	38	0.144	
17 week age group						
Controls	Age (weeks)	Ratio	**Experimental**	Age (weeks)	Ratio	
2009-05-11	17	0.145	2009-05-05	17	0.120	
			2009-05-25	18	0.128	
Average		0.146	Average		0.127	0.134

Table 7-4 Titin:MHC ratios in the LV endocardium and epicardium layers of Bio TO-2 and Bio F1B hamsters at 17 and 38 weeks of age

No statistically significant difference was found between the titin:MHC ratios in the endocardium and epicardium layers of the two groups, whether the groups included the 17 and 38 week old control and experimental LV walls, or just the 17 and 38 week old experimental LV walls.

7.3.4 N2BA isoform molecular weights

38 week age group							
Control		Age (weeks)	MW	**Experimental**		Age (weeks)	MW
2009-06-22	Endo	36	3191	2009-06-17	Endo	37	3177
2009-06-22	Epi	36	3184	2009-06-17	Epi	37	3177
	Average		3187		Average		3177
2009-09-21		44	3135	2009-07-06	Endo	38	3120
2009-12-14		41	3190	2009-07-06	Epi	38	3139
					Average		3130
				2009-09-08		37	3135
				2009-09-14		36	3130
				2009-11-30		38	3190
Average			3171	Average			3152

17 week age group							
Control		Age (weeks)	MW	**Experimental**		Age (weeks)	MW
2009-05-11	Endo	17	3176	2009-05-05	Endo	17	3176
2009-05-11	Epi	17	3163	2009-05-05	Epi	17	3176
	Average		3170		Average		3176
2009-11-03		17	3184	2009-05-25	Endo	18	3156
				2009-05-25	Epi	18	3148
					Average		3152
				2009-11-09		17	3184
Average			3177	Average			3171

Table 7-5 Molecular weights of the N2BA isoforms in the LVs of Bio TO-2 and Bio F1B hamsters at 17 and 38 weeks of age

No statistically significant difference was found between the MWs of the N2BA isoforms from the two animal and two age groups. The MW of the N2BA isoform from various species was found to range from ~3250 to ~3400 kDa (Neagoe *et al.*, 2003).

7.3.5 Animal weights and weights of solution filled hearts

38 week age group							
Control	Age (weeks)	Animal weight (kg)	Weight of sol. filled heart (g)	**Experimental**	Age (weeks)	Animal weight (kg)	Weight of sol. filled heart (g)
2009-06-08	36	0.110	0.65	2009-06-17	37	0.123	0.67
2009-06-22	36	0.123	0.69	2009-07-06	38	0.120	0.62
2009-08-31	36	0.130	0.69	2009-09-08	37	0.112	0.60
2009-09-21	44	0.136	0.70	2009-09-14	36	0.117	0.80
2009-12-14	41	0.112	0.61	2009-11-30	38	0.103	0.61
2012-02-06	39	0.178	0.79	2012-02-27	38	0.116	0.74
2012-03-05	39	0.130	0.66	2012-03-12	38	0.110	0.67
2012-03-19	43	0.159	0.77	2012-03-19	43	0.127	0.80
Average		0.135	0.70	Average		0.116	0.69

17 week age group							
Control	Age (weeks)	Animal weight (kg)	Weight of sol. filled heart (g)	**Experimental**	Age (weeks)	Animal weight (kg)	Weight of sol. filled heart (g)
2009-05-11	17	0.115	0.61	2009-05-05	17	0.098	0.57
2009-10-19	18	0.135	0.62	2009-05-25	18	0.115	0.52
2009-11-03	17	0.132	0.62	2009-10-27	17	0.099	0.50
				2009-11-09	17	0.102	0.53
Average		0.127	0.62	Average		0.103	0.53

Table 7-6 Weights of 17 and 38 week old Bio TO-2 and Bio F1B hamsters and of their solution filled hearts

Statistically significant differences were found between the animal weights of two animal and two age groups. Using a 2-way ANOVA parametric analysis, the 38 week old control animals were found to weigh more than the 38 week old experimental animals. Also, using a Mann Whitney-U non-parametric test, the 38 week old experimental animals were found to weigh more than the 17 week old experimental animals.

Using a 2-way ANOVA parametric analysis ($p=0.001$, 2-tailed) and a Mann Whitney-U non-parametric test ($p<0.002$, 2-tailed), a statistically significant difference was found between the weights of the solution filled hearts from the 17 and 38 week old experimental animals, the solution filled hearts from the 38 week old animals weighing more than those from the 17 week old animals.

7.3.6 N2BA:N2B ratios as a function of weights of solution filled hearts normalized to body weight

38 week age group							
Control	Age (weeks)	HW:BW Ratio	N2BA:N2B ratio	**Experimental**	Age (weeks)	HW:BW ratio	N2BA:N2B ratio
2009-06-22	36	0.0056	0.113	2009-06-17	37	0.0054	0.085
2009-08-31	36	0.0053	0.216	2009-07-06	38	0.0052	0.095
2009-09-21	44	0.0051	0.106	2009-09-08	37	0.0054	0.092
2009-12-14	41	0.0054	0.091	2009-09-14	36	0.0068	0.057
				2009-11-30	38	0.0059	0.068
Average		0.0054	0.132	Average		0.0057	0.080

17 week age group							
Control	Age (weeks)	HW:BW Ratio	N2BA:N2B ratio	**Experimental**	Age (weeks)	HW:BW ratio	N2BA:N2B ratio
2009-05-11	17	0.0053	0.083	2009-05-05	17	0.0058	0.088
2009-10-19	18	0.0046	0.121	2009-05-25	18	0.0045	0.123
2009-11-03	17	0.0047	0.090	2009-10-27	17	0.0051	0.099
				2009-11-09	17	0.0052	0.070
Average		0.0049	0.098	Average		0.0052	0.095

Table 7-7 N2BA:N2B ratios and weights of solution filled hearts normalized to body weight (HW:BW) for Bio TO-2 and Bio F1B hamsters at 17 and 38 weeks of age

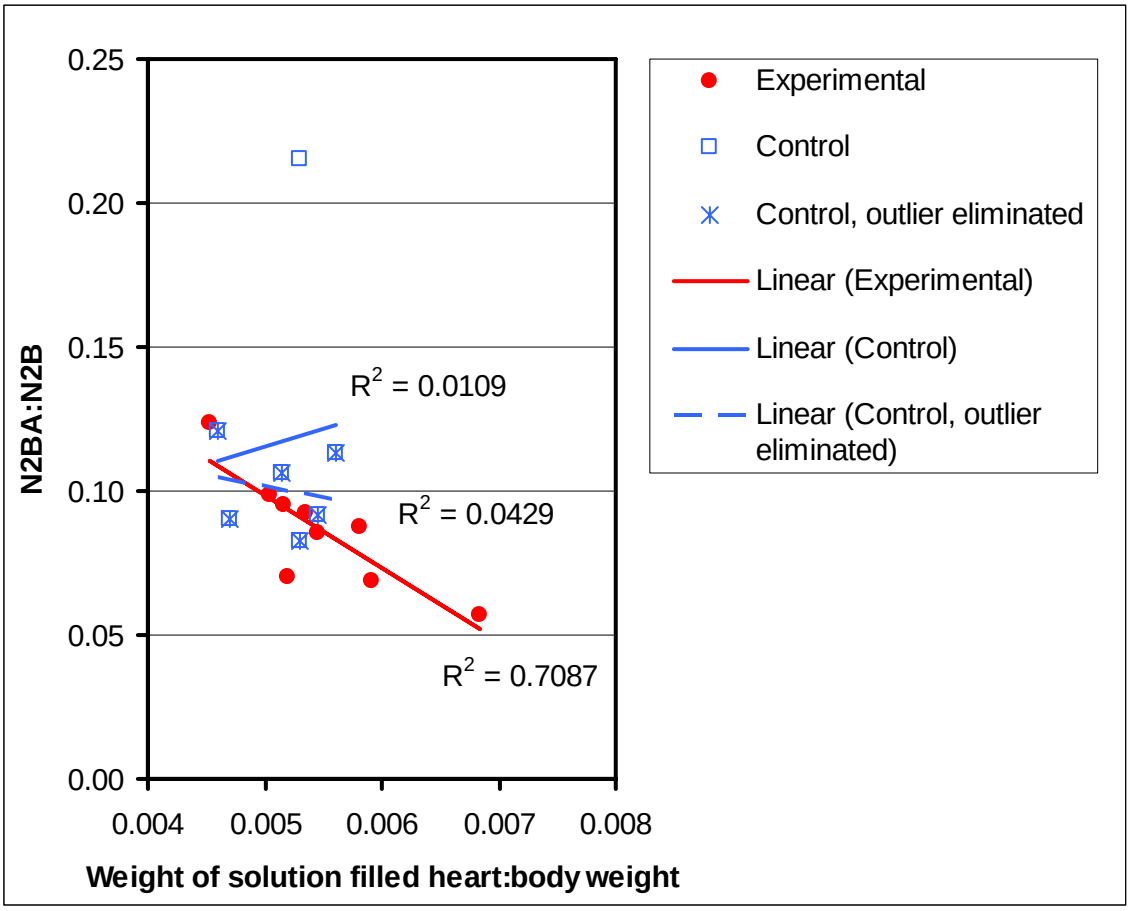

Figure 7-3 Linear relations between N2BA:N2B ratios and weights of solution filled hearts normalized to body weight for Bio TO-2 and Bio F1B hamsters tested at 17 and 38 weeks of age

The linear relation between the LV N2BA:N2B ratios and the weights of the solution filled hearts normalized to body weight, for the experimental animals tested at 17 and 38 weeks of age, was found to be statistically significant ($p<0.01$). The relation for the control animals tested at 17 and 38 weeks of age was not statistically significant whether the outlier was included or excluded from the data.

Here is a summary of the results on the titin expression for the two age and two animal groups:

1) A slightly statistically significant difference was found between the N2BA:N2B ratios of the 38 week old experimental and control LVs, the experimental N2BA:N2B ratios being lower than the control ratios (Table 7-1). This difference became no statistically significant when an outlier was excluded.
2) No statistically significant difference was found between the titin:MHC ratios of the two animal and two age groups (Table 7-2).
3) No statistically significant transmural difference was found in the N2BA:N2B and titin:MHC ratios (Table 7-3 and 7-4).
4) No statistically significant difference was found between the MWs of the N2BA isoforms from the two animal and two age groups (Table 7-5).
5) The 38 week old control animals were found to weigh more than the 38 week old experimental animals, and the 38 week old experimental animals were found to weigh more than the 17 week old experimental animals (Table 7-6).
6) The solution filled hearts of the 38 week old experimental animals were found to weigh more than those of the 17 week old experimental animals (Table 7-6).
7) A statistically significant linear relation exists between the LV N2BA:N2B ratios and the weights of the solution filled hearts normalized to body weight for the experimental animals tested at 17 and 38 weeks of age (Figure 7-3).

The significance of these results will be discussed in Chapter 8.

CHAPTER EIGHT: DISCUSSION

In general, the passive mechanical properties of the experimental myofibrils at 17 and 38 weeks of age did not differ from those of the control myofibrils. No statistically significant difference was found between the SL standard deviations at peak stress, SL standard deviations at steady state, stress decay magnitudes and stress decay quadratic coefficients of the myofibrils from the two animal groups at any given SL. A statistically significant difference was found between the adjusted mean peak stresses of the 17 week old experimental and control myofibrils at a SL of 2.1 µm, but no animal group difference was found at SLs of 2.0, 2.2, 2.3, 2.4, 2.5, 2.6 and 2.7 µm. Statistically significant differences were found between the adjusted mean steady state stresses of the 17 week old experimental and control myofibrils at SLs of 2.1, 2.3 and 2.4 µm, and the mean steady state stresses of the 17 week old experimental and control myofibrils at a SL of 2.2 µm, but no difference was found at SLs of 2.0, 2.5, 2.6 and 2.7 µm. Assuming that the molecular mechanism at the origin of most of the passive force generated by a myofibril upon stretch is the lengthening of the different elements of the extensible region of titin in a sequential manner with increasing SLs due to their different bending rigidities (Watanabe *et al.*, 2002), a difference between the peak and steady state passive stresses of the experimental and control myofibrils would be expected to increase with SL if such a difference really existed. Inaccuracies were introduced in the steady state passive stress measurements by the fact that the stress-time traces did not always reach steady-state following stress relaxation. Because titin is responsible for most of the passive force generated by an isolated myofibril (Granzier *et al.*, 2005) and the ensuing stress relaxation behaviour, these results suggest that there is no, or little, difference in titin expression between the Bio TO-2 and F1B hamsters.

Differences between the SL standard deviations of the experimental and control myofibrils were expected to be found based on the results reported by Mancinelli et al. discussed in section 4.4. They found shorter and longer average SLs in papillary muscles from Bio TO-2 hamsters fixed at the length at which they produced maximum force during twitch contractions, compared to those of papillary muscles from Bio F1B hamsters. Larger SL standard deviations were measure on some of the DCM papillary muscles compared to control muscles. It appears that the differences in average SLs and in SL standard deviations found by Mancinelly et al. using fixed papillary muscles were caused by differences in the sarcolemma and/or connective tissue between the two breeds, and not in subcellular components. The results from this research suggest that SL regulation is unaffected at the myofibrillar level in the LV of the Bio TO-2 hamster.

Some statistically significant differences related to age were found in the passive mechanical properties of the experimental and control myofibrils, but they may not be reflective of changes in the myofibrils. Statistically significant differences were found between the adjusted mean peak stresses of 17 and 38 week old experimental myofibrils at a SL of 2.1, and the mean peak stresses of 17 and 38 week old experimental myofibrils at a SL of 2.6 µm, but no difference was found at SLs of 2.0, 2.2, 2.3, 2.4, 2.5 and 2.7 µm. Statistically significant differences were found between the adjusted mean steady state stresses of the 17 and 38 week old experimental myofibrils at SLs of 2.1 and 2.4 µm, and the adjusted mean steady state stresses of the 17 and 38 week old control myofibrils at a SL of 2.1 µm, but no age difference was found at SLs of 2.0, 2.2, 2.3, 2.5, 2.6 and 2.7 µm. Statistically significant differences were found between the mean stress decay magnitudes of the 17 and 38 week old experimental myofibrils, and between those of the 17 and 38 week old control myofibrils at the SL bin ranging from 2.5 to 2.7 µm, but no difference was found at the SL bins ranging from 1.9 to 2.1, 2.1 to 2.3, 2.3 to 2.5, and 2.7 to 3.0 µm. Due to the fact that the passive mechanical properties of the

17 week old myofibrils were obtained using cantilevers of a higher stiffness than those used for the 38 week old myofibrils, these age differences could be due to an artifact. There may have been a difference between the stiffness values used in the stress calculations for the two types of cantilevers compared to the real stiffness values of the cantilevers since they were not calibrated. Inaccuracies in the steady state stress measurements, as previously mentioned, may also have contributed to these age differences. A statistically significant difference was found between the mean stress decay quadratic coefficients of the 17 and 38 week old experimental myofibrils at the SL bin ranging from 2.3 to 2.4 μm, but no difference was found at the SL bin ranging from 2.4 to 2.5 μm. This age difference in the stress decay quadratic coefficients may be attributable to inaccuracies in the measurements due to the fact that the stress relaxation portions of the stress-time traces did not always form a nice curve.

Small changes in the expression of titin between the experimental and control LVs were detected, but they were too small to be noticed in the passive mechanical properties. The N2BA:N2B ratios were found to be slightly significantly lower in the 38 week old experimental LVs than in the 38 week old control LVs. Although no significant difference was found between the N2BA:N2B ratios of the 17 and 38 week old control LVs, the slightly significant difference between the N2BA:N2B ratios of the 38 week old control and experimental LVs seems attributable to increased N2BA:N2B ratios in the control LVs with age as opposed to decreased N2BA:N2B ratios in the experimental LVs with age. This slightly significant difference became statistically not significant when an outlier was excluded. No statistically significant difference was found in the quantity of titin relative to MHC expressed in the experimental and control LVs. No transmural difference was found either in the N2BA:N2B and titin:MHC ratios. Furthermore, the experimental and control LVs were found to express N2B and N2BA titin of the same MWs. However, a statistically significant linear relation was discovered between the N2BA:N2B ratios and an indicator of the progression of DCM, the weights of the solution filled hearts normalized

to body weight, for the experimental animals tested at 17 and 38 weeks of age. This correlation implies that the LV cells from the Bio TO-2 hamster express more of the shorter and stiffer N2B isoform as the disease progresses. Because the data points forming the correlation did not separate into two defined clusters corresponding to the two age groups, it appears that the disease is progressing at different rates amongst the experimental animals. This could explain why no difference was found between the N2BA:N2B ratios of the 17 and 38 week old experimental LVs. According to the correlation, the N2BA:N2B ratio decreases from ~0.11 (10% N2BA) to ~0.05 (5% N2BA) as the ratio of weight of a solution filled heart to body weight increases from ~0.0045 to ~0.007. Using data from (Granzier & Labeit, 2004) who provided passive stress-SL relations for cardiac myocytes that predominantly express N2B titin and for some that predominantly express N2BA titin, it is estimated that a 5% decrease in the N2BA:N2B ratio would result in a ~1 $nN/\mu m^2$ increase in peak passive stress at a SL of 2.5 µm. Such an increase in the peak stress results would not be detectable with our system.

It appears as though the following steps are involved in the progression of DCM in the Bio TO-2 hamster:

1. Myocardial damage causes LV dilation. Because the Bio TO-2 hamster lacks the α-, β-, γ- and δ-SG proteins (Sakamoto *et al.*, 1997;Kawada *et al.*, 1999) and shows a partial loss of the α- and β-dystroglycan proteins (Sakamoto *et al.*, 1997), there is a loss of transmission of the force developed by the actin-myosin cross-bridges to the extracellular matrix and a loss of resistance to the over-expansion of the sarcolemma. It is likely that the LV dilation is a result of sarcomeres being added in series, possibly in response to increased diastolic strain (for a review (Russell *et al.*, 2010)), or diminished force transmission (for a review (Granzier & Labeit, 2004)).
2. Ventricular dilation initially provides a mechanism for maintaining adequate stroke volume in the presence of low ejection fraction, but results in increased systolic wall stresses due to

the added volume of blood. For a given aortic pressure, the dilated LV must create a greater tension to eject blood than the normal LV because it has a larger volume.

3. Ventricular stiffness increases almost entirely through changes in collagen expression, thereby providing a limitation in the degree of enlargement. It has been suggested that, in the normal heart, an increase in collagen expression is associated with a decrease in the N2BA:N2B ratio (Wu *et al.*, 2003). The contributions of titin and collagen to the stiffness of cardiac muscles which express predominantly N2B titin, predominantly N2BA titin, and a combination of N2B and N2BA titins were determined. The contributions of titin and collagen to stiffness both increased with the N2B titin content. In the Bio TO-2 hamster, this trend appears to be only partially maintained since a small shift in the expression of titin toward the N2B isoform was found in this study.
4. Excessive collagen expression results in excessive stiffness and progression to heart failure.

In human hearts failing due to DCM, an increase in collagen expression has also been reported (Burlew & Weber, 2002;Makarenko *et al.*, 2004;Neagoe *et al.*, 2002), but the LV N2BA:N2B ratio was found to be increased compared to normal donor hearts, not decreased. In the normal hearts, the percentage of N2BA titin ranged from 23 to 44%, and in the DCM heart, from 29 to 63%. The expression of the longer N2BA isoform possibly increased to counteract the effect of increased collagen expression on myocardial stiffness. It is unknown if an increase in N2B expression accompanied the increase in collage expression before the heart failure stage.

The costameres, Z-disc and titin with its three sensing and signalling centers (see section 2.6.6) have been identified as containing mechanotransduction sites (for a review (Russell *et al.*, 2010;Granzier & Labeit, 2004)) which could be involved in the different stages of the progression of DCM. The costameres play a role in the “transmission of force from the

sarcomere to the sarcolemma and extracellular matrix" (Peter *et al.*, 2011). "The Z-disc is also connected to the sarcolemma at […] costameres" (Granzier & Labeit, 2004). Titin interacts with several proteins contained in the Z-disc. Furthermore, it has been suggested that the Z-disc and titin's capping protein T-cap play a role in myogenesis. Therefore, the costameres, Z-disc and Z-disc region of titin are possible candidates to sense a loss of transmission of the force developed by the actin-myosin cross-bridges to the extracellular matrix or an over-expansion of the sarcolemma, and to be involved in initiating the LV dilation. It has been suggested that both the Z-disc and M-line regions of titin receive mechanical input from actin-myosin crossbridges. Therefore, it is possible that one or both of these sensing and signalling centers of titin are involved in detecting the greater tension produced by the LV myocytes in response to dilation, and in initiating an increase in collagen expression. In human hearts, excessive myocardial stiffness and an increased number of sarcomeres in series would likely result in decreased sarcomere stretch during diastole, and all three sensing and signalling centers of titin could possibly be involved in detecting a reduced titin-based tension and in initiating a shift in titin expression toward the longer N2BA isoform. The N2A element in the I-band region of N2BA titin has been reported to contain a binding motif that has been found to interact with the cardiac ankyrin repeat protein (CARP) (Miller *et al.*, 2003), a ligand involved in transcription through interactions with the transcriptional regulator YB-1 (Zou *et al.*, 1997). If the N2A element of titin is involved in initiating a shift in titin expression toward the longer N2BA isoform in human hearts failing due to DCM, that could explain why the N2BA:N2B ratio was not found to increase during the progression of DCM in the LV of the Bio TO-2 hamster, since it predominantly expresses N2B titin which has no N2A element.

CHAPTER NINE: SUMMARY AND FUTURE DIRECTIONS

Single LV myofibrils from the Bio TO-2 hamster model of DCM were isolated and mechanically tested passively for the first time in this study. Since changes in the expression of titin have been reported to alter the passive mechanical properties of myocardium (Wu *et al.*, 2002b;Cazorla *et al.*, 2000;Neagoe *et al.*, 2003;Schiaffino & Reggiani, 1996;Nagueh *et al.*, 2004;Makarenko *et al.*, 2004;Neagoe *et al.*, 2002) and have been associated with human cases of DCM (Nagueh *et al.*, 2004;Makarenko *et al.*, 2004;Neagoe *et al.*, 2002), the purpose of this study was to relate the mechanical properties of DCM myocardium at the myofibrillar level to the expression of titin during the progression of the disease in the LV of the Bio TO-2 hamster.

9.1 Conclusion

The results of this thesis suggest that there is no difference between the passive mechanical properties of myofbrils isolated from the LVs of Bio TO-2 and F1B hamsters, and that the Bio TO-2 hamster expresses slightly more of the shorter and stiffer N2B isoform compared to the N2BA isoform with the progression of DCM, but the change is too small to be detectable in the passive mechanical properties of experimental myofibrils with the testing system used. These results conflict with the increased N2BA:N2B ratio and decreased contribution of titin to passive tension previously reported in human hearts failing due to DCM.

9.2 Limitations

The measurements made on the passive mechanical properties varied a lot between myofibrils, which may have resulted in some differences between the experimental and control myofibrils being hidden considering the small sample sizes. These variations in the passive mechanical properties of the myofibrils could be real, or they could be attributable to many other

factors, such as inaccuracies in the estimation of the myofibrils' diameters used to calculate the cross-sectional areas, imprecise average SLs, variations in the stiffness of the cantilevers, and cantilever displacements not fully parallel to the image plane of the microscope. A large variance in passive mechanical properties can also be seen in the passive stresses measured on rabbit psoas myofibrils displayed in Figure 6-11 (Leonard & Herzog, 2010) and in the passive stresses measured on mouse and pig LV myocytes displayed in Figure 2-6 (Cazorla *et al.*, 2000).

The small number of myofibrils tested in the experimental group at 17 weeks of age (n=3) affected the power of the statistical analysis performed involving this group. However, the sample sizes of the control (n=8) and experimental groups (n=9) at 38 weeks of age were larger.

The sample sizes of the two animal and two age groups for the N2BA:N2B ratios (experimental at 38 weeks, n=5; control at 38 weeks, n=4; experimental at 17 weeks, n= 4; control at 17 weeks, n=3), titin:MHC ratios (experimental at 38 weeks, n=5; control at 38 weeks, n=4; experimental at 17 weeks, n= 3; control at 17 weeks, n=2), N2BA MWs (experimental at 38 weeks, n=5; control at 38 weeks, n=3; experimental at 17 weeks, n= 3; control at 17 weeks, n=2), and weights of solution filled hearts normalized to body weight (experimental at 38 weeks, n=5; control at 38 weeks, n=4; experimental at 17 weeks, n= 4; control at 17 weeks, n=3), were also small, which affected the power of the statistical analysis performed.

9.3 Future directions

This animal model could be used to study the addition of sarcomeres in series during the progression of the LV dilation in DCM. The number of sarcomeres in series in the fibres and the SLs could possibly be determined using the method described by (Chung & Granzier, 2011) of fixation of intact hearts by perfusion at constant pressure and laser diffraction.

Reference List

Allen DG & Kentish JC (1985). The cellular basis of the length-tension relation in cardiac muscle. *J Mol Cell Cardiol* **17**, 821-840.

Bell SP, Nyland L, Tischler MD, McNabb M, Granzier H, & LeWinter MM (2000). Alterations in the determinants of diastolic suction during pacing tachycardia. *Circ Res* **87**, 235-240.

Burlew BS & Weber KT (2002). Cardiac fibrosis as a cause of diastolic dysfunction. *Herz* **27**, 92-98.

Calaghan SC & White E (1999). The role of calcium in the response of cardiac muscle to stretch. *Prog Biophys Mol Biol* **71**, 59-90.

Cazorla O, Freiburg A, Helmes M, Centner T, McNabb M, Wu Y, Trombitas K, Labeit S, & Granzier H (2000). Differential expression of cardiac titin isoforms and modulation of cellular stiffness. *Circ Res* **86**, 59-67.

Cazorla O, Szilagyi S, Le Guennec JY, Vassort G, & Lacampagne A (2004). Transmural stretch-dependent regulation of contractile properties in rat heart and its alteration after myocardial infarction. *FASEB J* 04-2066fje.

Chung CS & Granzier HL (2011). Contribution of titin and extracellular matrix to passive pressure and measurement of sarcomere length in the mouse left ventricle. *J Mol Cell Cardiol* **50**, 731-739.

de Tombe PP (1998). Altered contractile function in heart failure. *Cardiovasc Res* **37**, 367-380.

De Tombe PP, Mateja RD, Tachampa K, Mou YA, Farman GP, & Irving TC (2010). Myofilament length dependent activation. *J Mol Cell Cardiol* **48**, 851-858.

Fabiato A (1981). Myoplasmic free calcium concentration reached during the twitch of an intact isolated cardiac cell and during calcium-induced release of calcium from the sarcoplasmic reticulum of a skinned cardiac cell from the adult rat or rabbit ventricle. *J Gen Physiol* **78**, 457-497.

Freiburg A, Trombitas K, Hell W, Cazorla O, Fougerousse F, Centner T, Kolmerer B, Witt C, Beckmann JS, Gregorio CC, Granzier HLM, & Labeit S (2000). Series of exon-skipping events in the elastic spring region of titin as the structural basis for myofibrillar elastic diversity. *Circ Res* **86**, 1114-1121.

Fuchs F & Martyn DA (2005). Length-dependent Ca(2+) activation in cardiac muscle: some remaining questions. *J Muscle Res Cell Motil* **26**, 199-212.

Fujita H, Labeit D, Gerull B, Labeit S, & Granzier HLM (2004). Titin isoform-dependent effect of calcium on passive myocardial tension. *Am J Physiol Heart Circ Physiol* **287**, H2528-H2534.

Fukuda N, Wu Y, Farman G, Irving TC, & Granzier HLM (2005a). Titin-based modulation of active tension and interfilament lattice spacing in skinned rat cardiac muscle. *Pflügers Arch - Eur J Physiol* **449**, 449-457.

Fukuda N, Wu Y, Nair P, & Granzier HL (2005b). Phosphorylation of titin modulates passive stiffness of cardiac muscle in a titin isoform-dependent manner. *J Gen Physiol* **125**, 257-271.

Goineau S, Pape D, Guillo P, Ramee MP, & Bellissant E (2001). Hemodynamic and histomorphometric characteristics of dilated cardiomyopathy of Syrian hamsters (Bio TO-2 strain). *Can J Physiol Pharmacol* **79**, 329-337.

Granzier H, Wu Y, Siegfried L, & LeWinter M (2005). Titin: physiological function and role in cardiomyopathy and failure. *Heart Fail Rev* **10**, 211-223.

Granzier HL & Labeit S (2004). The giant protein titin: a major player in myocardial mechanics, signaling, and disease. *Circ Res* **94**, 284-295.

Granzier HLM & Irving TC (1995). Passive tension in cardiac muscle: contribution of collagen, titin, microtubules, and intermediate filaments. *Biophys J* **68**, 1027-1044.

Granzier HLM & Labeit S (2007). Structure-function relations of the giant elastic protein titin in striated and smooth muscle cells. *Muscle Nerve* **36**, 740-755.

Hershberger RE, Morales A, & Siegfried JD (2010). Clinical and genetic issues in dilated cardiomyopathy: a review for genetics professionals. *Genet Med* **12**, 655-667.

Hershberger RE & Siegfried JD (2011). Update 2011: clinical and genetic issues in familial dilated cardiomyopathy. *J Am Coll Cardiol* **57**, 1641-1649.

Herzog W (1999). Muscle. In *Biomechanics of the Musculoskeletal System*, eds. Nigg BM & Herzog W, pp. 148-188. John Wiley & Sons Ltd., Chichester, England.

Holt KH, Lim LE, Straub V, Venzke DP, Duclos F, Anderson RD, Davidson BL, & Campbell KP (1998). Functional rescue of the sarcoglycan complex in the BIO 14.6 hamster using delta-sarcoglycan gene transfer. *Mol Cell* **1**, 841-848.

Ibrahim M, Gorelik J, Yacoub MH, & Terracciano CM (2011). The structure and function of cardiac t-tubules in health and disease. *Proc Biol Sci* **278**, 2714-2723.

Ichihara S, Yamada Y, Ichihara G, Kanazawa H, Hashimoto K, Kato Y, Matsushita A, Oikawa S, Yokota M, & Iwase M (2006). Attenuation of oxidative stress and cardiac dysfunction by bisoprolol in an animal model of dilated cardiomyopathy. *Biochem Biophys Res Commun* **350**, 105-113.

Jaber WA, Maniu C, Krysiak J, Shapiro BP, Meyer DM, Linke WA, & Redfield MM (2008). Titin isoforms, extracellular matrix, and global chamber remodeling in experimental dilated cardiomyopathy: functional implications and mechanistic insight. *Circ Heart Fail* **1**, 192-199.

Joumaa V, Rassier DE, Leonard TR, & Herzog W (2007). Passive force enhancement in single myofibrils. *Pflügers Arch - Eur J Physiol* **455**, 367-371.

Karkkainen S, Miettinen R, Tuomainen P, Karkkainen P, Helio T, Reissell E, Kaartinen M, Toivonen L, Nieminen MS, Kuusisto J, Laakso M, & Peuhkurinen K (2003). A novel mutation, Arg71Thr, in the delta-sarcoglycan gene is associated with dilated cardiomyopathy. *J Mol Med (Berl)* **81**, 795-800.

Kato Y, Iwase M, Takagi K, Nishizawa T, Kanazawa H, Matsushita A, Umeda H, Izawa H, Noda A, Koike Y, Nagata K, & Yokota M (2006). Differential myolysis of myocardium and skeletal muscle in hamsters with dilated cardiomyopathy: beneficial protective effect of diltiazem. *Circ J* **70**, 1497-1502.

Kawada T, Nakatsuru Y, Sakamoto A, Koizumi T, Shin WS, Okai-Matsuo Y, Suzuki J, Uehara Y, Nakazawa M, Sato H, Ishikawa T, & Toyo-oka T (1999). Strain- and age-dependent loss of sarcoglycan complex in cardiomyopathic hamster hearts and its re-expression by delta-sarcoglycan gene transfer in vivo. *FEBS Lett* **458**, 405-408.

Kawada T, Masui F, Kumagai H, Koshimizu M, Nakazawa M, & Toyo-oka T (2005). A novel paradigm for therapeutic basis of advanced heart failure--assessment by gene therapy. *Pharmacology & Therapeutics* **107**, 31-43.

Kentish JC, ter Keurs HE, Ricciardi L, Bucx JJ, & Noble MI (1986). Comparison between the sarcomere length-force relations of intact and skinned trabeculae from rat right ventricle. Influence of calcium concentrations on these relations. *Circ Res* **58**, 755-768.

Kossmann CE & Fawcett D.W. (1961). The Sarcoplasmic Reticulum of Skeletal and Cardiac Muscle. *Circulation* **24**, 336-348.

Kruger M, Kotter S, Grutzner A, Lang P, Andresen C, Redfield MM, Butt E, dos Remedios CG, & Linke WA (2009). Protein kinase G modulates human myocardial passive stiffness by phosphorylation of the titin springs. *Circ Res* **104**, 87-94.

Labeit D, Watanabe K, Witt C, Fujita H, Wu Y, Lahmers S, Funck T, Labeit S, & Granzier HLM (2003). Calcium-dependent molecular spring elements in the giant protein titin. *Proc Natl Acad Sci U S A* **100**, 13716-13721.

Labeit S & Kolmerer B (1995). Titins: Giant proteins in charge of muscle ultrastructure and elasticity. *Science* **270**, 293-296.

Lee WN, Pernot M, Couade M, Messas E, Bruneval P, Bel A, Hagege AA, Fink M, & Tanter M (2012). Mapping myocardial fiber orientation using echocardiography-based shear wave imaging. *IEEE Trans Med Imaging* **31**, 554-562.

Leeson, Leeson, & Paparo (1985). *Textbook of Histology*, 5th ed., pp. 186-192.

Leonard TR & Herzog W (2010). Regulation of muscle force in the absence of actin-myosin based cross-bridge interaction. *Am J Physiol Cell Physiol* **299**, C14-C20.

Linke WA, Ivemeyer M, Olivieri N, Kolmerer B, Ruedel R, & Labeit S (1996). Towards a molecular understanding of the elasticity of titin. *J Mol Biol* **261**, 62-71.

Linke WA & Leake MC (2004). Multiple sources of passive stress relaxation in muscle fibres. *Phys Med Biol* **49**, 3613-3627.

Lloyd-Jones D, Adams RJ, Brown TM, Carnethon M, Dai S, de SG, Ferguson TB, Ford E, Furie K, Gillespie C, Go A, Greenlund K, Haase N, Hailpern S, Ho PM, Howard V, Kissela B, Kittner S, Lackland D, Lisabeth L, Marelli A, McDermott MM, Meigs J, Mozaffarian D, Mussolino M, Nichol G, Roger VL, Rosamond W, Sacco R, Sorlie P, Roger VL, Thom T, Wasserthiel-Smoller S, Wong ND, & Wylie-Rosett J (2010). Heart disease and stroke statistics--2010 update: a report from the American Heart Association. *Circulation* **121**, e46-e215.

Luk A, Ahn E, Soor GS, & Butany J (2009). Dilated cardiomyopathy: a review. *J Clin Pathol* **62**, 219-225.

Luther PK & Squire JM (2002). Muscle Z-band ultrastructure: titin Z-repeats and Z-band periodicities do not match. *J Mol Biol* **319**, 1157-1164.

Makarenko I, Opitz CA, Leake MC, Neagoe C, Kulke M, Gwathmey JK, del MF, Hajjar RJ, & Linke WA (2004). Passive stiffness changes caused by upregulation of compliant titin isoforms in human dilated cardiomyopathy hearts. *Circ Res* **95**, 708-716.

Mancinelli R, Vargiu R, Cappai A, Floris G, Fraschini M, & Faa G (2005). A metabolic approach to the treatment of dilated cardiomyopathy in BIO T0-2 cardiomyopathic Syrian hamsters. *Biofactors* **25**, 127-135.

Mestroni L, Maisch B, McKenna WJ, Schwartz K, Charron P, Rocco C, Tesson F, Richter A, Wilke A, & Komajda M (1999). Guidelines for the study of familial dilated cardiomyopathies. Collaborative Research Group of the European Human and Capital Mobility Project on Familial Dilated Cardiomyopathy. *Eur Heart J* **20**, 93-102.

Miller MK, Bang ML, Witt CC, Labeit D, Trombitas C, Watanabe K, Granzier H, McElhinny AS, Gregorio CC, & Labeit S (2003). The muscle ankyrin repeat proteins: CARP, ankrd2/Arpp and DARP as a family of titin filament-based stress response molecules. *J Mol Biol* **333**, 951-964.

Minajeva A, Kulke M, Fernandez JM, & Linke WA (2001). Unfolding of titin domains explains the viscoelastic behaviour of skeletal myofibrils. *Biophys J* **80**, 1442-1451.

Nagueh SF, Shah G, Wu Y, Torre-Amione G, King NM, Lahmers S, Witt CC, Becker K, Labeit S, & Granzier HL (2004). Altered titin expression, myocardial stiffness, and left ventricular function in patients with dilated cardiomyopathy. *Circulation* **110**, 155-162.

Neagoe C, Kulke M, del Monte F, Gwathmey JK, De Tombe PP, Hajjar RJ, & Linke WA (2002). Titin isoform switch in ischemic human heart disease. *Circulation* **106**, 1333-1341.

Neagoe C, Opitz CA, Makarenko I, & Linke WA (2003). Gigantic variety: expression patterns of titin isoforms in striated muscles and consequences for myofibrillar passive stiffness. *J Muscle Res Cell Motil* **24**, 175-189.

Nishimura S, Yamashita H, Katoh M, Yamada KP, Sunagawa K, Saeki Y, Ohnuki Y, Nagai R, & Sugiura S (2005). Contractile dysfunction of cardiomyopathic hamster myocytes is pronounced under high load conditions. *J Mol Cell Cardiol* **39**, 231-239.

Peter AK, Cheng H, Ross RS, Knowlton KU, & Chen J (2011). The costamere bridges sarcomeres to the sarcolemma in striated muscle. *Progress in Pediatric Cardiology* **31**, 83-88.

Pollack GH & Huntsman LL (1974). Sarcomere length-active force relations in living mammalian cardiac muscle. *Am J Physiol* **227**, 383-389.

Prado LG, Makarenko I, Andresen C, Kruger M, Opitz CA, & Linke WA (2005). Isoform diversity of giant proteins in relation to passive and active contractile properties of rabbit skeletal muscles. *J Gen Physiol* **126**, 461-480.

Rassier DE, Herzog W, & Pollack GH (2003). Dynamics of individual sarcomeres during and after stretch in activated single myofibrils. *Proc R Soc Lond B* **270**, 1735-1740.

Rodriguez EK, Hunter WC, Royce MJ, Leppo MK, Douglas AS, & Weisman HF (1992). A method to reconstruct myocardial sarcomere lengths and orientations at transmural sites in beating canine hearts. *Am J Physiol* **263**, H293-H306.

Russell B, Curtis MW, Koshman YE, & Samarel AM (2010). Mechanical stress-induced sarcomere assembly for cardiac muscle growth in length and width. *J Mol Cell Cardiol*.

Sakamoto A, Ono K, Abe M, Jasmin G, Eki T, Murakami Y, Masaki T, Toyo-oka T, & Hanaoka F (1997). Both hypertrophic and dilated cardiomyopathies are caused by mutation of the same gene, delta-sarcoglycan, in hamster: an animal model of disrupted dystrophin-associated glycoprotein complex. *Proc Natl Acad Sci U S A* **94**, 13873-13878.

Schaper J, Froede R, Hein S, Buck A, Hashizume H, Speiser B, Friedl A, & Bleese N (1991). Impairment of the myocardial ultrastructure and changes of the cytoskeleton in dilated cardiomyopathy. *Circulation* **83**, 504-514.

Schiaffino S & Reggiani C (1996). Molecular diversity of myofibrillar proteins: gene regulation and functional significance. *Physiol Rev* **76**, 371-423.

Schwinger RH, Bohm M, Koch A, Schmidt U, Morano I, Eissner HJ, Uberfuhr P, Reichart B, & Erdmann E (1994). The failing human heart is unable to use the Frank-Starling mechanism. *Circ Res* **74**, 959-969.

Sparks HV (1987). The Heart as a Pump. In *Essentials of Cardiovascular Physiology* pp. 43-78. University of Minnesota Press, Minneapolis.

Stehle R, Kruger M, & Pfitzer G (2002a). Force kinetics and individual sarcomere dynamics in cardiac myofibrils after rapid ca(2+) changes. *Biophys J* **83**, 2152-2161.

Stehle R, Kruger M, Scherer P, Brixius K, Schwinger RH, & Pfitzer G (2002b). Isometric force kinetics upon rapid activation and relaxation of mouse, guinea pig and human heart muscle studied on the subcellular myofibrillar level. *Basic Res Cardiol* **97 Suppl 1**, I127-I135.

Stuyvers BD, Miura M, Jin JP, & ter Keurs HE (1998). Ca(2+)-dependence of diastolic properties of cardiac sarcomeres: involvement of titin. *Prog Biophys Mol Biol* **69**, 425-443.

Stuyvers BD, Miura M, & ter Keurs HE (1997a). Diastolic viscoelastic properties of rat cardiac muscle; involvement of Ca2+. *Adv Exp Med Biol* **430**, 13-28.

Stuyvers BD, Miura M, & ter Keurs HE (1997b). Dynamics of viscoelastic properties of rat cardiac sarcomeres during the diastolic interval: involvement of Ca2+. *J Physiol* **502 (Pt 3)**, 661-677.

Stuyvers BD, Miura M, & ter Keurs HE (2000). Ca(2+)-dependence of passive properties of cardiac sarcomeres. *Adv Exp Med Biol* **481**, 353-366.

Sylvius N, Duboscq-Bidot L, Bouchier C, Charron P, Benaiche A, Sebillon P, Komajda M, & Villard E (2003). Mutational analysis of the beta- and delta-sarcoglycan genes in a large number of patients with familial and sporadic dilated cardiomyopathy. *Am J Med Genet A* **120A**, 8-12.

Toyo-oka T, Kawada T, Nakata J, Xie H, Urabe M, Masui F, Ebisawa T, Tezuka A, Iwasawa K, Nakajima T, Uehara Y, Kumagai H, Kostin S, Schaper J, Nakazawa M, & Ozawa K (2004). Translocation and cleavage of myocardial dystrophin as a common pathway to advanced heart failure: a scheme for the progression of cardiac dysfunction. *Proc Natl Acad Sci U S A* **101**, 7381-7385.

Trombitas K, Jin JP, & Granzier HLM (1995). The mechanically active domain of titin in cardiac muscle. *Circ Res* **77**, 856-861.

Trombitas K, Wu Y, Labeit D, Labeit S, & Granzier HLM (2001). Cardiac titin isoforms are coexpressed in the half-sarcomere and extend independently. *Am J Physiol Heart Circ Physiol* **281**, H1793-H1799.

Tsubata S, Bowles KR, Vatta M, Zintz C, Titus J, Muhonen L, Bowles NE, & Towbin JA (2000). Mutations in the human delta-sarcoglycan gene in familial and sporadic dilated cardiomyopathy. *J Clin Invest* **106**, 655-662.

Vahl CF, Timek T, Bonz A, Fuchs H, Dillman R, & Hagl S (1998). Length dependence of calcium- and force-transients in normal and failing human myocardium. *J Mol Cell Cardiol* **30**, 957-966.

Vahl CF, Timek T, Bonz A, Kochsiek N, Fuchs H, Schaffer L, Rosenberg M, Dillmann R, & Hagl S (1997). Myocardial length-force relationship in end stage dilated cardiomyopathy and normal human myocardium: analysis of intact and skinned left ventricular trabeculae obtained during 11 heart transplantations. *Basic Res Cardiol* **92**, 261-270.

Vatta M, Stetson SJ, Perez-Verdia A, Entman ML, Noon GP, Torre-Amione G, Bowles NE, & Towbin JA (2002). Molecular remodelling of dystrophin in patients with end-stage cardiomyopathies and reversal in patients on assistance-device therapy. *Lancet* **359**, 936-941.

Warren CM, Jordan MC, Roos KP, Krzesinski PR, & Greaser ML (2003). Titin isoform expression in normal and hypertensive myocardium. *Cardiovasc Res* **59**, 86-94.

Warren CM, Krzesinski PR, Campbell KS, Moss RL, & Greaser ML (2004). Titin isoform changes in rat myocardium during development. *Mech Dev* **121**, 1301-1312.

Watanabe K, Nair P, Labeit D, Kellermayer MS, Greaser M, Labeit S, & Granzier H (2002). Molecular mechanics of cardiac titin's PEVK and N2B spring elements. *J Biol Chem* **277**, 11549-11558.

Weinhaus A.J. & Roberts K.P. (2009). Anatomy of the Human Heart. In *Handbook of Cardiac Anatomy, Physiology, and Devices* pp. 59-85. Springer.

Wu Y, Bell SP, Trombitas K, Witt CC, Labeit S, LeWinter MM, & Granzier H (2002a). Changes in titin isoform expression in pacing-induced cardiac failure give rise to increased passive muscle stiffness. *Circulation* **106**, 1384-1389.

Wu Y, Cazorla O, Labeit D, Labeit S, & Granzier H (2003). Changes in titin and collagen underlie diastolic stiffness diversity of cardiac muscle. *J Mol Cell Cardiol* **32**, 2151-2162.

Wu Y, Labeit S, LeWinter MM, & Granzier H (2002b). Titin: an endosarcomeric protein that modulates myocardial stiffness in DCM. *J Card Fail* **8**, S276-S286.

Wynne J & Braunwald E (2005). The cardiomyopathies. In *Heart disease: a textbook of cardiovascular medicine*, eds. Zipes DP, Libby P, Bonow RV, & Braunwald E, pp. 1659-1663. Elsevier-Saunders, Philadelphia.

Yamasaki R, Berri M, Wu Y, Trombitas K, McNabb M, Kellermayer MSZ, Witt C, Labeit D, Labeit S, Greaser M, & Granzier HLM (2001). Titin-Actin interaction in mouse myocardium: passive tension modulation and its regulation by calcium/S100A1. *Biophys J* **81**, 2297-2313.

Zou Y, Evans S, Chen J, Kuo HC, Harvey RP, & Chien KR (1997). CARP, a cardiac ankyrin repeat protein, is downstream in the Nkx2-5 homeobox gene pathway. *Development* **124**, 793-804.

APPENDIX A: PROTOCOL SOLUTIONS

For storage solution: Keep in refrigerator.	MW (g/mol)	mM	M	**500 ml** Mass (g)	**1 L** Mass (g)
K_2HPO_4 from 1 M stock solution		10	0.01	5 ml	10 ml
NaN_3	65.0	10	0.01	0.325	0.650
Mg-acetate$\cdot 4H_2O$	214.5	6	0.006	0.644	1.287

For storage and relaxing solution: Freeze in aliquots.	MW (g/mol)	mM	M	**500 ml** Mass (g)	**1 L** Mass (g)
KCl	74.6	500	0.5	18.640	37.280
EGTA	380.4	250	0.25	47.544	95.088
K_4Cl_2EGTA		250	0.25		

Adjust pH of solution to 7 at 20ºC with KOH. This is required for EGTA to dissolve.

For storage, relaxing and activating solutions: Freeze in aliquots.	MW (g/mol)	mM	M	**500 ml** Mass (g)	**1 L** Mass (g)
Na_2ATP	551.1	50	0.05	13.778	27.555
$MgCl_2\cdot 6H_2O$	203.3	50	0.05	5.083	10.165
Cl_2Na_2MgATP		50	0.05		

For activating solution: Freeze in aliquots.	MW (g/mol)	mM	M	**500 ml** Mass (g)	**1 L** Mass (g)
$CaCl_2\cdot H_2O$	147.0	250	0.25	18.378	36.755
EGTA	380.4	250	0.25	47.544	95.088
$K_4Cl_2CaEGTA$		250	0.25		

Adjust pH of solution to 7 at 20ºC with KOH. This is required for EGTA to dissolve.

For relaxing and activating solutions: Keep in refrigerator.	MW (g/mol)	mM	M	**500 ml** Mass (g)	**1 L** Mass (g)
$MgCl_2 \cdot 6H_2O$	203.3	6	0.006	0.610	1.220
Imidazole	68.1	20	0.02	0.681	1.362

For rigor solution: Keep in refrigerator.	MW (g/mol)	mM	M	**500 ml** Mass (g)	**1 L** Mass (g)
Tris	121.1	10	0.01	0.606	1.211
NaCL	58.4	132	0.132	3.857	7.714
KCl	74.6	5	0.005	0.186	0.373
$MgCl_2 \cdot 6H_2O$	203.3	1	0.001	0.102	0.203
NaN_3	65.0	1	0.001	0.033	0.065
EGTA	380.4	5	0.005	0.951	1.902

Adjust pH of solution to 7 at 20ºC.

Table A-1 Compositions of stock solutions

	Vol. (ml)	Mass (g)
Volume of rigor solution needed Monday:	80.0	
Rigor stock solution	80.0	
Add Glucose monohydrate		0.101
Add DTT		0.025

Table A-2 Preparation of rigor solution on Monday

	Vol. (ml)	Mass (g)	# of tablets
Volume of storage solution to be made for the week:	325.0		
Stock solution of K_2HPO_4, NaN_3 and Mg-acetate	162.5		
Add N_2CrP		4.997	
Add K_4Cl_2EGTA from frozen aliquot	6.5		
Add water to make	305.5		
Volume of storage solution needed Monday:	150.0		
Solution of K_2HPO_4, NaN_3, Mg-acetate, N_2CrP and K_4Cl_2EGTA	141.0		
Add PI			3
Add DTT		0.046	
After one hour:			
Add Cl_2Na_2MgATP from frozen aliquot	9.0		
Adjust pH to 7 at 10°C			
Volume of skinning solution needed Monday:	20.0		
Storage solution with PI, DTT and Cl_2Na_2MgATP	19.8		
Add Triton	0.2		

Table A-3 Preparation of storage and skinning solution on Monday

	Vol. (ml)	Mass (g)	# of tablets
Volume of storage solution needed Tuesday, Wednesday and Thursday:	50.0		
Solution of K_2HPO_4, NaN_3, Mg-acetate, N_2CrP and K_4Cl_2EGTA	47.0		
Add PI			1
Add DTT		0.015	
Put aside some storage solution for an experiment in the afternoon	14.1		
After one hour:			
Remaining volume of solution to be used for storage and homogenization	32.9		
Add Cl_2Na_2MgATP from frozen aliquot	2.1		
Adjust pH to 7 at 10°C			
Volume of storage solution put aside for homogenization in the afternoon:	14.1		
Add Cl_2Na_2MgATP from frozen aliquot	0.900		
Adjust pH to 7 at room temperature			

Table A-4 Preparation of storage solution on Tuesday, Wednesday and Thursday

	Vol. (ml)	Mass (g)	# of tablets
Volume of storage solution needed Friday:	25.0		
Solution of K_2HPO_4, NaN_3, Mg-acetate, N_2CrP and K_4Cl_2EGTA	23.5		
Add PI			0.5
Add DTT		0.008	
Put aside some storage solution for an experiment in the afternoon	11.8		
After one hour:			
Remaining volume of solution to be used for homogenization	11.8		
Add Cl_2Na_2MgATP from frozen aliquot	0.750		
Adjust pH to 7 at 10°C			
Volume of storage solution put aside for homogenization in the afternoon:	11.8		
Add Cl_2Na_2MgATP from frozen aliquot	0.750		
Adjust pH to 7 at room temperature			

Table A-5 Preparation of storage solution on Friday

	Vol. (ml)	Mass (g)
Volume of relaxing and activating solutions to be made for the week:	360.0	
Stock solution of imidazole and $MgCl_2$	180.0	
Add Na_2CrP		5.618
Add water to make	348.5	
Volume of imidazole, $MgCl_2$, Na_2CrP and DTT solution needed per half day:	45.0	
Solution of imidazole, $MgCl_2$ and Na_2CrP	43.6	
Add DTT		0.014
Volume of relaxing solution needed per half day:	20.00	
Solution of imidazole, $MgCl_2$, Na_2CrP and DTT	19.36	
Add K_4Cl_2EGTA from frozen aliquot	0.240	
Add Cl_2Na_2MgATP from frozen aliquot	0.400	
Adjust pH to 7 at room temperature.		
Volume of activating solution needed per half day:	20.00	
Solution of imidazole, $MgCl_2$, Na_2CrP and DTT	19.36	
Add $K_4Cl_{2Ca}EGTA$ from frozen aliquot	0.240	
Add Cl_2Na_2MgATP from frozen aliquot	0.400	
Adjust pH to 7 at room temperature.		

Table A-6 Preparation of relaxing and activating solutions on Tuesday

	Vol. (ml)	Mass (g)
Volume of imidazole, $MgCl_2$, Na_2CrP and DTT solution needed per half day:	45.0	
Solution of imidazole, $MgCl_2$ and Na_2CrP	43.6	
Add DTT		0.014
Volume of relaxing solution needed per half day:	20.00	
Solution of imidazole, $MgCl_2$, Na_2CrP and DTT	19.36	
Add K_4Cl_2EGTA from frozen aliquot	0.240	
Add Cl_2Na_2MgATP from frozen aliquot	0.400	
Adjust pH to 7 at room temperature.		
Volume of activating solution needed per half day:	20.00	
Solution of imidazole, $MgCl_2$, Na_2CrP and DTT	19.36	
Add $K_4Cl_{2Ca}EGTA$ from frozen aliquot	0.240	
Add Cl_2Na_2MgATP from frozen aliquot	0.400	
Adjust pH to 7 at room temperature.		

Table A-7 Preparation of relaxing and activating solutions on Wednesday, Thursday and Friday